AD_____

Award Number: DAMD17-99-1-9458

TITLE: Growth Factor Antagonism in Breast Cancer Chemotherapy

PRINCIPAL INVESTIGATOR: Andrew D. Hamilton, Ph.D.

CONTRACTING ORGANIZATION: Yale University
New Haven, Connecticut 06520-8337

REPORT DATE: May 2002

TYPE OF REPORT: Final

PREPARED FOR: U.S. Army Medical Research and Materiel Command
Fort Detrick, Maryland 21702-5012

REPORT DOCUMENTATION PAGE

Form Approved
OMB No. 074-0188

1. AGENCY USE ONLY (Leave blank)	2. REPORT DATE	3. REPORT TYPE AND DATES COVERED
	May 2002	Final (1 May 99 - 30 Apr 02)

4. TITLE AND SUBTITLE
Growth Factor Antagonism in Breast Cancer Chemotherapy

5. FUNDING NUMBERS
DAMD17-99-1-9458

6. AUTHOR(S)
Andrew D. Hamilton, Ph.D.

7. PERFORMING ORGANIZATION NAME(S) AND ADDRESS(ES)
Yale University
New Haven, Connecticut 06520-8337

E-Mail: andrew.hamilton@yale.edu

8. PERFORMING ORGANIZATION REPORT NUMBER

9. SPONSORING / MONITORING AGENCY NAME(S) AND ADDRESS(ES)
U.S. Army Medical Research and Materiel Command
Fort Detrick, Maryland 21702-5012

10. SPONSORING / MONITORING AGENCY REPORT NUMBER

11. SUPPLEMENTARY NOTES
Report contains color.

12a. DISTRIBUTION / AVAILABILITY STATEMENT
Approved for Public Release; Distribution Unlimited

12b. DISTRIBUTION CODE

13. ABSTRACT ***(Maximum 200 Words)***

The primary focus of this work is the identification of molecules that block the interaction of growth factors with their receptor tyrosine kinases (RTKs). We have designed, synthesized and evaluated a novel series of synthetic agents that bind to the surface of growth factors and block their interaction with their RTKs. We have now prepared two classes of protein binding agents. The first involves the attachment of four peptide loops to a central scaffold based on the calix[4]arene unit. The second is based around a tetraphenylporphyrin unit in which different recognition groups are attached. We have identified one molecule that binds to the surface of platelet derived growth factor and shows potent antitumor activity in a mouse xenograft model of a human cancer that is activated by PDGF. From a different family of agents we have identified a molecule that binds tightly to epidermal growth factor.

14. SUBJECT TERMS	15. NUMBER OF PAGES
breast cancer, growth factor antagonism, protein surface binding agents, tyrosine kinases, synthetic agents	64
	16. PRICE CODE

17. SECURITY CLASSIFICATION OF REPORT	18. SECURITY CLASSIFICATION OF THIS PAGE	19. SECURITY CLASSIFICATION OF ABSTRACT	20. LIMITATION OF ABSTRACT
Unclassified	Unclassified	Unclassified	Unlimited

NSN 7540-01-280-5500

Standard Form 298 (Rev. 2-89)
Prescribed by ANSI Std. Z39-18
298-102

Table of Contents

Cover.....1

SF 298.....2

Table of Contents.....3

Introduction.....4

Body.....4

Key Research Accomplishments.....14

Reportable Outcomes.....14

Conclusions.....15

References.....15

Appendices.....17

Introduction

The primary focus of this project is the first step in the aberrant cell signaling pathways that lead to uncontrolled proliferation and cancer, namely the interaction of growth factors with their receptor tyrosine kinases (RTKs). Overexpression of RTKs as well as high serum levels of of the activating growth factor are seen in certain breast and ovarian carcinomas. Furthermore, elevated levels of RTKs in breast cancer patients correlate with poor response to chemotherapy and shorter survival times. The design of growth factor antagonists that can inhibit ligand-induced receptor activation is a potentially novel route to new anti-cancer drugs. In recent years this strategy has been supported by the development of antibodies (e.g. Herceptin) against RTKs that have been shown to be active against breast cancer in the clinic. The main goals of this project are to design, synthesize and evaluate a novel series of synthetic agents that bind to the surface of growth factors and block their interaction with their RTKs. We have now prepared two classes of protein binding agents. The first involves the attachment of four peptide loops to a central scaffold (based on the calix[4]arene unit). The second is based around a tetraphenylporphyrin unit in which different recognition groups are attached. A key component of the second year of this project was to further confirm the proof of concept that molecular entities can be designed to bind to growth factor targets and block their function in living cells.

Body of Text

Task 1. To further refine the first generation of protein surface recognition agents based on four β-turn cyclic peptide mimetics linked to a calix[4]arene core scaffold (months 1-12).

We have made excellent progress in the completion of task 1. We have prepared a large number of cyclic peptide derivatives based on the 3-aminomethylbenzoic acid scaffold and attached them to the core calixarene scaffold. A selection of these sequences is shown in Figure 1.

However, the calixarene unit suffers several complications, including difficulty of synthesis and tendency to aggregation. We have improved this synthetic approach by studying different organic scaffolds onto which recognition sites can be attached. Porphyrins, owing to their large size, rigidity and photophysical properties are interesting candidates as the central core scaffold component. During the past year we have investigated the design, synthesis and recognition properties of a series of tetraphenylporphyrins that bind, in certain cases with high affinity, to protein surfaces. We have tested the protein binding of these molecules against cytochrome c. Cytochrome c is a particularly attractive target since it is a well-characterized protein that plays a critical role, by binding to Apaf1, in initiating programmed cell death or apoptosis. The porphyrin-based receptors were prepared by the generation of the tetra-acid chloride ($(COCl)_2$, DMF) starting from m-tetrakis-(4-carboxyphenyl) porphyrin **1**, and subsequent coupling with the corresponding t-butyl protected amino acid or peptide amines. Deprotection of t-butyl groups with trifluoroacetic acid provided receptors **2-4**. Acidic and hydrophobic attachments were chosen to complement the cationic and hydrophobic surface surrounding the RTK binding region of many growth factors, e.g. PDGF.

Compounds **1-4**, and coproporphyrin I, a naturally occuring tetraanionic porphyrin, were initially screened for binding to horse heart ferricytochrome c using fluorescence spectroscopy. Addition of cytochrome c to solutions containing **1-4** resulted in quenching of porphyrin fluorescence emission (ex=420nm, em=650nm) due to the enforced proximity of the Fe(III)

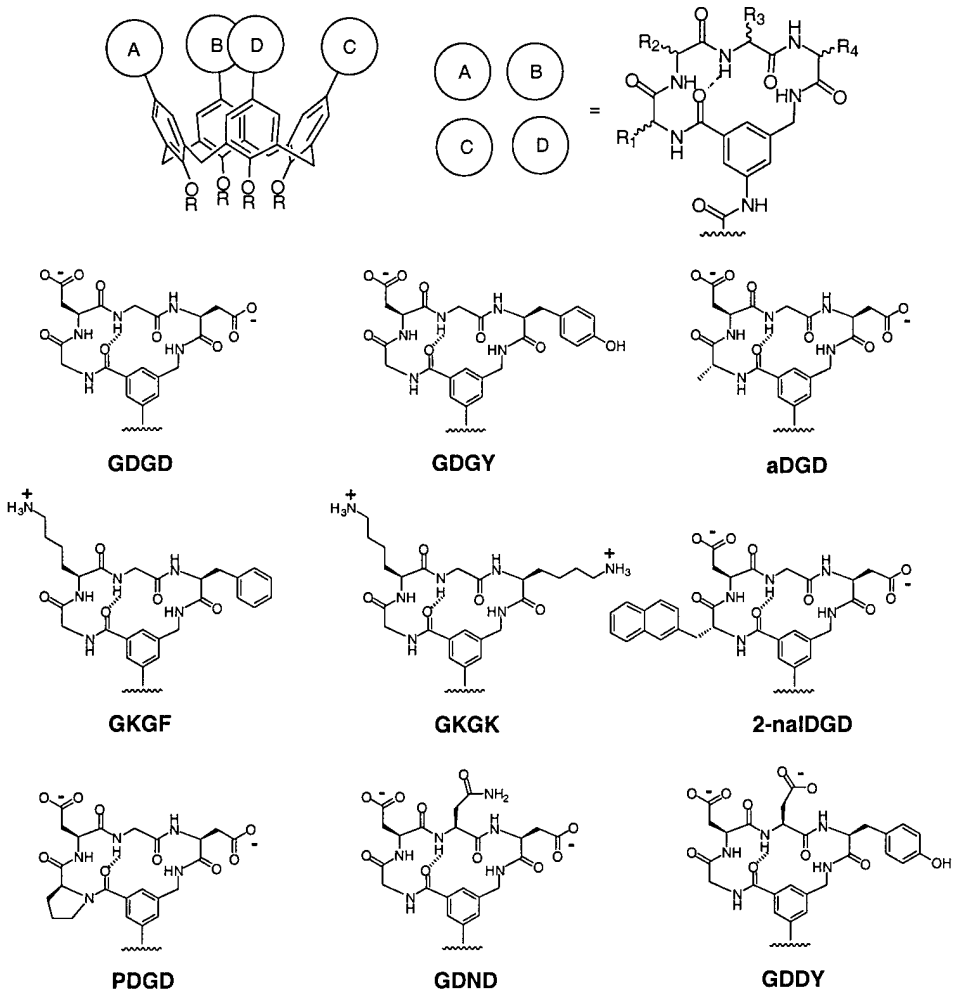

Figure 1. Recent progress in the synthesis of cyclic peptide derivatives and their incorporation in calixarene-based growth factor binding agents.

heme that results from complex formation between the protein and the receptors. In contrast, titrations with tetracationic m-tetrakis-(4-trimethylaminophenyl) porphyrin (TTMAPP), showed no quenching even at high concentrations indicating the absence of nonspecific binding. Typical titrations of **3**, **4** and TTMAPP with cytochrome c are shown in Figure 2. Receptor **4** contains eight negatively charged groups and 8 phenyl groups. The titration curve (Figure 2) shows a sharper achievement of saturation with **4** compared to **3**. This corresponds to a K_d of 20 ±5 nM for **4** binding to cytochrome c and represents an eight fold increase in affinity compared to **3**. To our knowledge, **4** is one of the strongest synthetic receptors for cytochrome c, under these experimental conditions. The binding experiments between **4** and cytochrome c were carried out in 5mM phosphate buffer at pH 7.4. Remarkably, receptor **4** with a molecular weight of ~1900 Da can bind to cytochrome c 100 fold stronger than its natural protein partners such as cytochrome c peroxidase, which has a K_d of 2.4μM measured at 5mM phosphate buffer, pH=7.2 Full details of this work are described in papers in *Organic Letters* and *Chemical Communications* (see appendix).

We have also made important steps in the wider application of the calix[4]arene approach with the preparation of a series of unsymmetrical receptors in which two different loops are attached to the core calixarene (Figure 3).

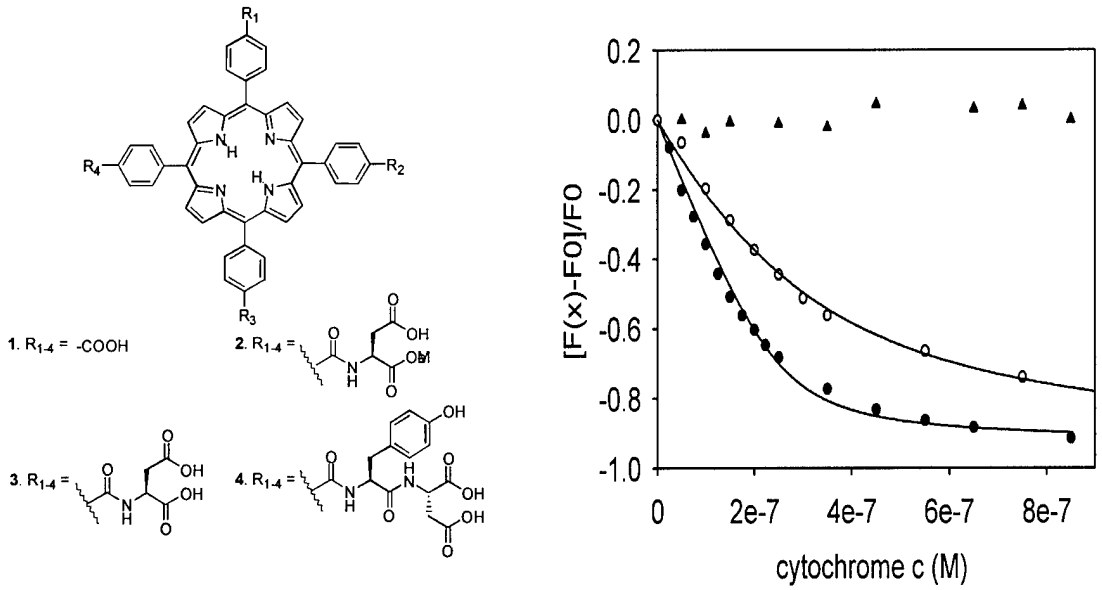

Figure 2. Fluorescence quenching of **4** (●), **3** (o) and TTMAPP (▲) upon addition of cytochrome c. The curve fit indicates a K_d of 20 ±5nM for **4** and 160 ±20nM for **3**. Titrations were carried out under 250nM initial receptor concentration in 5mM sodium phosphate buffer, pH = 7.4, at 298K.

Calix[4]arene has been widely used in the field of supramolecular chemistry due to its well-defined shape.[1] However, few examples exist in which the upper rim of calixarene has been differentially functionalized.[2] In our effort to attach two different peptide loops onto the calixarene scaffold, we envisioned that three partially protected calix[4]arene tetracarboxylic acid derivatives, such as (**5**), (**6**), (**7**) (Scheme 1), should lead to unsymmetrical receptors through sequencial coupling steps. Initial attempts to selectively protect butoxycalix[4]arene tetracarboxylic acid were unsuccessful, resulting in inseparable mixtures. However, stepwise functionalization of the upper rim of calix[4]arene could be carried out efficiently and gave all

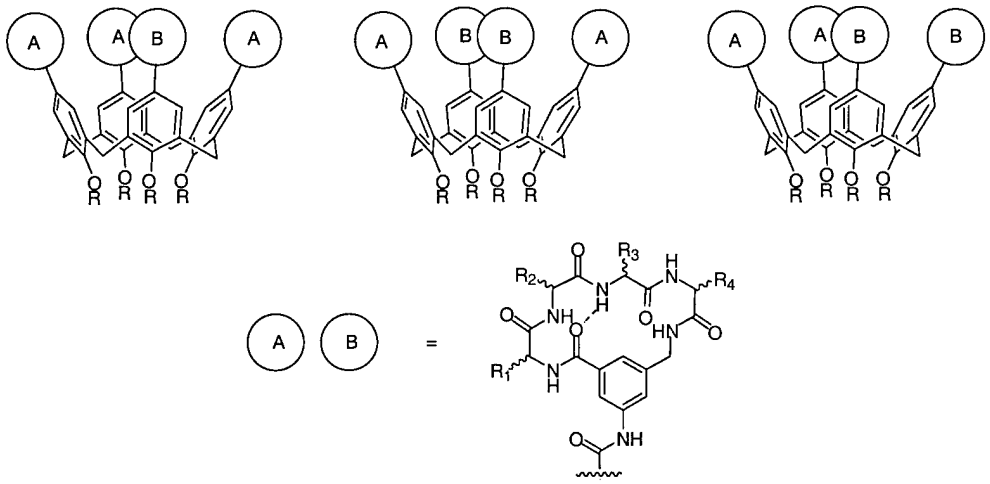

Figure 3. Design of unsymmetrical ligands based on a calix[4]arene scaffold.

three partially protected derivatives in good yields (Scheme 1).[3] Treating butoxycalix[4]arene with 1 eq. Cl_2CHOCH_3 in the presence of 1 eq. $TiCl_4$ gave primarily mono-formylated product in 60% yield. Subsequent oxidation and protection afforded a mono-calix[4]arene carboxylester.

The p-nitrobenzyl ester was chosen due to its easy removal by hydrogenation after coupling to the peptide loops (Scheme 2). Further formylation with excess $TiCl_4$ and oxidation with $NaClO_2$ furnished the final product as a mono-protected butoxycalix[4]arene tetracarboxylic acid (**5**). The other scaffolds were prepared in an analogous manner. Formylation of butylcalix[4]arene with CH_2Cl_2 and $SnCl_4$ gave a mixture of bis-formylated derivatives which could not be separated by flash chromatography. The mixture was carried on to the bis-ester stage after which the two isomers can be easily separated by column in a 1:1.3 cis:trans ratio. The bis-acids were protected as p. nitrobenzyl esters. Further formylation and oxidation afforded the final products, cis-calix[4]arene bis-acid bis-ester (**6**) and trans-calix[4]arene bis-acid bis-ester (**7**), which set up all three required scaffolds for our receptor constructions.

The use of the scaffold **5** for the preparation of the unsymmetrical receptors is illustrated in Scheme 2. The first coupling proceeded using a normal acid chloride method.[4] After removal of the p. nitrobenzyl protecting group under hydrogenation condition, the acid was converted to Yamaguchi-type anhydride[5], and subsequently reacted with the second peptide loop to give the fully protected calix[4]arene tetracyclic peptide receptor. TFA treatment gave the final product. A series of X-3-XYZW-1-X′Y′Z′W′ receptors were prepared in good yields by this route (Table 1). Similar routes were sucessfully performed on the preparations of cis-A2B2 and trans-A2B2

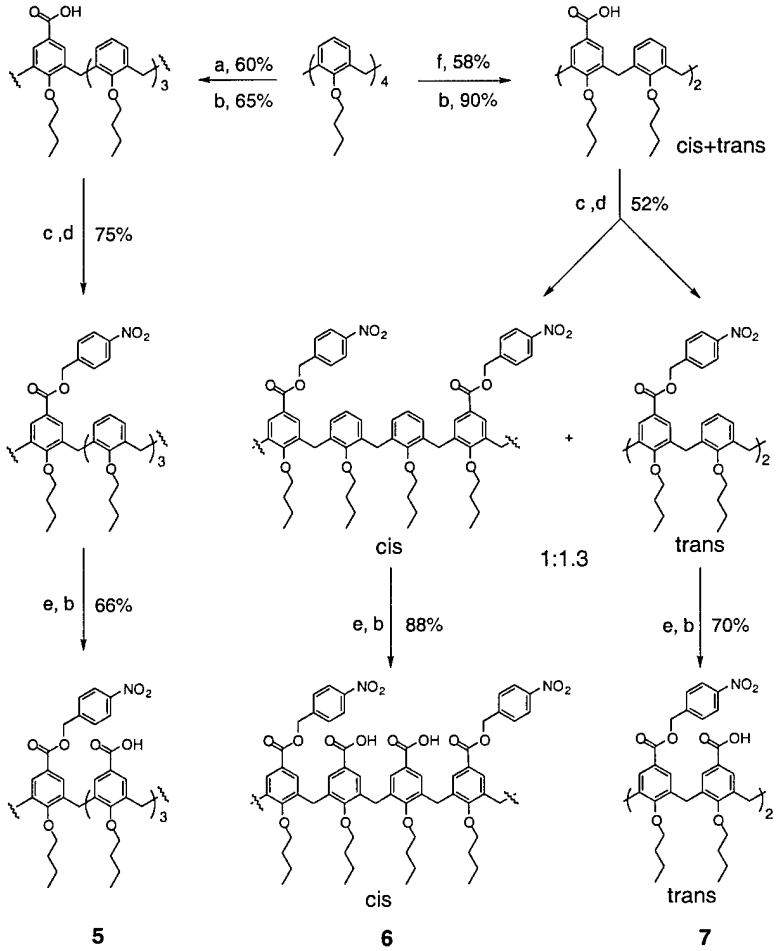

Scheme 1 a) 1 eq. Cl_2CHOCH_3, 1 eq. $TiCl_4$, CH_2Cl_2, -10°C; b)$NaClO_2$, H_2NSO_3H, CH_2Cl_2, Acetone, H_2O; c) $(COCl)_2$, cat. DMF, CH_2Cl_2; d) *p*-nitrobenzyl alcohol, DIEA, CH_2Cl_2; e) Cl_2CHOCH_3, $TiCl_4$ (excess), CH_2Cl_2, -10°C; f) Cl_2CHOCH_3, $SnCl_4$, CH_2Cl_2, -10°C.

types of receptors (Scheme 3). In summary, we have developed an efficient route for stepwise functionalizations of calix[4]arene upper rim. It should be noted that functional groups other than carboxylate can also be incorporated into the synthetic scheme. A series of unsymmetrical

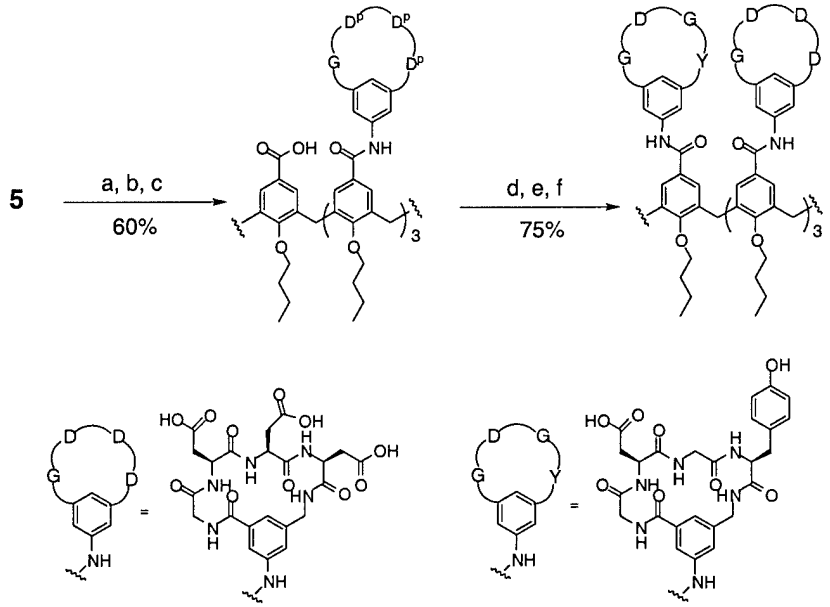

Scheme 2. a) $(COCl)_2$, cat. DMF, CH_2Cl_2; b) cyclo-(Gly-Asp(O^{t}Bu)-Asp(O^{t}Bu)-Asp(O^{t}Bu)-Spc)-NH_2, DIEA, CH_2Cl_2; c) 10% Pd/C, H_2, MeOH; d) 2,4,6-trichlorobenzol chloride, TEA, THF; e) cyclo-(Gly-Asp(O^{t}Bu)-Gly-Tyr(O^{t}Bu)-Spc)-NH_2, DMAP, Benzene/CH_2Cl_2; f) 25% TFA/ CH_2Cl_2.

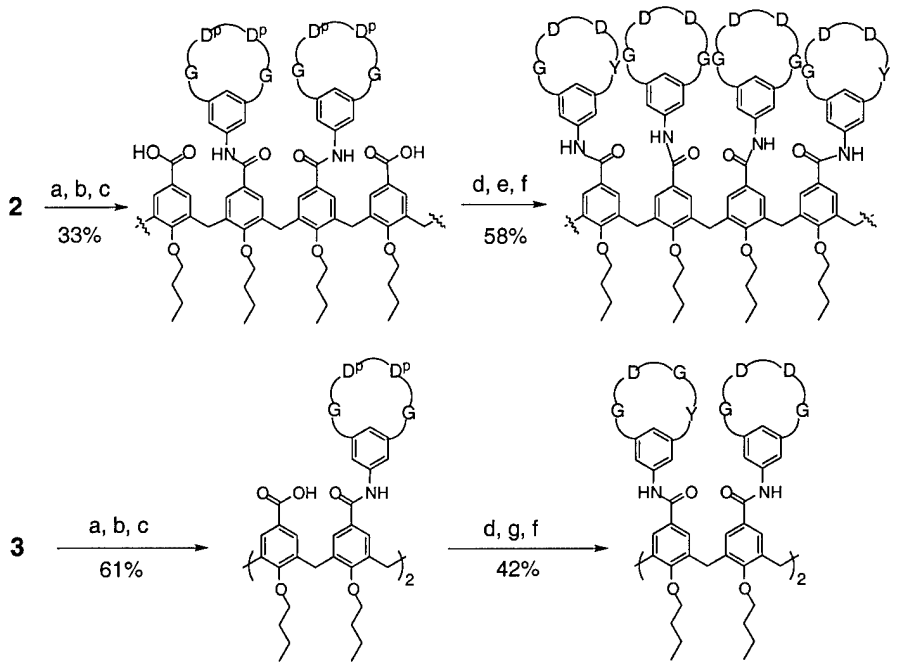

Scheme 3. a) $(COCl)_2$, cat. DMF, CH_2Cl_2; b) *cyclo*-(Gly-Asp(O^{t}Bu)-Asp(O^{t}Bu)-Gly-Spc)-NH_2, DIEA, CH_2Cl_2; c) 10% Pd/C, H_2, MeOH; d) 2,4,6-trichlorobenzol chloride, TEA, THF; e) *cyclo*-(Gly-Asp(O^{t}Bu)- Asp(O^{t}Bu)-Tyr(O^{t}Bu)-Spc)-NH_2, DMAP, Benzene/CH_2Cl_2; f) 25% TFA/CH_2Cl_2; g)) *cyclo*-(Gly-Asp(O^{t}Bu)-Gly-Tyr(O^{t}Bu)-Spc)-NH_2, DMAP, CH_2Cl_2.

Table 1 Unsymmetrical Receptors.

sequence	yield	molecular weight	
		expected($M+H^+$)	determined(ES-MS)
X-3(GDDD)-GDGY	45%	2945.82	2925.50 ± 0.55
X-3(GDGY)-GDDG	45%	2867.88	2867.37 ± 0.46
X-3(GDGY)-GDDY	52%	2974.00	2973.75 ± 0.87
X-3(GDGY)-GDDD	51%	2925.91	2926.01 ± 0.31
X-3(GDGD)-GDGY	43%	2771.71	2771.22 ± 1.30
X-3(GDGD)-GDDD	57%	2778.98	2778.22
X-3(GDGD)-GDDY	54%	2829.75	2828.74 ± 0.45
trans-X-2(GDDG)-2(GDGY)	26%	2819.80	2818.79 ± 0.72
cis-X-2(GDDG)-2(GDDY)	19%	2935.88	2935.62 ± 0.07

receptors based on partially protected calix[4]arene tetra carboxylic acid was thus contructed. The biological testing of unsymmetrical receptors for various growth factor targets are underway. A paper outlining this strategy has recently been submitted to *Comptes Rendues*(Reportable outcomes #5).

Task 2. To develop combinatorial libraries of protein surface binding agents that can be targeted to a range of growth factor structures (months 12-24).

The work described under task 1 summerizes our progress towards parallel libraries based on unsymmetrically substituted calixarenes. In the search for an alternative synthetic route to receptor libraries, an obvious choice is a solution phase two-step mixture coupling method. In this method, n different cyclic peptides are put into the coupling solution. If we assume they have equal reactivities, we should anticipate a mixture library being generated that contains a large number of receptors whose percentage in the library should follow a statistical rule. If we look more closely at this mixture, we should find all six possible unsymmetric receptors (Figure 4) in addition to the four-fold symmetric ones, which are otherwise very difficult to prepare. However, at the same time, the *degeneracy* occurs as a result of the scaffold symmetry (Table 2). For example, we may have six different arrangements (six different compounds) for the ABCD-type receptor. Considering the degeneracy and the combinatorial rule, a theoretical calculation of the size of a receptor library is shown in Table 2, and exemplified in Table 3. For example, a library of 1,044 receptors can be generated by mixing only 8 different cyclic peptides with the activated calixarene scaffold.

To identify the effective protein surface receptors from the mixture libraries, a simple detection method is needed. Mass spectrometry has proved itself highly suitable for such applications for its sensitivity, speed of analysis, and automation capability with solution phase techniques such as HPLC and CE. The success of a quantitative mass monitoring will critically depend on that the individual mass peaks of library compounds being distinguishable, and having similar physical properties such as laser desorption abilities. To test the viability of the MALDI-TOF method in our library monitoring process, a library was generated by coupling four cyclic peptides: *cyclo*-GDGDSp, *cyclo*-GDNDSp, *cyclo*-aDGDSp, *cyclo*-GDDYSp, and one equivalent of H_2O with the scaffold. The above cyclic peptides were selected from a pool of cyclic peptides with the aid of a computer program (MASP) such that the resulting library mixture does not have overlapped peaks in the mass spectrum.

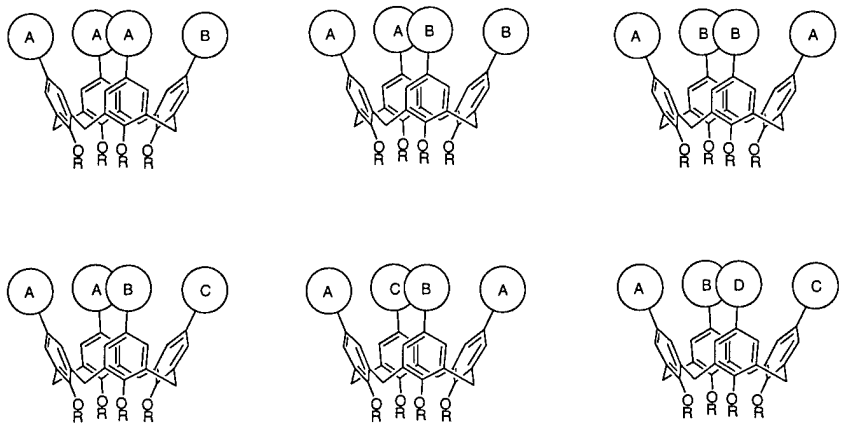

Figure 4 Six types of unsymmetrical receptors in mixture libraries.

Table 2 Calculated number of receptors produced with *n* cyclic peptides.[a]

Combination type	Degeneracy	Combinatorial rule	Combinations
AAAA	1	n	n
AAAB	1	n (n-1)	n (n-1)
AABB	2	n (n-1) / 2	n (n-1)
AABC	3	n (n-1) (n-2) / 2	3n (n-1) (n-2) / 2
ABCD	6	n (n-1) (n-2) (n-3) / 4!	n (n-1) (n-2) (n-3) / 4

[a]The total number of compounds equals the sum of the number of compounds of all five combination types.

Table 3 Examples of library sizes for *n* cyclic peptides.

Combination type	n = 4	n = 6	n = 8	n = 10	n = 20
AAAA	4	6	8	10	20
AAAB	12	30	56	90	380
AABB	12	30	56	90	380
AABC	36	180	504	1,080	10,260
ABCD	6	90	420	1,260	29,070
Total	70	336	1,044	2,530	40,110

Calculation of the expected mass distribution shows that a 170-membered multi-loop library can be generated with four cyclic peptides and one equivalent of water. Specifically, 26 bis-loop receptors, 74 tris-loop receptors, and 70 tetra-loop receptors are in the library (Figure 5A). Indeed, the MALDI-TOF mass spectrum for this library (Figure 5B) showed an exact distribution of multi-loop receptors as well as peak intensity as predicted by calculation, indicating the similar reactivities of the cyclic peptide amines.

These results provide good support for the strategy of solution generation of libraries. We are currenly investigating mass spectrometric methods that allow us to selectively detect which members of the library are binding to protein targets.

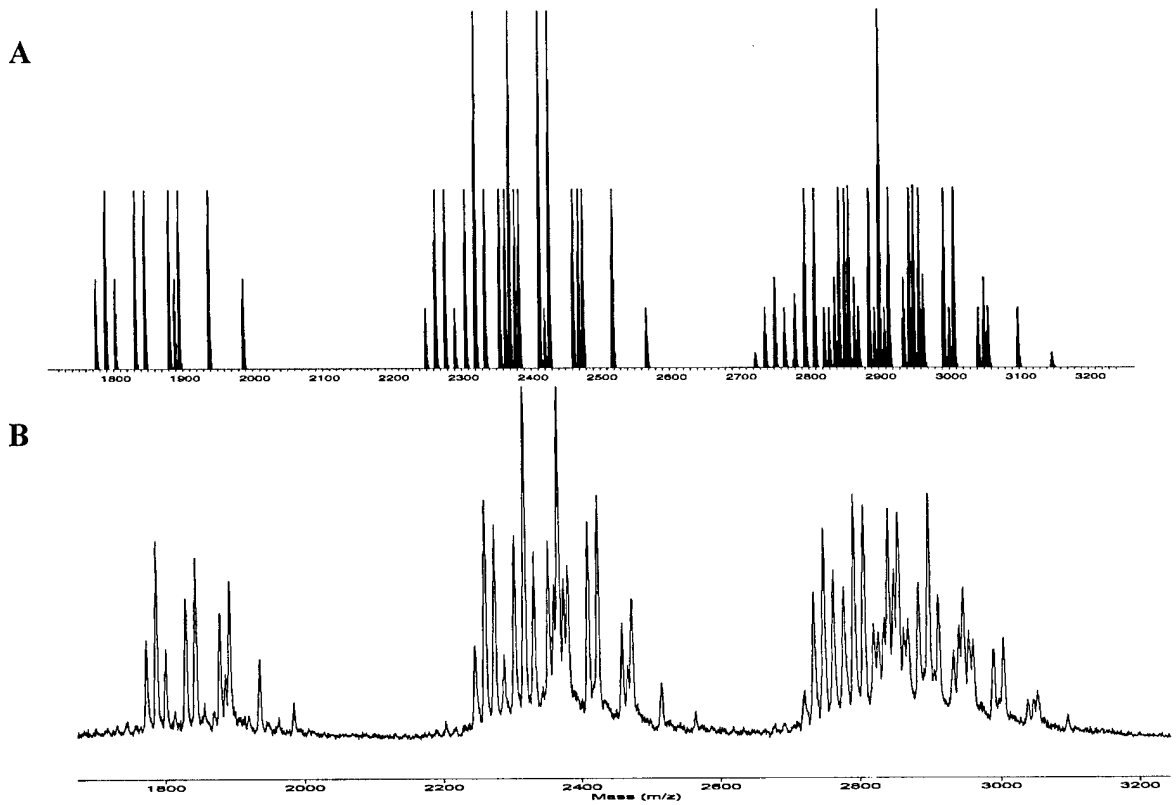

Figure 5. MALDI-TOF mass spectra of a mixture library: (A) the predicted mass spectrum using a computer program MASP; (B) the observed mass spectrum.

These results provide good support for the strategy of solution generation of libraries. We are currenly investigating mass spectrometric methods that allow us to selectively detect which members of the library are binding to protein targets.

Task 3. To develop synthetic antagonists for PDGF activation of its receptor tyrosine kinase that are active both in purified protein and in whole cell assays (months 1-18).

We have made excellent progress in the completion of task 3. We have prepared a large number of cyclic peptide derivatives based on the 3-aminomethylbenzoic acid scaffold and attached them to the core calixarene scaffold. These have been tested for their ability to interact with platelet derived growth factor using fluorescence spectroscopy, non-denaturing gel electrophoresis and protein binding assays. We have further shown that one key molecule can disrupt the growth of PDGF activated human tumor cell growth in a nude mouse model. This work has been published in *Nature Biotechnology* (**Ref. 2**, Reportable Outcomes) and in *Oncogene* (**Ref. 3**, Reportable Outcomes) and copies of the papers are appended.

Task 4. To target other growth factors involved in aberrant breast cell proliferation pathways, including VEGF, EGF and heregulin (months 18-36).

During the past year we have made excellent progress towards the primary goals outlined in Task 4. We have prepared a series of molecules based around a tetraphenylporphyrin scaffold (Figure 6). This structure has the attraction of providing a large (~300Å^2) hydrophobic surface that can be readily functionalized with a polar substituents on the four meso positions.

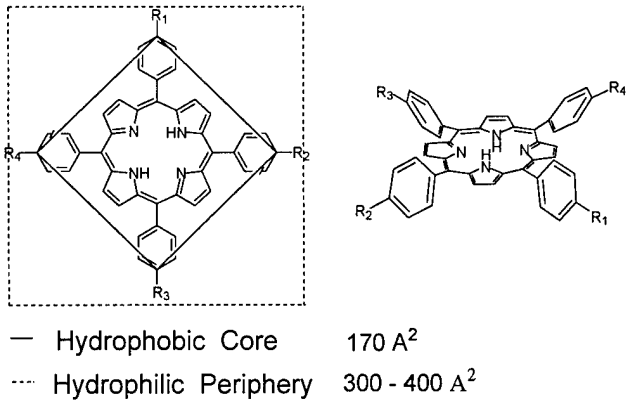

Figure 6. Tetraphenyl porphyrin scaffold for forming growth factor binding agents.

Figure 7.

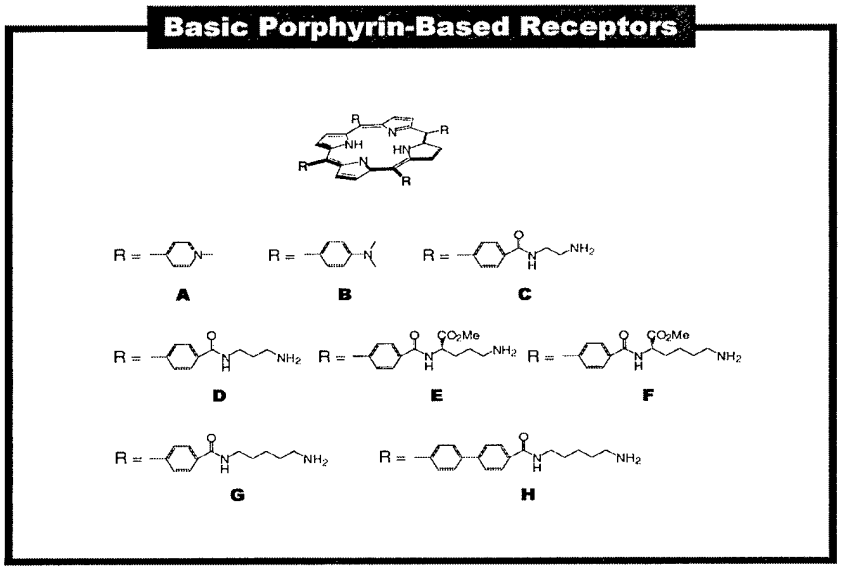

An example of a small library based on cationic substituents around the porphyrin is shown in Figure 7. These molecules were prepared by reacting different amine derivatives with the tetra acid chloride of tetracarboxytetraphenyl porphyrin. We have targeted this library to epidermal growth factor (Figure 8) which contains on its exterior surface a number of hydrophobic and anionic residues that could be complementary to the correctly configured cationic porphyrin shown in Figure 7.

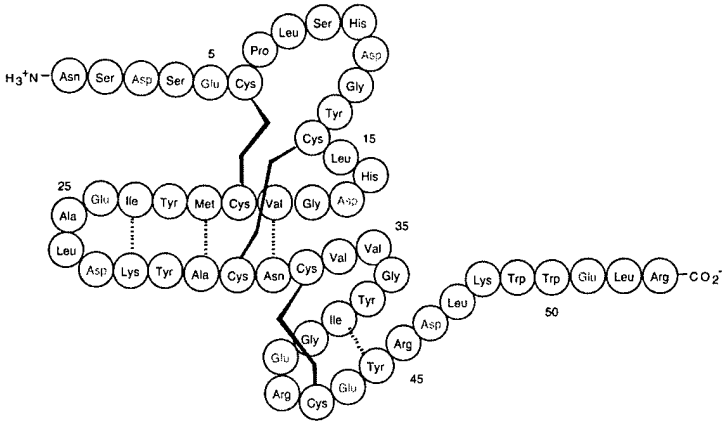

Figure 8. Structure of epidermal growth factor

An initial screen of EGF binding was established using an ELISA assay in which the growth factor was laid down on the solid surface and different porphyrins were assessed for their ability to block its interaction with an antiEGF antibody. The presence or absence of antiEGF antibody binding was assessed using a secondary antibody linked to horseradish peroxidase. Figure 9 shows the results obtained with the porphyrin library shown in Figure 7 at three different concentrations, 200, 100 and 20 nM. These results clearly point to an

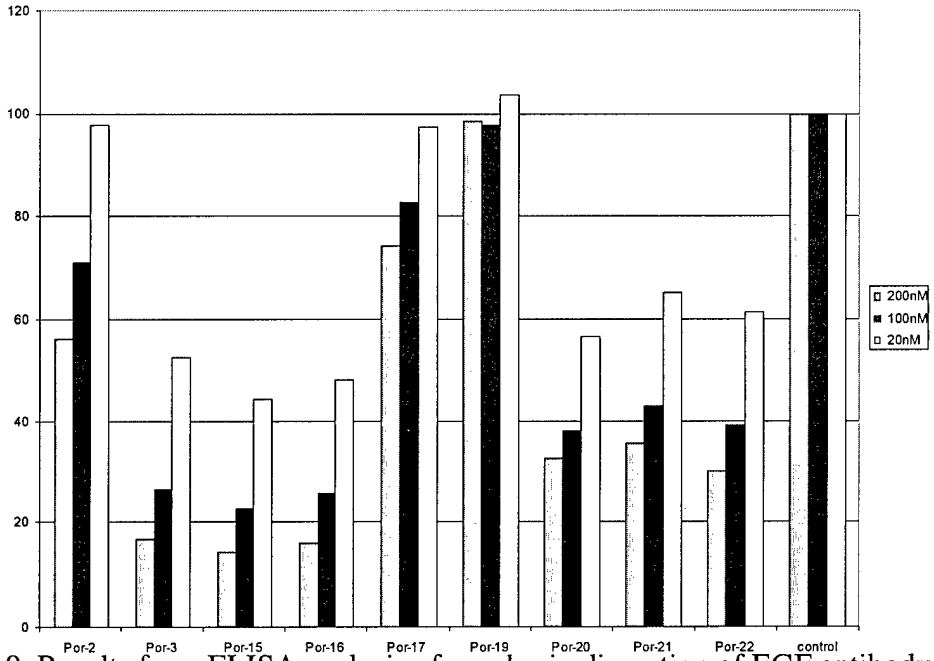

Figure 9. Results from ELISA analysis of porphyrin disruption of EGF antibody binding.

effective disruption of the protein-protein interactions by compound #15 and 16, corresponding to compounds G and F in Figure 7. The strong binding of F was confirmed by following changes in the fluorescence emission of Trp residues in EGF that are influenced by the porphyrin. The fluorescence titration gave a binding isotherm from which a Kd of 58nM was measured. The 1:1 stoichiometry of the interaction was further confirmed by non-denaturing gel electrophoresis (Figure 10) which showed a clear gel shift on addition of porphyrin F to EGF

Figure 10

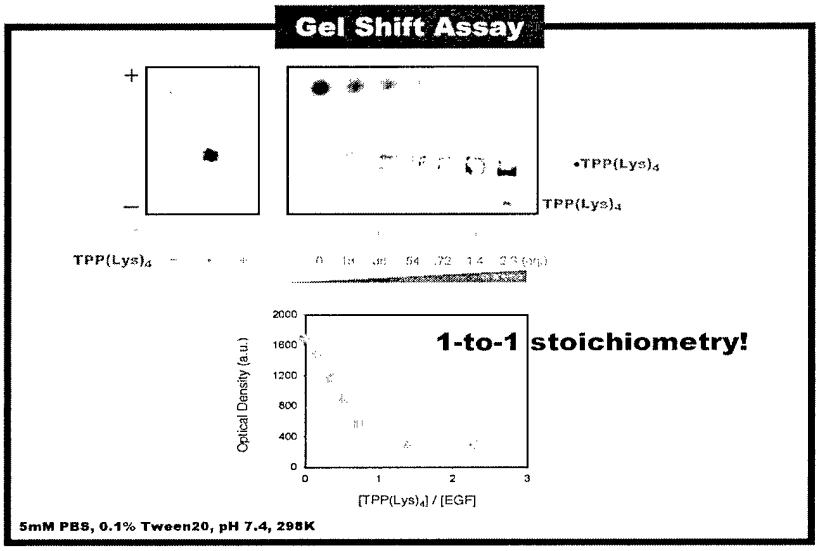

that reaches saturation at one equivalent. An important feature of this study is that the effect of EGF binding is structure specific. Only those derivatives that have a distance between the porphyrin center and the terminal ammonium group of 10-12Å are effective (Figure 11A). This

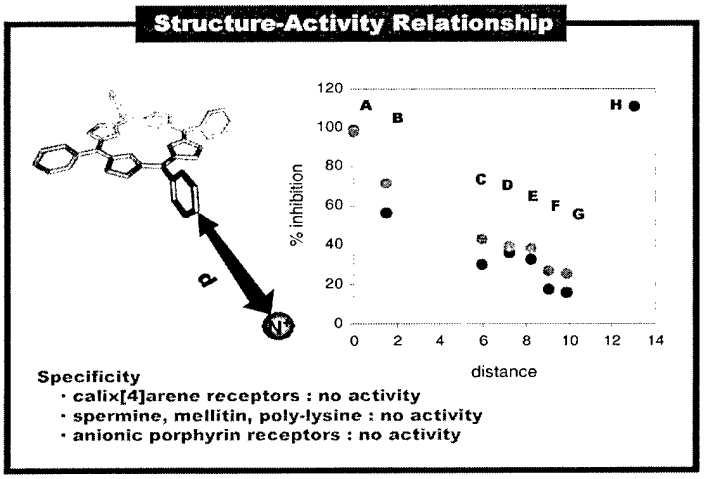

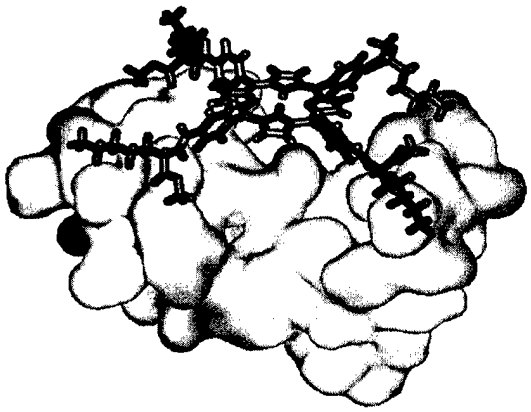

A B

Figure 11A. SAR for porphyrin binding to EGF. Figure 11B. Postulated EGF-porphyrin complex.

is consistent with a structure for the complex in which the porphyrin makes contact with a hydrophobic patch and the positively charged substituents stretch to make contact with carboxylate groups on the protein surface (Figure 11B).

Key Research Accomplishments

- Developed stepwise synthetic routes to unsymmetrical calixarene derivatives containing different peptide loop recognition domains.
- Designed, synthesized and evaluated a novel series of protein surface receptors based on a tetraphenylporphyrin scaffold and showed that certain compounds can bind with high affinity to cytochrome c.
- Developed parallel and solution phase methods for the preparation of combinatorial libraries of protein surface binding agents. Established a mass spectrometric approach to determine the diversity of the solution based libraries.
- Showed that one calixarene tetraloop derivative is able to bind to platelet derived growth factor and inhibit it from binding and activating its receptor tyrosine kinase. This compound was also shown to have potent anti-tumor activity in a nude mouse xenograft model.
- Identified strong EGF binding molecules from a small library of cationic porphyrin derivatives

Reportable Outcomes

1) Jain, R.; Hamilton, A. D. "Protein Surface Recognition by Synthetic Receptors Based on a Tetraphenylporphyrin Scaffold", *Organic Letters*, **2000**, 1721-1723.

2) Blaskovich, M. A.; Lin, Q.; Delarue, F. L.; Sun, J.; Park, H. S.; Coppola, D.; Hamilton, A. D.; Sebti, S. M. "Design of GFB-111 a Platelet-derived Growth Factor Binding Molecule with Anti-angiogenic and Anti-cancer Activity Against Human Tumors in Mice" *Nature Biotechnology*, **2000**, *18*, 1065-1070.

3) Sebti, S. M.; Hamilton, A. D. "Design of Growth Factor Antagonists with Antiangiogenic and Antitumor Properties" *Oncogene*, **2000**, *19*, 6566-6573.

4) Wei, Y.; McLendon, G. L.; Hamilton, A. D.; Case, M. A.; Purring, C. B.; Lin, Q.; Hyung Soon Park, Chang-Sun Lee, Tianning Yu"Disruption of Protein-Protein Interactions: Design of A Synthetic Receptor that Blocks the Binding of Cytochrome c to Cytochrome c Peroxidase". *J. Chem. Soc. Chem. Commun*, **2001**, 1580-1581.

5) Lin, Q.; Hamilton, A. D. "Design and Synthesis of Multiple-Loop Receptors Based on a Calix[4]arene Scaffold for Protein Surface Recognition", *Comptes Rendues*, Submitted.

Conclusions

During this project we have establishing the concept that synthetic agents can be used to bind to growth factor surfaces and to block their oncogenic function in activating tumor cell growth. We have significantly advanced our synthetic work on the design of agents for the complexation of protein exterior surfaces. We have extended our design strategy with the synthesis of unsymmetrical calixarene derivatives with different peptide loops arrayed around the upper rim. We have also developed parallel and solution phase approaches to libraries of protein surface binding agents. These methods should allow us to rapidly screen for strong binding agents against a range of protein targets. We have identified one molecule that not only binds to the surface of platelet derived growth factor with high affinity (IC50 < 250nM) under physiological conditions but also blocks its activation of PDGF receptor tyrosine kinase. This molecule also shows potent antitumor activity in a mouse xenograft model of a human cancer that is activated by PDGF. We have also synthesized a library of porphyrin derivatives that contain a hydrophobic core and a periphery of modifiable, hydrophilic substituents. From this library we have isolated different derivatives that bind to cytochrome c or to epidermal growth factor. The compounds identified in this project have the potential to be the first in a new class of rationally designed antitumor agents that function similarly to new antibody based therapies in blocking growth factor function but that are based around relatively low molecular weight synthetic derivatives.

References

1. For reviews, see: (a) Gutsche, C.D. Calixarenes Revisited. In Monographs in Supramolecular Chemistry; Stoddart, J.F., Ed.; Royal Society of Chemistry, London, **1998**. (b) Bohmer, V. *Angew. Chem. Int. Ed. Engl.* **1995**, *34*, 713-745.

2. For a few examples, see: (a) Pinkhassik, E.; Stibor, I.; Casnati, A.; Ungaro, R. *J. Org. Chem.* **1997**, *62*, 8654-8659. (b) Kanamathareddy, S.; Gutsche, C.D. *J. Am. Chem. Soc.* **1998**, *120*, 12226-12231. (c) Timmerman P.; Verboon, W.; Reinhoudt, D.N.; Arduini, A.; Grandi, S.; Sicui,

A.R.; Pochini, A.; Ungaro, R. *Synthesis* **1994**, 185. (d) Arduini, A.; McGregor, W.M.; Pochini, A.; Secchi, A.; Ugozzoli, F.; Ungaro, R. *J. Org. Chem.* **1996**, *61*, 6881-6887. (e) Arduini, A.; mirone, L.; Paganuzzi, D.; Pinalli, A.; Pochini, A.; Secchi, A.; Ungaro, R. *Tetrahedron*, **1996**, *52*, 6011-6018.

3. Arduini, A.; Fanni, S.; Manfredi, G.; Pochini, A.; Ungaro, R.; Sicuri, A.R.; Ugozzoli, F. *J. Org. Chem.* **1995**, *60*, 1448-1453.

4. For synthesis of cyclic peptides, see: Lin, Q.; Park, H.S.; Hamuro, Y.; Lee, C.S.; Hamilton, A.D. *Biopolymers (Peptide Science)* **1998**, *47*, 285-297.

5. Inanaga, J.; Hirata, K.; Saeki, H.; Katsuki, T.; Yamaguchi, M. *Bull. Chem. Soc. Jpn.* **1979**, *52*, 1989-1993.

Protein Surface Recognition by Synthetic Receptors Based on a Tetraphenylporphyrin Scaffold

Rishi K. Jain and Andrew D. Hamilton

Department of Chemistry, P.O. Box 208107, 225 Prospect Street, Yale University, New Haven, Connecticut 06520-8107

Organic LETTERS

Reprinted from
Volume 2, Number 12, Pages 1721–1723

ORGANIC LETTERS

2000
Vol. 2, No. 12
1721–1723

Protein Surface Recognition by Synthetic Receptors Based on a Tetraphenylporphyrin Scaffold

Rishi K. Jain and Andrew D. Hamilton*

Department of Chemistry, P.O. Box 208107, 225 Prospect Street, Yale University, New Haven, Connecticut 06520-8107

andrew.hamilton@yale.edu

Received March 29, 2000

ABSTRACT

Receptors based on a tetraphenylporphyrin scaffold bearing different charged and hydrophobic groups have been synthesized. The interactions of these with horse heart cytochrome *c* were studied by fluorescence spectroscopy. Receptor 4 was identified to be the strongest synthetic receptor (K_d = 20 nM) for cytochrome *c*. The differences in affinity among the receptors reflected a dependence on the number of anionic and hydrophobic groups.

The past two decades have seen enormous progress in the design of synthetic molecules targeted to disrupt protein–ligand interactions.[1] The majority of these medicinally important molecules disrupt interactions occurring inside well-defined cavities on the proteins. In contrast, synthetic molecules that mediate protein function through binding to the solvent-exposed *exterior surface* are largely unexplored.[2] This is surprising since such molecules may provide a fundamentally different mechanism for modulating protein function, by sterically preventing protein–ligand and protein–protein interactions. This strategy may not only result in the discovery of novel drug candidates but may also provide opportunities to systematically understand the role of protein exterior surfaces in molecular recognition.

Recently, we have reported a novel family of synthetic receptors that target protein exteriors.[3] The initial design, involving four peptide loops arrayed around a central calix[4]arene core, was shown to inhibit the approach of small molecule substrates to cytochrome *c* and chymotrypsin at submicromolar concentrations. However, the calixarene unit suffers several complications, including difficulty of synthesis and tendency to aggregation. We sought to improve this synthetic approach by studying different organic scaffolds onto which recognition sites can be attached. Porphyrins, owing to their large size, rigidity, and photophysical properties, have been used in numerous artificial receptors and model systems in bioorganic and bioinorganic chemistry.[4] In this Letter, we report on the design, synthesis, and recognition properties of a series of tetraphenylporphyrins that bind, in certain cases with high affinity, to the surface of cytochrome *c*.

(1) Babine, R. E.; Bender, S. L. *Chem. Rev.* **1997**, *97*, 1359–1472.

(2) (a) Cushman, M.; Kanamathareddy, S.; De Clerq, E.; Schols, D.; Goldman, M. E.; Bowen, J. A. *J. Med. Chem.* **1991**, *34*, 337–342. (b) Regan, J.; McGarry, D.; Bruno, J.; Green D.; Newman, J.; Hsu, C. Y.; Kline, J.; Barton, J.; Travis, J.; Choi, Y. M.; Volz, F.; Pauls, H.; Harrison, R.; Zilberstein, A.; Ben-Sasson, S. A.; Chang, M. *J. Med. Chem.* **1997**, *40*, 3408–3422.

(3) (a) Hamuro, Y.; Calama, M. C.; Park, H. S.; Hamilton, A. D. *Angew. Chem., Int. Ed. Engl.* **1997**, *36*, 2680–2683. (b) Park, H. S.; Lin, Q.; Hamilton, A. D. *J. Am. Chem. Soc.* **1999**, *121*, 8–13. (c) Lin, Q.; Park, H. S.; Hamuro, Y.; Lee, C. S.; Hamilton, A. D. *Biopolymers* **1998**,*47*, 285–297.

(4) Ogoshi, H.; Mizutani, T. *Curr. Opin. Chem. Biol.* **1999**, *3*, 736–739.

10.1021/ol005871s CCC: $19.00
Published on Web 05/23/2000

Cytochrome *c* is a particularly attractive target since it plays key roles in electron transfer and apoptosis, which are mediated by complex formation to other proteins (cytochrome *c* oxidase, Apaf1, etc.). One critical recognition region involves an array of lysine and arginine residues surrounding the exposed heme edge surface.[5] The tetraphenylporphyrin scaffold closely matches the arrangement of hydrophobic and charged domains present in this region (Figure 1). In pioneering work, Fisher recognized this

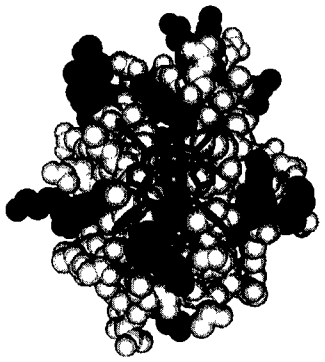

Figure 1. A space filling representation of horse heart cytochrome *c* based on its X-ray crystal structure.[7] The heme group which directly faces the reader is drawn in gray spheres. Black spheres represent positively charged lysine and arginine residues. White spheres correspond to all other residues. A tetraphenylporphyrin scaffold (black cylindrical bonds) is drawn in the center.

geometrical relationship and showed that tetracarboxyphenyl porphyrin **1** binds to cytochrome *c* with a K_d of ~5 μM.[6]

To determine the optimum combination of recognition features in synthetic receptors of this type, we designed a series of tetraphenylporphyrins with various amino acid derivatives attached. The resulting receptors contain a large, flat, and semirigid molecular surface of approximately 300–400 Å^2 in area. The receptors were prepared by the generation of the tetra-acid chloride ($(COCl)_2$, DMF) starting from *m*-tetrakis(4-carboxyphenyl) porphyrin **1** and subsequent coupling with the corresponding *tert*-butyl-protected amino acid or peptide amines. Deprotection of the *tert*-butyl groups with trifluoroacetic acid provided receptors **2**–**4**. Acidic and hydrophobic attachments were chosen to complement the cationic and hydrophobic surface surrounding the heme edge of cytochrome *c*.

Compounds **1**–**4**, and coproporphyrin I, a naturally occurring tetraanionic porphyrin, were initially screened for binding to horse heart ferricytochrome *c* using fluorescence spectroscopy. Addition of cytochrome *c* to solutions containing **1**–**4** resulted in quenching of porphyrin fluorescence emission (ex = 420 nm, em = 650 nm) due to the enforced proximity of the Fe(III) heme that results from complex formation between the protein and the receptors.

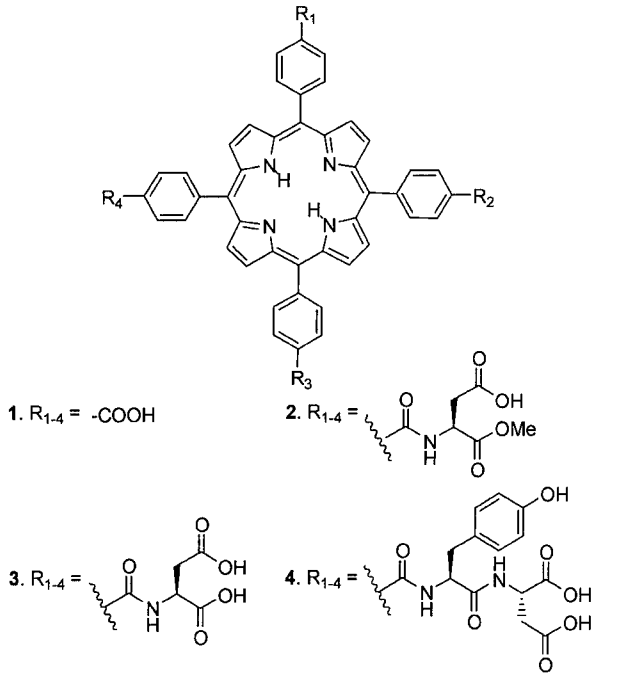

In contrast, titrations with tetracationic *m*-tetrakis(4-trimethylaminophenyl) porphyrin (TTMAPP), showed no quenching even at high concentrations, indicating the absence of nonspecific binding. Typical titrations of **3**, **4**, and TTMAPP with cytochrome *c* are shown in Figure 2 (see Supporting Information for others).

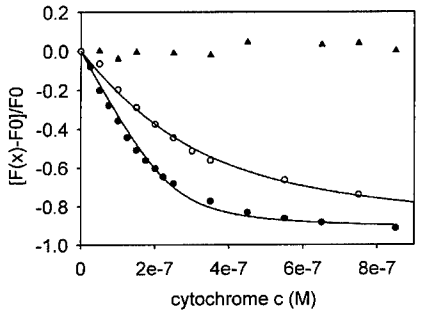

Figure 2. Fluorescence quenching of **4** (●), **3** (○), and TTMAPP (▲) upon addition of cytochrome *c*. The curve fit indicates a K_d of 20 ±5 nM for **4** and 160 ±20 nM for **3**. Titrations were carried out under 250 nM initial receptor concentration in 5 mM sodium phosphate buffer, pH = 7.4, at 298 K.

Dissociation constants were derived by curve fitting to a 1:1 binding equation[8] with stoichiometries being fixed at $n = 1$ for all compounds. Preference for 1:1 binding was confirmed for receptors **3** and **4** by Job's method[9] (see Supporting Information). K_d values for all compounds are summarized in Table 1.

(5) Scott, R. A.; Mauk, A. G. *Cytochrome c:a Multidisciplinary Approach*; University Science Books: Sausalito, 1996.

(6) Clark-Ferris, K. K.; Fisher, J. *J. Am. Chem. Soc.* **1985**, *107*, 5007–5008.

(7) Bushnell, G. W.; Louie, G. V.; Brayer, G. D. *J. Mol. Biol.* **1990**, *214*, 585–595.

(8) Wilcox, C. S. In *Frontiers in Supramolecular Organic Chemistry and Photochemistry*; Schneider, H. J., Dürr, H., Eds.; VCH: Weinheim, 1990; pp 123–143.

(9) Job, P. *Ann. Chim.* **1928**, *9*, 113–203.

Table 1. Dissociation Constants[a] and Structural Properties of Synthetic Receptors and Other Water-Soluble Porphyrins

compound	K_d (nM)	charge	aryl groups
1	950 ± 250	−4	4
2	860 ± 90	−4	4
3	160 ± 20	−8	4
4	20 ± 5	−8	8
coproporphyrin I	7700 ± 270	−4	0
uroporphyrin I	1000[b]	−8	0

[a] Determined at 5 mM sodium phosphate, pH 7.4, 298 K. [b] From ref 10, at m = 4 mM sodium phosphate, pH 7.26, 298 K.

Significant changes in affinity for cytochrome *c* were observed by altering the relative proportions of acidic and aromatic functionalities in the receptors (Table 1). Receptors **2** and **3** differ only by the substitution of four methyl esters by carboxylic acids, respectively, providing controls for probing the charge requirements for cytochrome *c* recognition. A ~5-fold increase in affinity was seen, on going from receptor **2** to receptor **3**, indicating a preference for octaanionic receptors over their tetraanionic counterparts. Receptors **1** and **2**, with the same number and type of charged groups, show little difference in their binding affinities. Similar trends were observed when aromatic groups were incorporated into the receptor while keeping the number of charged groups constant. Rodgers had earlier shown that uroporphyrin I, containing eight carboxylate groups, binds cytochrome *c* with μM affinity.[10] However, receptor **3** which has eight anionic groups and 4 phenyl groups binds to cytochrome *c* approximately 6-fold stronger than uroporphyrin. In a similar analysis, receptor **2** binds cytochrome *c* 9-fold tighter than tetraanionic coproporphyrin I. These results suggested that an appropriate combination of charged and hydrophobic groups on the porphyrin periphery would give a molecule with exceptionally high affinity for cytochrome *c*. To confirm this, we designed receptor **4** to contain eight negatively charged groups and eight phenyl groups. The titration curve (Figure 1) shows a sharper achievement of saturation with **4** compared to **3**. This corresponds to a K_d of 20 ±5 nM for **4** binding to cytochrome *c* and represents an 8-fold increase in affinity compared to **3** (Table 1).To our knowledge, **4** is one of the strongest synthetic receptors for cytochrome *c*, under these experimental conditions. The binding experiments between **4** and cytochrome *c* were carried out in 5 mM phosphate buffer at pH 7.4. Remarkably, receptor **4** with a molecular weight of ~1900 Da can bind to cytochrome *c* 100 fold stronger than its natural protein partners such as cytochrome *c* peroxidase, which has a K_d of 2.4 μM measured at 5 mM phosphate buffer, pH = 7.[11] The combination of many electrostatic and hydrophobic interactions over a large contact surface is primarily responsible for the formation of high-affinity protein−protein complexes in nature.[12] The synthetic receptors reported here behave similarly, attaining large enhancements in affinity through the incorporation of both anionic and aromatic groups. The tetraphenylporphyrin scaffold appears to provide a template in which the peripheral anionic and aromatic groups take up a good geometrical relationship to the cationic and hydrophobic side chains of cytochrome *c*. On the basis of these findings, it should be possible to extend this approach to identify new receptors for protein targets that are known to interact with simple porphyrin derivatives.[13]

In summary, we have designed and synthesized synthetic receptors that recognize a protein surface with high affinity in aqueous medium. Analogues of receptor **4** with less symmetrical substitution patterns may provide a clearer understanding of the detailed recognition properties of the cytochrome *c* protein surface. In addition to providing a new strategy for protein surface recognition, these findings may have important medicinal consequences. Cytochrome *c* has been shown to interact with Apaf1, leading to the activation of programmed cell death or apoptosis.[14] Receptor **4** may serve as a valuable lead in the search for efficient disruptors of Apaf1−cytochrome *c* interaction.

Acknowledgment. This work was supported by the National Institute of Health (GM35208) and the U.S. Army (DAMD17-99-1-9458).

Supporting Information Available: Experimental procedure and characterization for compounds **2**−**4**. Fluorescence titration plots for **1**−**2** and coproporphyrin I and Job's plots for **3** and **4**. This material is available free of charge via the Internet at http://pubs.acs.org.

OL005871S

(10) Zhou, J. S.; Granada, E. S. V.; Leontis, N. B.; Rodgers, M. A. J. *J. Am. Chem. Soc.* **1990**, *112*, 5074−5080.

(11) Nicholls, P.; Mochan, E. *Biochem. J.* **1971**, *121*, 55−67.

(12) Stites, W. E. *Chem. Rev.* **1997**, *97*, 1233−1250.

(13) (a) Priola, S. A.; Raines, A.; Caughey, W. S. *Science* **2000**, *287*, 1503−1506. (b) Debnath, A. K.; Jiang, S.; Strick, N.; Lin, K.; Haberfield, P.; Neurath, A. R. *J. Med. Chem.* **1994**, *37*, 1099−1108.

(14) Green, D.; Reed, J. *Science* **1998**, *281*, 1309−1312.

Design of GFB-111, a platelet-derived growth factor binding molecule with antiangiogenic and anticancer activity against human tumors in mice

Michelle A. Blaskovich[1], Qing Lin[2], Frederic L. Delarue[1], Jiazhi Sun[1], Hyung Soon Park[2], Domenico Coppola[1], Andrew D. Hamilton[1] * and Saïd M. Sebti[1] *

[1]Drug Discovery Program, H. Lee Moffitt Cancer Center and Research Institute, Departments of Biochemistry and Molecular Biology and of Pathology, University of South Florida, Tampa, FL 33612, and [2]Department of Chemistry, Yale University, New Haven, CT 06511.
**Coresponding authors (sebti@moffitt.usf.edu and ahamilton@ursula@chem.yale.edu).*

Received 9 March 2000; accepted 31 July 2000

We have designed a molecule, GFB-111, that binds to platelet-derived growth factor (PDGF), prevents it from binding to its receptor tyrosine kinase, and blocks PDGF-induced receptor autophosphorylation, activation of Erk1 and Erk2 kinases, and DNA synthesis. GFB-111 is highly potent (IC_{50} = 250 nM) and selective for PDGF over EGF, IGF-1, aFGF, bFGF, and HRGβ (IC_{50} values > 100 μM), but inhibits VEGF-induced Flk-1 tyrosine phosphorylation and Erk1/Erk2 activation with an IC_{50} of 10 μM. GFB-111 treatment of nude mice bearing human tumors resulted in significant inhibition of tumor growth and angiogenesis. The results demonstrate the feasibility of designing novel growth factor–binding molecules with potent anticancer and antiangiogenic activity.

Keywords: platelet-derived growth factor, angiogenesis, oncogenesis, cancer drug discovery

Platelet-derived growth factor (PDGF) is a potent inducer of growth and motility in several cell types such as fibroblasts, endothelial cells, and smooth muscle cells. It induces cell proliferation, angiogenesis, wound healing, and chemotaxis, and inhibits apoptosis[1-3]. Additionally, PDGF has been directly implicated in malignant diseases involving uncontrolled cell proliferation such as cancer, where overexpression of PDGF and/or PDGF receptors is common in human tumors including glioblastomas and sarcomas[2]. Also, PDGF stimulates the proliferation and migration of endothelial cells leading to formation of new blood vessels, a process that is required for the growth of tumors[4-7]. Furthermore, PDGF has also been shown to stimulate endothelial cells to express high levels of vascular endothelial growth factor (VEGF), a potent angiogenesis inducer[7,8]. Finally, the importance of PDGF in angiogenesis has also been documented by the fact that mice deficient in PDGF-BB or its receptor β are defective in blood vessel development[9,10].

To elicit the above biological response, PDGF binds to its cell surface receptor, PDGFR, a tyrosine kinase[1,11-13]. Binding results in dimerization, receptor auto (cross) phosphorylation, and recruitment by means of the resulting phosphotyrosine of SH2 domain-containing signaling proteins such as Grb2/Sos1, PLC-γ, PI-3 kinase, and Src[11,12]. These proteins trigger several arms of the PDGF signal transduction pathways that are involved in different cellular responses. For example, Grb2/Sos1 activates the GTPase Ras, resulting in the activation of a cascade of mitogen-activated protein kinases (MAPK), such as Erk1 and Erk2, and this contributes to the proliferation arm of the PDGF signaling pathway[13]. Others, such as PI3 kinase, activate yet another kinase, AKT, which is responsible for the survival or the anti-apoptotic arm of PDGF signaling pathways[1].

The involvement of PDGF overactivity in proliferative diseases prompted many researchers to target PDGF as a therapeutic strategy[14-22]. The approaches used to interfere with aberrant PDGF function in disease include PDGFR antibodies that block PDGF binding[14], linear or cyclic peptides corresponding to areas of PDGF that bind its receptor[15,16], receptor dimerization antagonists[17], and inhibitors of the tyrosine kinase activity of the receptor[18,19]. An underexploited area in the search for antagonists of PDGF overactivity is that of rationally designed agents that bind to PDGF and inhibit it from activating its receptor. In this area only a few strategies such as antibodies against PDGF[20], soluble forms of PDGFR[21], and DNA aptamers[22] have been tried with marginal success. These are all based on biosynthetically derived compounds that are limited in structural building blocks to the four nucleosides or 20 amino acids. Synthetic derivatives that antagonize PDGF binding have the potential advantages of being stable to proteolytic or nuclease cleavage, having smaller molecular weights and utilizing a wider range of structural scaffolds that might complement the protein surface. To date there have been no examples of nonnatural systems that antagonize PDGFR activation by discrete binding to the growth factor surface. This is primarily due to the difficulty of designing agents to disrupt protein–protein interactions that are mediated over large surface binding areas. We have previously reported the synthesis of a protein-binding molecule that interacts with strongly cationic regions on chymotrypsin[23] and cytochrome *c*[24]. In the present paper we significantly expand this strategy with the synthesis of a library of binding agents from which we identify a molecule (GFB-111) that targets the regions of PDGF (loops I and III) that are involved in binding to its receptor. GFB-111 treatment of nude mice bearing human tumors resulted in significant inhibition of tumor growth and angiogenesis.

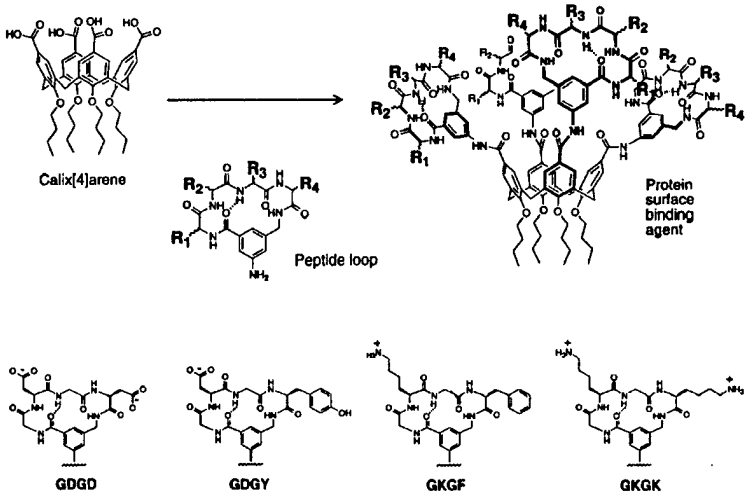

Figure 1. Structure of growth factor binders (GFBs). GFBs were synthesized as described[23,24].

Results

Design of GFB-111, a synthetic molecule that binds PDGF. To design molecules that bind PDGF and disrupt its signaling function, we have prepared a novel series of protein surface binding agents. The molecules are composed of a central calix[4]arene scaffold to which are attached four peptide loop domains (Fig. 1). The peptide loop component is based on a cyclic hexapeptide in which two residues were replaced by a 3-aminomethylbenzoate dipeptide mimetic containing a 5-amino substituent for attachment to the scaffold. The resulting molecules (Fig. 1 and Table 1) contain a functionalized and variable surface ~500 Å^2 in area. Several peptide loop sequences were synthesized (Table 1) to provide molecular surfaces with negatively and positively charged as well as hydrophobic regions designed to bind to complementary areas on the target growth factor. To identify PDGF-binding molecules from this library, we first used a cell-based screening assay with NIH 3T3 cells to detect molecules capable of blocking PDGF-BB-induced tyrosine autophosphorylation of the PDGFR. The ability of the identified molecules to bind PDGF-BB and inhibit interaction with its receptor was then confirmed biochemically. Starved NIH 3T3 cells were pretreated for 5 min with the synthetic molecules before stimulation with PDGF for 10 min. The effects of the molecules on PDGF-stimulated receptor tyrosine phosphorylation were determined by antiphosphotyrosine western blotting. Screening the library for potential PDGF binders identified GFB-111 as a potent (IC_{50} = 250 nM) inhibitor of PDGF-BB stimulation of PDGFR tyrosine autophosphorylation (Table 1). GFB-111 has four-fold symmetry, containing four identical peptide loops with negative and hydrophobic residues, GDGY, that are designed to be complementary to the PDGF surface involved in binding to PDGFR. The area of PDGF-BB that binds PDGFR is composed primarily of positive and hydrophobic residues[25,26]. Substitution of aspartic acid in the loop by positively charged lysine is not tolerated (compare GFB-111 (GDGY) (IC_{50} = 250 nM) to GFB-115 (GKGF) (IC_{50} = 50 μM) and GFB-116 (GKGK) (IC_{50} = 40 μM)), indicating that negatively charged residues are important for the inhibitory activity of GFB-111. However, negatively charged residues are not sufficient, and the presence of an aromatic hydrophobic residue in the loop is also critical (compare GFB-111(GDGY) to GFB-107 (GDGD) (IC_{50} = 2.5 μM), as well as GFB-122 (GDDY) (IC_{50} = 1.7 μM) to GFB-106 (GDDD) (IC_{50} = 8 μM)) (Table 1).

The structure/activity relationship results in Table 1 are consistent with GFB-111 being a PDGF-BB-binding molecule. To confirm this, we determined whether GFB-111 binds PDGF-BB by gel electrophoresis and also inhibits binding of ^{125}I-labeled PDGF (^{125}I-

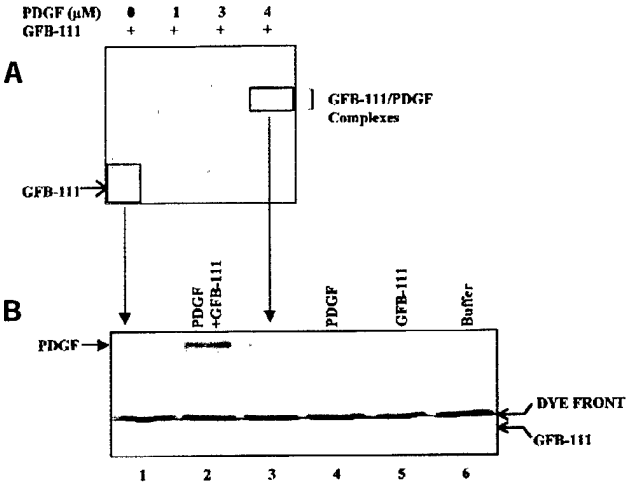

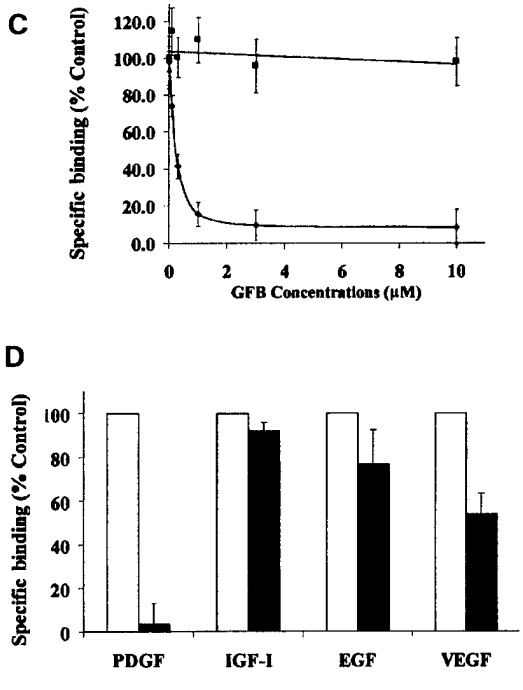

Figure 2. GFB-111 binds PDGF and inhibits ^{125}I-PDGF binding to its receptor on NIH 3T3 cells. (A) GFB-111 was incubated with increasing concentrations of PDGF-BB and the mixtures were then loaded onto native PAGE. Bands corresponding to the boxed area were cut out of the lanes of the gel, denatured, and loaded onto SDS-PAGE gel. (B) Lanes 1–6 correspond to GFB-111 from the native gel; PDGF + GFB-111 standards; GFB-111–PDGF complex from the native gel; PDGF standard; GFB-111 standard; and buffer, respectively. Data are representative of three independent experiments. (C, D) NIH 3T3 (PDGF) or NIH 3T3 cells overexpressing EGFR (EGF), IGFR (IGF), or Flk-1 (VEGF) were incubated with ^{125}I-PDGF, ^{125}I-EGF, ^{125}I-IGF, or ^{125}I-VEGF, respectively. (C) Specific ^{125}I-PDGF binding to NIH 3T3 cells with increasing concentrations of GFB-111 (◆) or GFB-116 (■) were used. (D) Specific binding with GFB-111 at 10 μM. Empty and filled bars represent control and GFB-111 treated samples, respectively. Cells were incubated at 4°C and washed. Lysates plus wash were counted. Excess of cold growth factors was used to obtain nonspecific binding levels. Data are representative of three independent experiments.

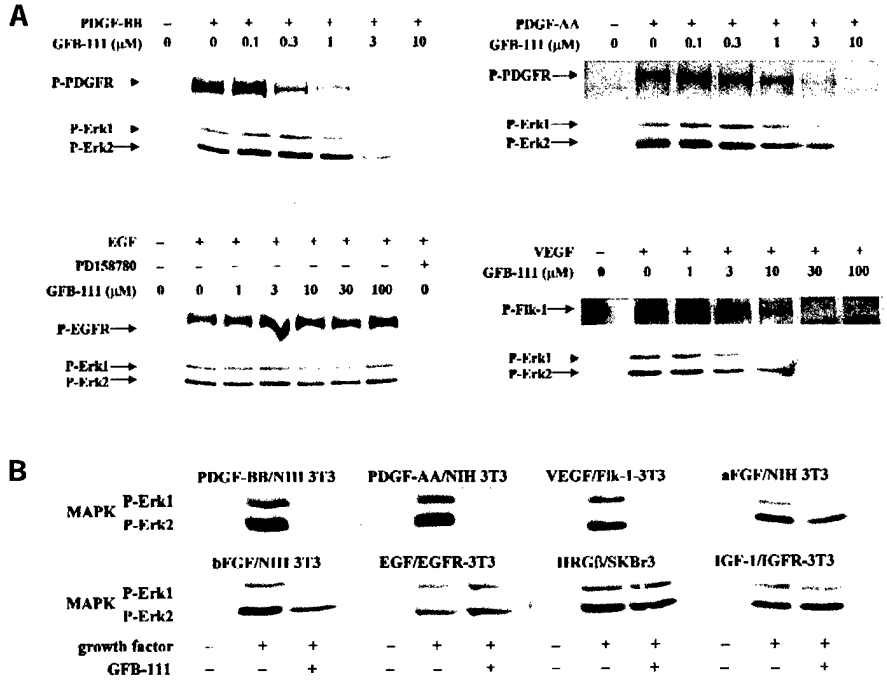

Figure 3. GFB-111 inhibits selectively PDGF-stimulated receptor tyrosine autophosphorylation and activation of MAPK. (A) Starved NIH 3T3 cells (PDGF-BB and PDGF-AA), and NIH 3T3 cells overexpressing either EGFR (EGF) or Flk-1 (VEGF) were pretreated with GFB-111 before stimulation with PDGF-BB, PDGF-AA, EGF, and VEGF. Cell lysates were run on SDS–PAGE gels, then transferred to nitrocellulose and western blotted with anti-phosphotyrosine or anti-phosphorylated Erk1/Erk2. (B) Starved NIH 3T3 cells (PDGF-AA, PDGF-BB, aFGF, bFGF), NIH 3T3 cells overexpressing EGFR, IGF-1R, or Flk-1, and the human breast carcinoma SkBr3 that overexpresses ErbB2 (HRGβ) were pretreated with GFB-111 (100 μM) for 5 min before 10 min stimulation with the indicated growth factors. Cell lysates were then immunoblotted with anti-phosphorylated Erk1/Erk2 as described for (A). Data are representative of three independent experiments.

PDGF) to its receptor on NIH 3T3 cells. Figure 2A shows that mixing GFB-111 with PDGF-BB resulted in a concentration-dependent disappearance of GFB-111 that was paralleled by the appearance of a slower migrating band on native polyacrylamide gel electrophoresis (PAGE). In this native PAGE system, PDGF-BB itself migrates toward the cathode and hence does not penetrate the gel. To demonstrate that the slower migrating band is formed by the complex between GFB-111 and PDGF-BB, the band was cut out of the native gel, processed and loaded onto denaturing SDS–PAGE gel. Figure 2B shows that the GFB-111 standard (lane 5), as well as the GFB-111 band cut out of the Figure 2A gel (lane 1), migrated on SDS–PAGE as a single band that eluted faster than the dye front. Mixing PDGF-BB standard (lane 4) and GFB-111 standard (lane 5) confirmed their separation on SDS–PAGE (lane 2). Most important is that the band cut out of the native gel presumed to contain the complex did indeed contain both PDGF-BB and GFB-111 (Fig. 2B, lane 3). The interaction was structure-dependent in that the positively charged derivative GFB-116 (Table 1) did not bind to PDGF-BB as demonstrated by gel electrophoresis (data not shown). Furthermore, GFB-111 did not bind to the related peptide growth factors epidermal growth factor (EGF) and insulin-like growth factor-1 (IGF-1), demonstrating that GFB-111 is selective for PDGF (data not shown).

GFB-111 blocks ^{125}I-PDGF binding. The complementarity of the recognition domain of GFB-111 (negatively charged and hydrophobic residues) with the receptor binding surface of PDGF (positively charged and hydrophobic sites) suggested that GFB-111 would block binding of PDGF to PDGFR. To support this, we determined whether GFB-111 can block ^{125}I-PDGF-BB specific binding in NIH 3T3 cells. Figure 2C shows that in the absence of GFB-111, NIH 3T3 cells bound ^{125}I-PDGF-BB. However, pretreatment with increasing concentrations

Table 1. Inhibition of PDGF-dependent receptor tyrosine phosphorylation by growth factor binders (GFBs)[a]

Compounds	Loop sequence	IC_{50} (μM)
GFB-105	GDFD	2.4
GFB-106	GDDD	8
GFB-107	GDGD	2.5
GFB-108	d-ADGD	9
GFB-109	GDLD	7.5
GFB-110	GDAD	1.7
GFB-111	GDGY	0.25
GFB-112	ADGD	29
GFB-113	GDSD	2.8
GFB-115	GKGF	50
GFB-116	GKGK	40
GFB-117	GDND	5.8
GFB-119	PDGD	20
GFB-120	GDDG	1.3
GFB-122	GDDY	1.7

[a]Starved NIH 3T3 cells were pretreated with the various GFBs for 5 min before stimulation with PDGF. The cells were then harvested and lysed, and the proteins from the lysates separated by SDS–PAGE and immunoblotted with an anti-phosphotyrosine antibody. The phosphotyrosine PDGF receptor bands were scanned and the concentrations of GFBs that inhibited the ability of PDGF to stimulate PDGFR tyrosine phosphorylation by 50% were determined. Data for each compound are representative of at least two independent experiments.

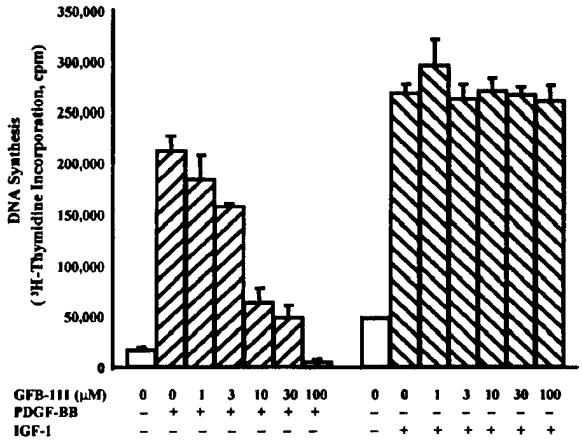

Figure 4. GFB-111 selectively inhibits PDGF-stimulated DNA synthesis. Starved NIH 3T3 or NIH 3T3 cells overexpressing IGFR were treated with GFB-111 and either PDGF or IGF-1, respectively, then labeled with [^{3}H]thymidine. [^{3}H]thymidine incorporation was quantified by scintillation counting. Data are representative of three independent experiments.

Table 2. GFB-111 inhibits tumor growth in nude mice[a]

Cell line	Tumor origin	Tumor growth inhibition (%) Experiment 1	2	3	4
U87MG	Human brain	61% (35) 50mpk	56% (32) 50mpk	81% (32) 100mpk	88% (32) 200mpk
A-549	Human lung	62% (30) 50mpk	53% (31) 50mpk	64% (27) 50mpk	N/D
C6	Rat brain	54% (15) 50mpk	64% (15) 50mpk	46% (18) 50mpk	N/D
DaOY	Human brain	21% (48) 50mpk	0% (37) 50mpk	N/D	N/D

[a]The antitumor studies were performed exactly as described under legend to Figure 5A except that the human lung adenocarcinoma (A-549), human brain medulloblastoma (DaOY) or rat glioma (C6) were implanted s.c. in nude mice. The number in each parenthesis represents the day the % inhibition was calculated which is also the day the experiment was terminated (N/D, not determined; mpk, mg/kg.)

of GFB-111 resulted in a concentration-dependent decrease in PDGF-BB binding. The IC_{50} value of binding inhibition was 250 nM (Fig. 2C), which is similar to the IC_{50} value measured for GFB-111 inhibition of PDGF-BB-stimulated PDGFR tyrosine phosphorylation (Table 1). Figure 2C also shows that PDGF-BB binding to its receptor was blocked by GFB-111 but not GFB-116. Similar experiments with EGF, IGF-1, and VEGF demonstrated that GFB-111 (10 μM) had no significant effects on ^{125}I-EGF or ^{125}I-IGF-1 binding but inhibited ^{125}I-VEGF binding by 50% in NIH 3T3 cells overexpressing EGFR, IGF-1R, and VEGFR (Flk-1), respectively (Fig. 2D).

GFB-111 selectively blocks PDGF-induced receptor tyrosine phosphorylation and MAP kinase activation. We next determined the selectivity of GFB-111 by evaluating its ability to block growth factor–stimulated tyrosine phosphorylation of several receptor tyrosine kinases and subsequent activation of two MAPKs, Erk1 and Erk2. Figure 3A shows that PDGF-BB stimulation of starved NIH 3T3 cells in the absence of GFB-111 resulted in PDGFR autophosphorylation and Erk1/Erk2 activation. However, pretreatment of these cells with GFB-111 (0.1–10 μM) for 5 min resulted in a concentration-dependent inhibition of PDGF-BB stimulation of receptor tyrosine phosphorylation with an IC_{50} of 250 nM and a complete block at 3 μM GFB-111. Figure 3A also shows that GFB-111 is a potent inhibitor of PDGF-dependent activation of Erk1 and Erk2 (IC_{50} of 0.8 and 1.2 μM, respectively). PDGF-AA stimulation of PDGFR phosphorylation and Erk1/Erk2 activation was also blocked with GFB-111 with a similar potency. In contrast, GFB-111 at concentrations as high as 100 μM did not affect the ability of EGF to stimulate EGFR tyrosine phosphorylation and Erk1/Erk2 activation. For comparison, PD158780, a known EGFR tyrosine kinase inhibitor, blocks EGFR tyrosine phosphorylation and Erk1/Erk2 activation (Figure 3A). To further evaluate GFB-111 selectivity, we have demonstrated that this compound was able to inhibit VEGF-stimulated Flk-1 tyrosine phosphorylation and MAPK activation, but at concentrations higher (IC_{50} = 10 μM) than those required for PDGF (IC_{50} = 250 nM). Furthermore, activation by IGF-1, acidic or basic fibroblast growth factors (aFGF, bFGF), and HRGβ of Erk1/Erk2 was minimally affected by GFB-111 at concentrations as high as 100 μM (Fig. 3B). Thus, GFB-111 blocks PDGF signaling at very low concentrations, inhibits VEGF signaling at higher concentrations (10 μM), but has little effect on EGF, IGF-1, aFGF, bFGF, and HRGβ signaling at very high concentrations.

GFB-111 selectively inhibits PDGF-stimulated DNA synthesis. To confirm whether this selectivity applies to PDGF-induced cellular responses, we next evaluated the selectivity of GFB-111 to inhibit growth factor–stimulated DNA synthesis using a [^{3}H]thymidine incorporation assay. In NIH 3T3 cells PDGF-BB stimulated DNA synthesis by 10-fold, and GFB-111 suppressed this stimulation in a dose-dependent manner with an IC_{50} of 6.5 μM (Fig. 4). In contrast GFB-111 was ineffective at inhibiting IGF-1–stimulated DNA synthesis at concentrations as high as 100 μM (Fig. 4). These data further confirm the highly selective character of GFB-111 toward PDGF.

GFB-111 inhibits the growth of human tumors in nude mice. The ability of GFB-111 to potently and selectively block PDGF-dependent signaling and DNA synthesis, coupled with the ability of PDGF to stimulate angiogenesis and contribute to cancer cell growth, prompted us to determine the in vivo antitumor efficacy of GFB-111 in the nude mouse human xenograft model. Daily intraperitoneal administration with GFB-111 (50, 100, and 200 mg/kg) to nude mice implanted subcutaneously with the human

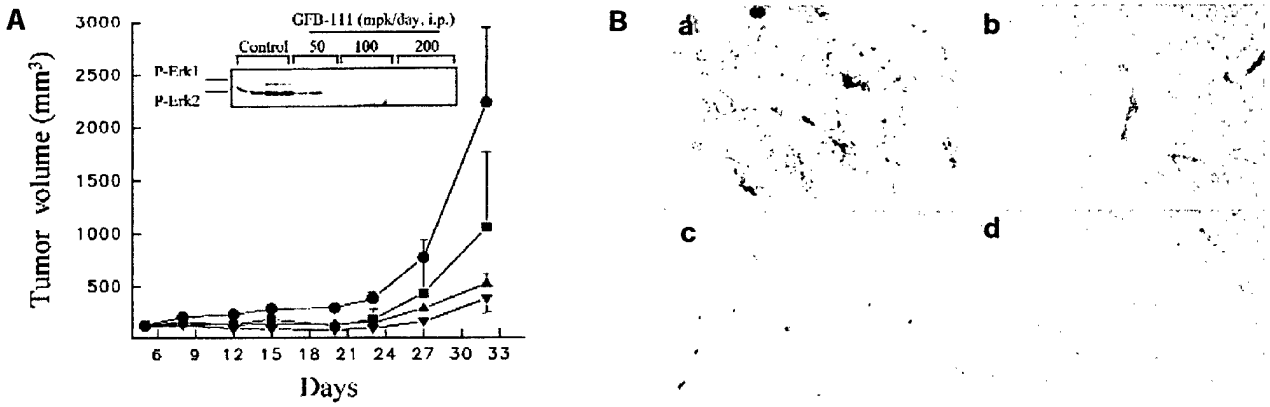

Figure 5. GFB-111 inhibits tumor growth and angiogenesis in nude mice. (A) GFB-111 inhibits the growth of the human glioblastoma U87MG in nude mice. U87MG cells were injected subcutaneously into nude mice, and when tumors reached about 100 mm³, animals were dosed intraperitoneally with 0.2 ml once daily. Control animals (●) received a saline vehicle, whereas treated animals were injected with GFB-111 at 50 (■), 100 (▲), or 200 (▼) mg/kg/day. For detection of phosphorylated/activated Erk1/Erk2 in tumors in vivo, the tumors were processed as described in the Experimental Protocol. The lysates were electrophoresed on SDS–PAGE, and immunoblotted, with anti-phospho-p44/p42 MAPK (Thy202/Tyr204). Data are representative of three independent experiments. (B) GFB-111 inhibits angiogenesis. On the indicated termination day of each experiment (see Table 2), the U87MG tumors were extracted. Tissue sections were stained with H&E and also subjected to immunostaining for Factor VIII. Control (panel a), 50 mg/kg (panel b), 100 mg/kg (panel c), and 200 mg/kg (panel d). Data are representative of two independent experiments.

Table 3. GFB-111 inhibits tumor angiogenesis[a]

Tumor	Group	Microvessel Count (Mean ± sd)	
		250X	400X
A-549	Control	15.66 ± 7.00	7.74 ± 2.88
	GFB-111 (50 mg/kg)	3.63 ± 1.36	2.34 ± 1.01
U87MG	Control	66.40 ± 1.36	31.53 ± 7.58
	GFB-111 (50 mg/kg)	23.13 ± 15.69	12.33 ± 8.37
U87MG	Control	23.48 ± 6.21	15.68 ± 3.25
	GFB-111 (50 mg/kg)	10.50 ± 2.12	6.00 ± 1.13
	GFB-111 (100 mg/kg)	7.73 ± 2.61	5.20 ± 1.71
	GFB-111 (200 mg/kg)	5.13 ± 3.10	3.07 ± 1.94
C6	Control	20.23 ± 7.84	9.77 ± 3.13
	GFB-111 (50 mg/kg)	14.27 ± 4.79	7.97 ± 2.83
DaOY	Control	8.07 ± 1.47	4.73 ± 0.90
	GFB-111 (50 mg/kg)	7.20 ± 2.52	4.80 ± 1.37

[a]For micro blood vessel counting, the five areas of highest tumor neovascularization were microscopically selected using a low-power view (4×). After the areas of highest neovascularization had been identified, individual microvessels were counted on a 250× (25× objective lens and 10× ocular lens), and a 400× (40× objective lens and 10× ocular lens) field. Brown-staining endothelial cells or endothelial cell clusters were considered as a single, countable microvessel following Weidner et al. criteria[34]. Vessel lumina and/or red blood cells were not used to define a microvessel[34]. Data represent average value from at least two independent experimental groups for each tumor type.

glioblastoma U87MG resulted on day 32 in a dose-dependent inhibition of tumor growth of 56, 81, and 88%, respectively (Fig. 5A and Table 2). Extraction and processing of tumors on day 32 show that Erk1/Erk2 activation was blocked in the tumors from the animals treated with 100 and 200 mg/kg GFB-111 (Fig. 5A, inset). The ability of GFB-111 to inhibit tumor growth was not limited to U87MG. GFB-111 was also effective at inhibiting the tumor growth in nude mice of the human lung adenocarcinoma A-549 and the rat glioma C6 (Table 2). However, the growth of the human medulloblastoma DaOY was minimally affected (Table 2).

GFB-111 inhibits angiogenesis in vivo. Because GFB-111 was effective at inhibiting the tumor growth of human cancer cells that express a PDGF/PDGFR autocrine loop (U87MG) as well as those that express neither PDGF nor PDGFR (A-549), and because PDGF promotes angiogenesis, we next explored whether GFB-111 inhibits angiogenesis in vivo. Tissue sections from U87MG tumor biopsy specimens collected on day 32 were immunostained with the vascular marker Factor VIII. Tumors from control animals showed very marked staining (Fig. 5B). In contrast, the Factor VIII immunostaining was decreased in a dose-dependent manner in tumors from animals treated with 50, 100, and 200 mg/kg GFB-111 (Fig. 5B). Quantification of microvessels at two field magnifications (250× and 400×) clearly demonstrated that GFB-111 inhibited angiogenesis strongly in U87MG and A-549 tumors, to a lesser degree in C6 tumors, and had no effect on angiogenesis in DaOY tumors (Table 3).

Discussion

In this study we have used a new approach to inhibiting receptor tyrosine kinase signaling by targeting the binding of growth factors to their receptor. The discovery of GFB-111 demonstrates that a designed synthetic molecule can bind to a growth factor, and disrupt its biological activity by preventing it from binding to its receptor. This is a critical finding that supports the disruption of protein–protein interactions as a sound approach for modern anticancer therapy. An advantage of this strategy is the direct access to the target, avoiding problems associated with cellular uptake and intracellular metabolism and degradation. This approach also has the potential for high selectivity because it targets interactions that do not involve the common adenosine triphosphate (ATP) binding site of receptor tyrosine kinases.

GFB-111 is selective for the disruption of PDGFR binding, tyrosine phosphorylation, and Erk1/Erk2 activation compared to EGF and, to a lesser extent, VEGF binding to their respective receptors. This is consistent with differences in their overall structure, particularly in areas involved in receptor binding. The binding of PDGF to its receptor is mediated by mainly hydrophobic and basic amino acid residues found in the loops connecting the β-sheets of the PDGF peptide[25,26]. Although VEGF shares some overall structural homology with PDGF, there are critical differences in their receptor binding regions. In particular, the receptor binding loop regions of VEGF are mainly composed of hydrophobic and acidic residues[27]. Epidermal growth factor has no structural homology with PDGF and VEGF and has a receptor binding domain composed of hydrophobic groups and a single basic residue (Arg 41) located in a hairpin turn[28]. Similarly, FGF has no structural relationship with PDGF and has a large receptor binding surface composed primarily of hydrophobic and positively charged or hydrogen-bonding (arginine and asparagine) residues[29]. IGF-1 has strong homology with insulin but bears no similarity to PDGF. The recognition surface of IGF-1 has been shown to include several critical tyrosine residues as well as two important arginine groups[30]. Finally, heregulin is similar in structure to EGF but bears little sequence homology. Alanine scanning experiments have shown the importance of hydrophobic as well as both positively (Arg 44 and 31) and negatively (Glu 19) charged residues in the binding of heregulin to different ErbB receptors[31]. Overall, these comparisons point to unique shape and surface residue distributions in the receptor binding domain of each of the growth factors that can be exploited in the design of synthetic agents that are selective for binding to PDGF.

The lack of correlation between GFB-111 inhibition of tumor growth and PDGF/PDGFR expression in the cancer cells suggested that tumor growth inhibition may be due to either inhibition of cell proliferation that depends on PDGF/PDGFR and/or angiogenesis. Indeed, PDGF has been directly implicated in promoting angiogenesis by mediating endothelial cell migration and proliferation. Furthermore, PDGF also induces endothelial cells to express VEGF, a very potent angiogenic growth factor. Therefore, by blocking PDGF binding to its receptor on endothelial cells, GFB-111 could inhibit endothelial cell migration and proliferation as well as VEGF expression, hence blocking angiogenesis. In addition, GFB-111 at higher concentrations could block VEGF binding to Flk-1 on endothelial cells and inhibit angiogenesis. Thus, our results demonstrate that selective PDGF binding molecules such as GFB-111 that are capable of blocking signaling, tumor growth, and angiogenesis may lead to the development of a new class of anticancer drugs capable of treating a wide spectrum of human cancers.

Experimental protocol

Inhibition of PDGF-dependent receptor tyrosine phosphorylation by growth factor binders (GFBs). Starved NIH 3T3 cells were pretreated with the various GFBs (0–100 μM) for 5 min before stimulation with PDGF (10 ng/ml) for 10 min. The cells were then harvested and lysed, and the proteins from the lysates separated by SDS–PAGE and immunoblotted with an anti-phosphotyrosine antibody (4G10; Upstate Biotechnology, Lake Placid, NY) as described by us[32]. The phosphotyrosine PDGF receptor bands were scanned using a BioRad Model GS-700 Imaging Densitometer (Bio-Rad Laboratories, Inc., Hercules, CA) and the concentrations of GFBs that inhibited the ability of PDGF to stimulate PDGFR tyrosine phosphorylation by 50% were determined.

PDGF binding. GFB-111 (50 μM) was incubated with buffer A (phosphate-buffered saline,PBS–0.5% bovine serum albumin, BSA) or PDGF-BB (1, 3, and 4 μM in buffer A) at room temperature for 10 min. The mixtures were then loaded onto a native 4% PAGE. The gel was then stained with silver nitrate. Duplicate lanes were run in the same gel but were not

stained. Bands corresponding to the boxed area were cut out of the lanes of the nonstained gel, denatured with SDS–PAGE loading buffer, loaded onto a 4% SDS–PAGE gel, and silver stained.

Binding of ^{125}I-PDGF to NIH 3T3 cells and inhibition by GFBs. NIH 3T3 (PDGF) or NIH 3T3 cells overexpressing either EGFR (EGF), IGFR (IGF-1), or Flk-1 (VEGF), were incubated with ^{125}I-PDGF, ^{125}I-EGF, ^{125}I-IGF, or ^{125}I-VEGF, respectively (50,000 c.p.m. per well) and increasing concentrations of GFB-111 or GFB-116. Cells were incubated at 4°C for 1–3 h, then washed three times with PBS and three times with 25 mM Tris pH 8.0, 1% Triton X-100, 10% glycerol, 1% SDS. Lysates plus wash were counted. Excess of cold growth factors was used to obtain nonspecific binding levels.

PDGF-stimulated receptor tyrosine autophosphorylation and activation of MAPK. Starved NIH 3T3 cells (PDGF-BB and PDGF-AA), NIH 3T3 cells overexpressing either EGFR (EGF) or Flk-1 (VEGF) were pretreated with the indicated concentrations of GFB-111 for 5 min before 10 min stimulation with PDGF-BB (10 ng/ml), PDGF-AA (10 ng/ml), EGF (100 ng/ml), and VEGF (50 ng/ml). Cell lysates were run on SDS–PAGE gels, then transferred to nitrocellulose and western blotted with anti-phosphotyrosine (4G10) or anti-phosphorylated Erk1/Erk2 (New England Biolabs, Beverly, MA)[32].

In other experiments, starved NIH 3T3 cells (PDGF-AA, PDGF-BB, aFGF, bFGF), NIH 3T3 cells overexpressing EGFR, IGF-1R, or Flk-1 and the human breast carcinoma SkBr3 that overexpresses ErbB2 (HRGβ) were pretreated with GFB-111 (100 μM) for 5 min before 10 min stimulation with the indicated growth factors at the concentrations shown above and aFGF (10 ng/ml), bFGF (50 ng/ml), IGF-1 (50 ng/ml), and HRGβ (10 ng/ml). Cell lysates were then immunoblotted with anti-phosphorylated Erk1/Erk2 (New England Biolabs).

PDGF-stimulated DNA synthesis. Starved NIH 3T3 or NIH 3T3 overexpressing IGFR were treated for 16 h with indicated concentrations of GFB-111 and either 10 ng/ml PDGF or 50 ng/ml IGF-1, respectively, then labeled for 2 h (NIH 3T3) or 4 h (IGFR) with [^{3}H]thymidine. Cells were then washed in PBS, lysed in 0.1 N NaOH, and spotted onto glass fiber filters. DNA was precipitated with ice-cold ethanol and then [^{3}H]thymidine incorporation quantified by scintillation counting.

Antitumor efficacy studies in nude mice. U87MG cells (human glioblastoma) were harvested, resuspended in PBS, and injected subcutaneously into the right and left flank (10×10^6 cells per flank) of eight-week-old female nude mice. When tumors reached about 100 mm^3, animals were dosed intraperitoneally with 0.2 ml once daily. Control animals received saline vehicle whereas treated animals were injected with GFB-111 (50, 100, or 200 mg/kg/day). The tumor volumes were determined by measuring length (l) and width (w) and calculating volume ($V = lw^2/2$) as described[33]. For detection of phosphorylated/activated Erk1/Erk2 in tumors in vivo, the tumors were extracted 20 min after the last GFB-111 injection on day 32, rinsed, and the tissue homogenized in *N*-[2-hydroxyethyl]piperazine-*N*'-[2-ethanesulfonic acid] (HEPES) lysis buffer (30 mM HEPES, pH 7.5, 1% Triton X-100, 10% glycerol, 10 mM NaCl, 5 mM $MgCl_2$, 25 mM NaF, 1 mM EGTA, 2 mM Na_3VO_4, 10 μg/ml trypsin inhibitor, 25 μg/ml leupeptin, 10 μg/ml aprotinin, 2 mM phenylmethylsulfonyl fluoride, PMSF). The lysates (50–100 μg) were electrophoresed on a 15% SDS–PAGE gel, transferred to nitrocellulose membranes, and immunoblotted, with anti-phosphorylated Erk1/Erk2 (New England Biolabs).

Angiogenesis studies. On the indicated termination day of each nude mouse experiment described above, the tumors were extracted and fixed in 10% neutral buffered formalin for 6 h. After fixation the tissue samples were processed into paraffin blocks. Tissue sections (4 μm thick) were obtained from the paraffin blocks and stained with hematoxylin and eosin (H&E) using standard histological techniques. Tissue sections were also subjected to immunostaining for Factor VIII (Dako, Carpinteria,CA) using the avidin biotin peroxidase complex technique. Rabbit polyclonal FVIII antibody was used at 1:400 dilution, following microwave antigen retrieval (four cycles of 5 min each on high in 0.1 M citrate buffer).

Acknowledgments

This work was supported by NIH PO1 CA78038-01A1 and United States Army grant DAMD17-99-1-9458. We would also like to thank Dr. Axel Ullrich (Max-Planck-Institute for Biochemistry) and Dr. Richard Jove (Moffitt Cancer Center and USF) for NIH3T3 cells overexpressing the VEGF/flk-1 receptor and EGFR, respectively.

1. Heldin, C.H., Ostman, A. & Ronnstrand, L. Signal transduction via platelet-derived growth factor receptors. *Biochim. Biophys. Acta* **1378**, F79–F113 (1998).
2. Heldin, C.H. & Westermark, B. In *The molecular and cellular biology of wound repair.* Edn. 2 (Plenum Press, New York; 1996).
3. Raines, E.W., Bowen-Pope, D.F. & Ross, R. Platelet-derived growth factor. In *Handbook of experimental pharmacology. Peptide growth factors and their receptors.* (Springer, Heidelberg; 1990).
4. Forsberg, K., Valyi-Nagy, I., Heldin, C.H., Herlyn, M. & Westermark, B. Platelet-derived growth factor (PDGF) in oncogenesis: development of vascular connective tissue stroma in xenotransplanted human melanoma producing PDGF-BB. *Proc. Natl. Acad. Sci. USA* **90**, 393–397 (1993).
5. Battegay, E.J., Rupp, J., Iruela-Arispe, L., Sage, E.H. & Pech, M. PDGF-BB modulates endothelial proliferation and angiogenesis in vitro via PDGF beta-receptors. *J. Cell. Biol.* **125**, 917–928 (1994).
6. Thommen, R. et al. PDGF-BB increases endothelial migration on cord movements during angiogenesis in vitro. *J. Cell. Biochem.* **64**, 403–413 (1997).
7. Kumar, R., Yoneda, J., Bucana, C.D. & Fidler, I.J. Regulation of distinct steps of angiogenesis by different angiogenic molecules. *Int. J. Oncol.* **12**, 749–757 (1998).
8. Wang, D., Huang, H.J., Kazlauskas, A. & Cavenee, W.K. Induction of vascular endothelial growth factor expression in endothelial cells by platelet-derived growth factor through the activation of phosphatidylinositol 3-kinase. *Cancer Res.* **59**, 1464–1472 (1999).
9. Leveen, P. et al. Mice deficient for PDGF-B show renal, cardiovascular and hematological abnormalities. *Genes Dev.* **8**, 1875–1887 (1994).
10. Soriano, P. Abnormal kidney development and hematological disorders in PDGF beta-receptor mutant mice. *Genes Dev.* **8**, 1888–1896 (1994).
11. Kazlauskas, A. & Cooper, J.A. Autophosphorylation of the PDGF receptor in the kinase insert region regulates interactions with cell proteins. *Cell* **58**, 1121–1133 (1989).
13. Lowenstein, E.J. et al. The SH2 and SH3 domain-containing protein GRB2 links receptor tyrosine kinases to *ras* signaling. *Cell* **70**, 431–442 (1992).
14. Ramakrishnan, V. et al. A novel monoclonal antibody dependent on domain 5 of the platelet-derived growth factor beta receptor inhibits ligand binding and receptor activation. *Growth Factors* **8**, 253–265 (1993).
15. Engstrom, U., Engstrom, A., Ernlund, A., Westermark, B. & Heldin, C.H. Identification of a peptide antagonist for platelet-derived growth factor. *J. Biol. Chem.* **267**, 16581–16587 (1992).
16. Brennand, D.M. et al. Identification of a cyclic peptide inhibitor of platelet-derived growth factor-BB receptor-binding and mitogen-induced DNA synthesis in human fibroblasts. *FEBS Lett.* **413**, 70–74 (1997).
17. Shulman, T., Sauer, F.G., Jackman, R.M., Chang, C.N. & Landolfi, N.F. An antibody reactive with domain 4 of the platelet-derived growth factor β receptor allows BB binding while inhibiting proliferation by impairing receptor dimerization. *J. Biol. Chem.* **272**, 17400–17404 (1997).
18. Klohs, W.D., Fry, D.W. & Kraker, A.J. Inhibitors of tyrosine kinase. *Curr. Opin. Oncol.* **9**, 562–568 (1997).
19. Levitzki, A. & Gazit, A. Tyrosine kinase inhibition: an approach to drug development. *Science* **267**, 1782–1788 (1995).
20. Ferns, G.A. et al. Inhibition of neointimal smooth muscle accumulation after angioplasty by an antibody to PDGF. *Science* **253**, 1129–1132 (1991).
21. Duan, D.S., Pazin, M.J., Fretto, L.J. & Williams, L.T. A functional soluble extracellular region of the platelet-derived growth factor (PDGF) β receptor antagonizes PDGF-stimulated responses. *J. Biol. Chem.* **266**, 413–418 (1991).
22. Green, L.S. et al. Inhibitory DNA ligands to platelet-derived growth factor B-chain. *Biochemistry* **35**, 14413–14424 (1996).
23. Park, H.D., Lin, Q. & Hamilton, A.D. Protein surface recognition by synthetic receptors: a route to novel sub-micromolar inhibitors for chymotrypsin. *J. Am. Chem. Soc.* **121**, 8–13 (1999).
24. Hamuro, Y., Calama, M.C., Park, H.S. & Hamilton, A.D. A calixarene with four peptide loops: an antibody mimic for recognition of protein surfaces. *Angew. Chem. Int. Edn. Engl.* **36**, 2680–2683 (1997).
25. Oefner, C., Arey, A.D., Winkler, F.K., Eggimann, B. & Hosang, M. Crystal structure of human platelet derived growth factor, *EMBO J.* **11**, 3921–3926 (1996).
26. Anderson, M. et al. Involvement of loop 2 of platelet derived growth factor-AA and -BB in receptor binding. *Growth Factors* **12**, 159–164 (1995).
27. Muller, Y.A. et al. Vascular endothelial growth factor: crystal structure and functional mapping of the kinase domain receptor binding site. *Proc. Natl. Acad. Sci. USA* **94**, 7192–7197, 1997.
28. Campion, S.R. & Niyogi, S.K. Interaction of the epidermal growth factor with its receptor. *Prog. Nucleic Acid Res. Mol. Biol.* **49**, 353–383 (1994).
29. Stauber, D.J., DiGabriele, A.D. & Hendrickson, W.A. Structural interactions of fibroblast growth factor receptor with its ligands. *Proc. Natl. Acad. Sci. USA* **97**, 49–54 (2000).
30. McInnes, C. & Sykes, B.D. Growth factor receptors: structure, mechanism and drug discovery. *Biopolymers* **43**, 339–366 (1997).
31. Jones, J.T. et al. Binding interaction of the heregulinβ *egf* domain with ErbB3 and ErbB4 receptors assessed by alanine scanning mutagenesis. *J. Biol. Chem.* **273**, 11667–11674 (1998).
32. McGuire, T., Qian, Y., Hamilton, A.D. & Sebti, S.M. Platelet derived growth factor receptor tyrosine phosphorylation requires protein geranylgeranylation and not farnesylation. *J. Biol. Chem.* **271**, 27402–27407 (1996).
33. Sun, J. et al. Antitumor efficacy of a novel class of non-thiol-containing peptidomimetic inhibitors of farnesyltransferase and geranylgeranyltransferase I: combination therapy with the cytotoxic agents cisplatin, taxol and gemcitabine. *Cancer Res.* **59**, 4919–4926 (1999).
34. Weidner, N., Semple, J.P., Welch, W.R. & Folkman, J. Tumor angiogenesis and metastasis—correlation in invasive breast carcinoma. *N. Engl. J. Med.* **324**, 1–8 (1991).

Oncogene (2000) 19, 6566–6573

www.nature.com/onc

Design of growth factor antagonists with antiangiogenic and antitumor properties

Saïd M Sebti*,[1] and Andrew D Hamilton*,[2]

[1]*Drug Discovery Program, H. Lee Moffitt Cancer Center and Research Institute, Department of Oncology and Biochemistry and Molecular Biology, University of South Florida, Tampa, Florida, FL 33612, USA;* [2]*Department of Chemistry, Yale University, New Haven, Connecticut, CT 06511, USA*

This review describes our recent efforts in the development of novel therapies for cancer. Our primary approach is to design synthetic agents that antagonize the function of growth factors that are critically involved in oncogenesis and angiogenesis. We achieve this by designing synthetic molecules that can recognize the exterior surface of the growth factor and so block the interaction with its receptor tyrosine kinase. A key step is the construction of synthetic agents that contain a large (>400Å²) and functionalized surface area to recognize a complementary surface on the target growth factor. In the course of this work we have discovered a molecule, GFB-111, that binds to PDGF, prevents it from binding to its receptor tyrosine kinase, blocks PDGF-induced receptor autophosphorylation, activation of Erk1 and Erk2 kinases and DNA synthesis. The binding affinity for PDGF is high (IC_{50} = 250 nM) and selective over EGF, IGF-1, aFGF, bFGF and HRGβ. In nude mouse models GFB-111 also shows significant inhibition of tumor growth and angiogenesis. *Oncogene* (2000) **19,** 6566–6573.

Keywords: platelet-derived growth factor; angiogenesis; oncogenesis; cancer drug discovery

Introduction

The search for new therapies in the war against cancer remains a top priority in biomedical research. In many cases current clinical therapies have changed little in several decades. The key to successfully developing novel clinical strategies against these cancers is twofold. First, critical protein targets that are known to be essential in the growth of tumors must be identified and validated as cancer therapy targets. Second, a novel approach to disrupting the function of these essential targets must be developed and shown to selectively block the growth of transformed cells. Our strategy is to disrupt the interaction of key growth factors with their receptor tyrosine kinase (RTK) targets in the cell membrane. To this end, we use an entirely novel strategy based on the design of synthetic agents that selectively and strongly bind to the surface of the growth factor and so block its oncogenic signaling function (Figure 1).

Our primary goal is to design synthetic agents that can recognize the exterior surface and antagonize the function of growth factors that are critically involved in oncogenesis. In our early work we have placed particular focus on platelet derived growth factor (PDGF) and its complementary receptor tyrosine kinase, platelet derived growth factor receptor (PDGFR). Overexpression of PDGFR is seen in many carcinomas and some cancer patients have high serum levels of PDGF. These elevated levels of PDGF and PDGFR in cancer patients also correlate with poor response to chemotherapy and shorter survival times. Synthetic agents that can block the uncontrolled signaling function of overexpressed receptor tyrosine kinases have the potential to slow the growth of tumors and greatly improve the quality of life for cancer patients (Figure 1).

*Correspondence: SM Sebti and AD Hamilton

Receptor tyrosine kinases as targets for cancer chemotherapy

Interaction of a quiescent cell with an external growth factor such as PDGF or epidermal growth factor (EGF) results in the activation of a complex network of signaling pathways that lead ultimately to cell division. The first step in this pathway involves the binding of the growth factor to the extracellular region of a membrane bound protein receptor tyrosine kinase (PDGFR or EGFR). Binding leads to dimerization of the receptor and activation of autophosphorylation of tyrosines on the receptor surface (Rockwell and Goldstein, 1995). This initiates the recruitment of several signaling proteins (including phosphatidylinositol-3-kinase, Src, Grb2/m-SOS-1 (a nucleotide exchange factor for Ras) and signal transducers and activators of transcription (STATs)) each of which contains src-homology-2 (SH-2) domains. Binding of the SH-2 regions of these proteins to the phosphotyrosines on the RTKs activates several pathways that are critical for triggering the cell cycle machinery.

The most well studied pathway passes through the GTP-binding protein Ras and activates the mitogen activated kinase (MAPK) cascade and subsequently transcription factors in the nucleus (Figure 2). Mutations in the Ras protein are present in 30% of human cancers and have been the subject of intense recent interest. We have reported extensively over the past seven years on the design of inhibitors for farnesyltransferase, a key enzyme in the posttranslational modification of Ras (Sebti and Hamilton, 2000). These compounds not only disrupt Ras farnesylation in whole cells but also block the growth of human tumors in nude mice models, and are on the verge of phase I clinical trials (Sun *et al.*, 1999). None of this work will be discussed here, however it provides a proof of

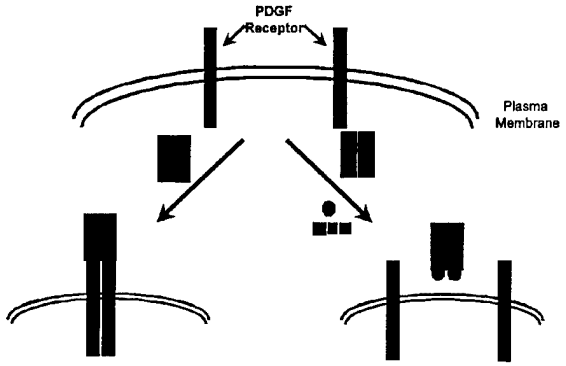

Figure 1 Schematic approach to growth factor binding agents (GFBs)

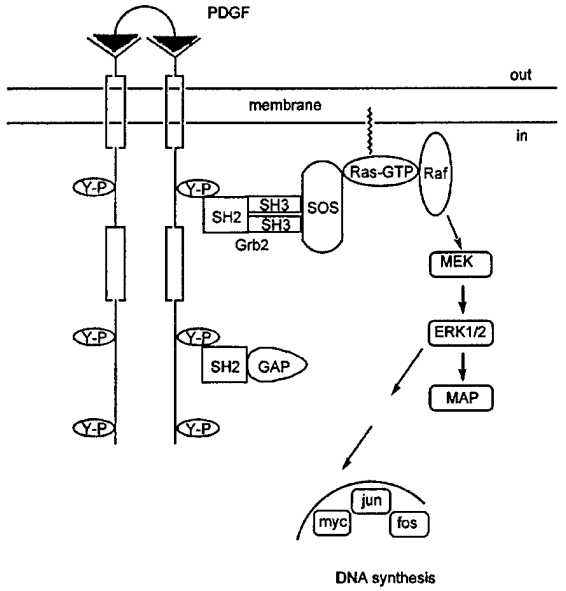

Figure 2 Simplified PDGF-activated signaling pathway

principle for targeting RTK signaling pathways in cancer therapy.

The primary focus of this review is the first step in the aberrant cell signaling pathways that lead to uncontrolled proliferation and cancer, namely the interaction of growth factors with RTKs. For example, PDGF, which plays an important role in many human malignancies (Heldin, 1992) exists in three isoforms (homodimers PDGF-AA and PDGF-BB and heterodimer PDGF-AB) and exerts its biological effects via specific binding to PDGF receptors (PDGFRs) (Hart *et al.*, 1988). Overexpression of PDGFR is seen in certain breast (Seymour *et al.*, 1993) and ovarian (Henriksen *et al.*, 1993) carcinomas as well as high serum levels of PDGF. Furthermore, elevated levels of PDGF and PDGFR in breast cancer patients correlate with poor response to chemotherapy and shorter survival times (Seymour *et al.*, 1993). The design of PDGF antagonists that can inhibit ligand-induced receptor activation has been suggested as a route to new anti-cancer drugs (Fiona and William, 1994). This strategy is supported by antibodies against PDGF which show anti-mitogenic activity (Johnson *et al.*, 1985) and a 110 kDa soluble form of the receptor has been shown to inhibit both the binding of PDGF-BB to PDGFR and the receptor tyrosine kinase activity (Duan *et al.*, 1991). These results strongly suggest that PDGF and PDGFR represent compelling targets for anti cancer drug design. Furthermore, PDGF has been shown to be critically involved in the angiogenesis process. PDGF can not only stimulate the proliferation of endothelial cells but also can stimulate the secretion of vascular endothelial growth factor. Moreover, PDGF knockout mice are deficient in processes of angiogenesis (Blaskovich, 2000).

The crystal structure of PDGF shows it to be a head-to-tail dimer, with each peptide folded into two long antiparallel pairs of β-strands with three intramolecular disulfide bonds (Figure 3) (Oefner *et al.*, 1992). The three surface loops connecting the strands (designated as I, II and III) are clustered at one end of the elongated dimer upon dimerization. Mutational analyses of individual amino acid residues or short peptide sequences in PDGF-B (Fenstermaker *et al.*, 1993; Ostman *et al.*, 1991; LaRoclelle *et al.*, 1992) have indicated that the key binding regions on PDGF occur in loops I and III. There is also some indication that residues from loop II from the other subunit of the dimer may also be involved in receptor binding (Anderson *et al.*, 1995). Inspection of the X-ray structure of PDGF-BB shows that the hairpin turns in loops I and III are separated by 10-12Å. Loop I projects a hydrophobic sequence (ANFLVW), loop III contains a highly cationic region (EIVRKKP) and loop II has a combination of both (NNRNV) (Engstom *et al.*, 1992).

Design of novel synthetic agents for protein surface binding

Protein recognition can be divided into two categories in terms of the interaction sites: (1) interactions that occur inside proteins, e.g. enzyme active sites; (2) interactions that occur on the surface of proteins. During the past two decades large numbers of synthetic molecules targeted to disrupt interior protein interactions have been shown to have medically important biological activities (Babine and Bender, 1997). However, artificially designed molecules that target the protein surface and disrupt its biological activity are rare (Hartwell *et al.*, 1997). Considering the unique composition of charged, hydrophobic and hydrophilic domains on every protein's surface, synthetic molecules that match the electrostatic features and topology of the protein targets might be expected to bind to the exterior and sterically prevent protein–protein interactions.

A model for protein surface recognition is provided by the immune system which generates a large number of antibodies that show high sequence and structural selectivity in binding to a range of protein surfaces (Brandon and Tooze, 1991). Our approach to growth factor binding agents involves the attachment of several peptide loops onto a core scaffold (Figure 4a) in direct analogy to the six hypervariable loops that are

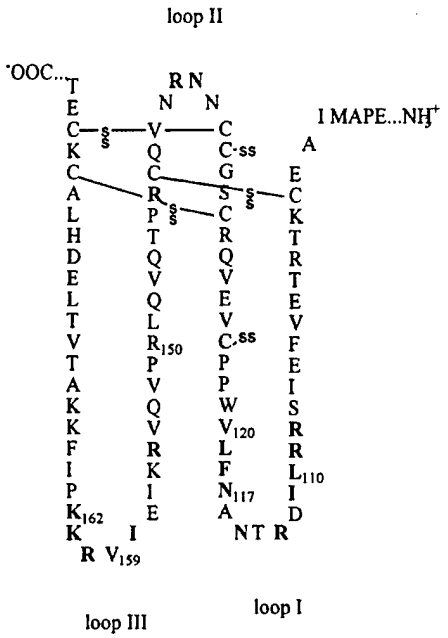

Figure 3 Amino acid sequence of PDGF-B chain. Residues important for receptor binding are in bold

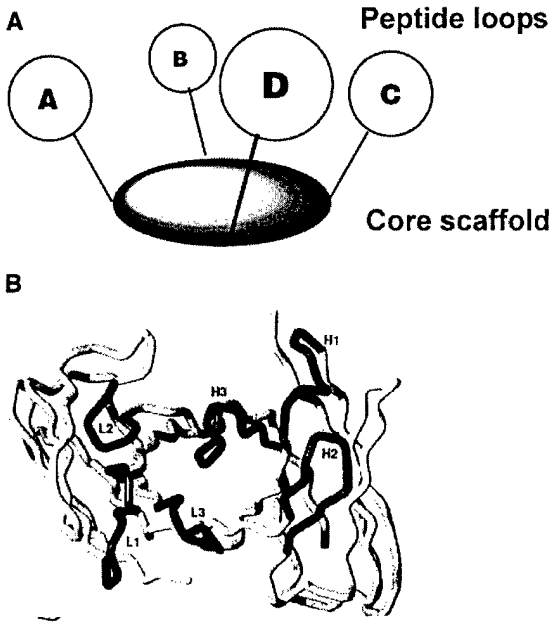

Figure 4 (a) Design for a protein binding agent. (b) Hypervariable loops in the FAB fragment

found in the antigen recognition region of the antibody FAB fragment (Figure 4b). The advantages of using this design for the recognition of protein surfaces are fourfold: (1) large surface areas can be created (>400 Å^2); (2) modular design enables us to generate a large diversity from a small number of cyclic peptide or scaffold components; (3) various non-natural groups can be incorporated into the loop structures and (4) scaffolds are relatively flexible which allows an 'induced fit' mechanism of binding.

We have recently prepared the first of a new class of protein surface receptors involving the attachment of four peptide loops to a central scaffold (based on the calix[4]arene unit **1**) (Hamuro *et al.*, 1997). The peptide loop component was based on a cyclic hexapeptide **2** in which two residues were replaced by a 3-aminomethylbenzoyl (3 amb) dipeptide mimetic (Bach *et al.*, 1994) containing a 5-amino substituent for linkage to the scaffold. The resulting molecule **3** contains a functionalized surface approximately 400Å^2 in area. The GDGD sequence in **2** was chosen to provide a surface containing both negatively charged and hydrophobic regions that would bind to a complementary surface on a target protein. We have prepared analogs of **3** in which the sequence of the cyclic peptide is varied to include anionic, hydrophobic and cationic residues, such as GDGD (**3**), GDGY (**5**), GKGF (**6**) and GKGK (**7**). This provided us with a first generation library of protein binding agents that were screened for their ability to bind to the surface of PDGF (Scheme 1).

Disruption of growth factor signaling by synthetic protein binding agents

Our first assessment of whether these molecules were able to interact with growth factors involved testing their ability to block PDGF-induced autophosphorylation of PDGFR. NIH3T3 cells were treated with the synthetic growth factor binding agents and PDGF (30 ng/ml) for 10 min, followed by lysis of the cells, SDS–PAGE and Western blot analysis using an antiphosphotyrosine antibody. Figure 5 shows the ability of the first generation GFB series at 5 μM concentrations to inhibit PDGF stimulation of the receptor tyrosine phosphorylation. We found that the molecule containing GlyAspGlyTyr (GDGY) sequences in each of the four peptide loops of (GFB-111) blocked PDGF-BB-stimulation of PDGF receptor tyrosine autophosphorylation with an IC_{50} value of 250 nM (Table 1). This fourfold symmetrical arrangement of negative and hydrophobic residues shows a strong complementary to the region of PDGF that interacts with the recognition surface of PDGFR. The critical receptor binding area on PDGF-BB contains lysine and arginine residues as well as a significant number of amino acids with hydrophobic side chains. Mutational analysis has shown that growth factor binding to its receptor diminishes when these residues are changed (Oefner *et al.*, 1996; Anderson *et al.*, 1995).

Similarly, there is a loss in binding ability when the key Asp and Tyr residues in the cyclic peptides in GFB-111 are changed. For example, substitution of negatively charged Asp by positively charged Lys, as with GFB-115 (GKGF) (IC_{50}=50 μM) and GFB-116 (GKGK) (IC_{50}=40 μM), causes an almost 200-fold reduction in antagonist potency. Changing the hydrophobic Tyr for Asp, as in GFB-107 (GDGD) (IC_{50}=2.5 μM), leads to an order of magnitude loss in activity. The specific sequence of the cyclic peptide also appears to be important. Rearranging the anionic and hydrophobic residues in the four cyclic peptides as in GFB-122 (GDDY) (IC_{50}=1.7 μM) leads to a sevenfold reduction in binding activity compared to GFB-111 (GDGY) (Table 1).

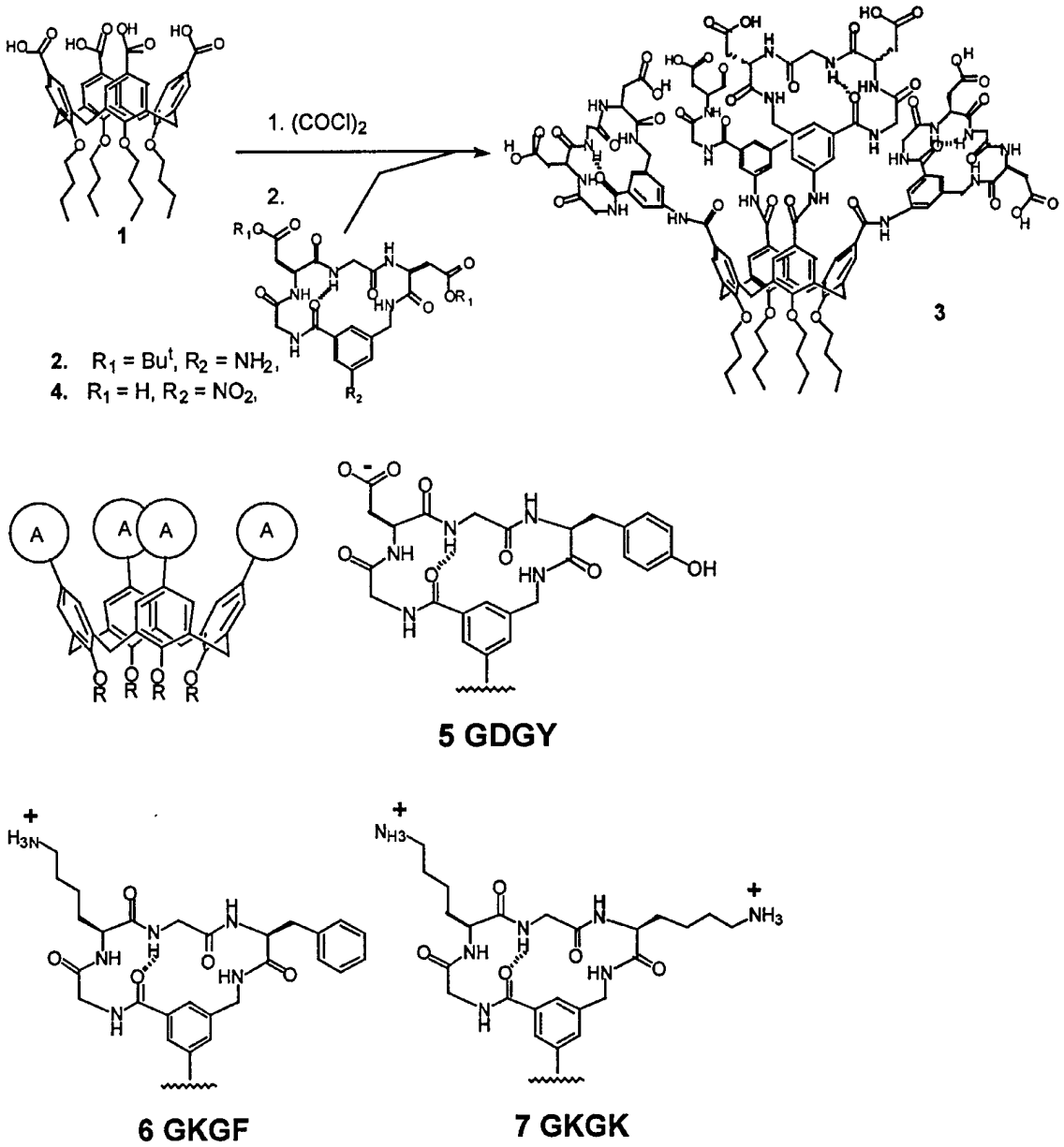

Scheme 1

Further insight into the mechanism by which GFB-111 was able to disrupt PDGF induced PDGFR phosphorylation was gained from a direct binding assay between [I-125]-labeled PDGF and PDGFR on the surface of NIH3T3 cells. Under normal circumstances [125-I]-PDGF-BB binds effectively to the receptor on the surface of NIH3T3 cells. However, pre-treatment with increasing concentrations of GFB-111, caused a decrease in PDGF-BB binding that followed normal dose dependent behavior (Figure 6). We measured an IC_{50} value for disruption of PDGF binding of 250 nM which corresponds well with the value measured for GFB-111 in the PDGFR tyrosine phosphorylation assay (Table 1). A similar experiment using GFB-116 (Figure 6) showed that PDGF-BB binding to its receptor was not blocked and confirmed the importance of the GDGY sequence. Excellent protein binding selectivity was also established in these experiments. GFB-111 (10 μM) was found to have no effect on the binding of [125-I]-EGF or [125-I]-IGF-1 to their corresponding receptors, EGFR and IGFR. A small effect was seen with [I-125]-VEGF (vascular endothelial growth factor) where GFB-111 at (10 μM) blocked binding by 50% in NIH3T3 cells overexpressing VEGFR/Flk-1 (Figure 7).

This selectivity for PDGF over related growth factors such as EGF, and to a lesser extent VEGF, is consistent with differences in their overall structure, particularly in areas involved in receptor binding. The critical residues for PDGF binding to its receptor are a

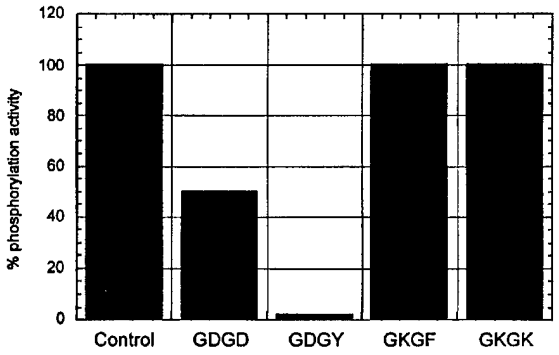

Figure 5 Inhibition of PDGF-stimulated tyrosine phosphorylation of PDGFR by the first generation of GFBs

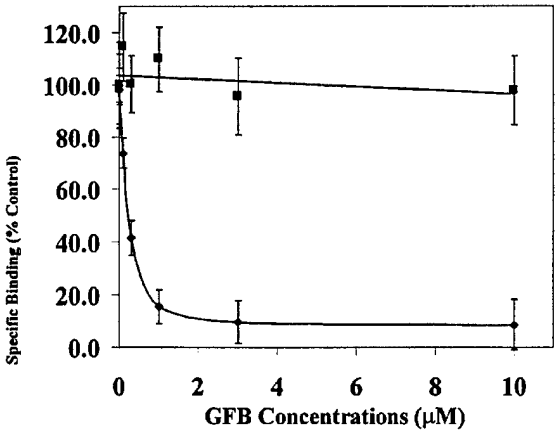

Figure 6 Inhibition of [125-I]PDGF binding to its receptor on NIH3T3 cells with increasing concentrations of GFB-111 (◆) or GFB-116 (■)

Table 1 Inhibition of PDGF-dependent receptor tyrosine phosphorylation by growth factor binders (GFBs)

Compounds	*Loop Sequence*	IC_{50} (μM)
GFB-105	GDFD	2.4
GFB-106	GDDD	8
GFB-107	GDGD	2.5
GFB-108	D-ADGD	9
GFB-109	GDLD	7.5
GFB-110	GDAD	1.7
GFB-111	GDGY	0.25
GFB-112	ADGD	29
GFB-113	GDSD	2.8
GFB-115	GKGF	50
GFB-116	GKGK	40
GFB-117	GDND	5.8
GFB-119	PDGD	20
GFB-120	GDDG	1.3
GFB-122	GDDY	1.7

series of hydrophobic and positively charged amino acids in loops I and III of one monomer, and loop II of the head-to-tail linked second monomer in dimeric PDGF (Oefner *et al.*, 1996; Anderson *et al.*, 1995). VEGF shares some structural homology with PDGF, but its receptor binding regions are made up principally of hydrophobic and negatively charged residues (Muller *et al.*, 1997). EGF has a completely different structure to PDGF and VEGF. The critical receptor binding region has been shown to contain several hydrophobic groups and a positively charged arginine residue (Arg41) (Campion and Niyogi, 1994). The receptor binding domains of these three growth factors are thus quite different suggesting that the negatively charged and hydrophobic surface of GFB-111 achieves its selectivity by matching the positive and hydrophobic surface of PDGF.

There is a strong possibility that the amphipathic GFB-111 is binding to the cationic and hydrophobic regions of the PDGF dimer and in doing so blocking its association to the receptor surface. A calculated structure for the interaction of this region of PDGF (using the crystal structure coordinates) with GFB-111 is shown in Figure 8. Similar interactions have been proposed for suramin binding to PDGF (Middaugh *et al.*, 1992) and heparin binding to fibroblast growth factor (Thompson *et al.*, 1994).

These early results clearly pointed to an interaction between GFB-111 and PDGF and a disruption of the initial activation of PDGFR tyrosine phosphorylation. The next question concerned whether this complex formation would lead to a disruption in downstream cell signaling pathways (Figure 2). We assessed the ability of GFB-111 to block growth factor-stimulated tyrosine phosphorylation of several receptor tyrosine kinases and subsequent activation of two mitogen-activated protein kinases (MAPK), Erk1 and Erk2. Treatment of starved NIH3T3 cells with PDGF-BB led to PDGFR autophosphorylation and Erk1/Erk2 activation (Figure 9). However, in the presence of GFB-111 (0.1–10 μM) there was a concentration-dependent inhibition of activation of Erk1 and Erk2 (IC_{50} of 0.8 and 1.2 μM, respectively). A similar effect was seen on PDGF-AA stimulation of PDGF receptor phosphorylation and Erk1/Erk2 activation. However selectivity among different growth factors was seen since GFB-111 at concentrations as high as 100 μM did not affect the ability of EGF to stimulate EGFR tyrosine phosphorylation and Erk1/Erk2 activation. As a positive control a known EGFR tyrosine kinase inhibitor, PD158780, blocks EGFR tyrosine phosphorylation and Erk1/Erk2 activation (Figure 9). Furthermore, IGF-1-, aFGF-, bFGF- and HRGβ-activation of Erk1/Erk2 was minimally affected by GFB-111 at concentrations as high as 100 μM (Figure 9). The results are consistent with the earlier radiolabeled growth factor data which showed a significant protein binding selectivity in the effects of GFB-111.

Anticancer activity of GFB-111

The above investigations showed that GFB-111 was able to bind to PDGF and block in a potent and selective manner PDGF-dependent signaling. However, a critical test for the strategy concerned the ability of GFB-111 to interfere with the function of PDGF in animal models. PDGF is well known to contribute to cancer cell growth by, in part, stimulating angiogenesis. This prompted us to investigate the *in vivo* anti-tumor

efficacy of GFB-111 in a nude mouse human xenograft model. The experiment involved nude mice implanted s.c. with the human glioblastoma U87MG. The tumor growth of a control group (treated with saline solution) was compared to that of a group treated daily with GFB-111 at 50, 100 and 200 mg per kg. Figure 10 shows that the treated group exhibited a dose-dependent inhibition of tumor growth of 56, 81 and 88%, respectively. Daily treatment with GFB-111 went on for more than one month yet there were no signs of gross toxicity among the animals. This provides good support that the molecules are exerting their effect through interference with a specific growth mechanism rather than through any systemic toxicity. At the end of the experiment the tumors from the mice were extracted and analysed to determine the extent of PDGF-dependent signaling. Figure 10 shows that Erk1/Erk2 activation was diminished in the tumors treated with 50 mg per kg and almost completely blocked in those treated with 100 and 200 mg per kg, confirming that our designed molecule was causing an inhibition of the PDGF-activated signaling pathway.

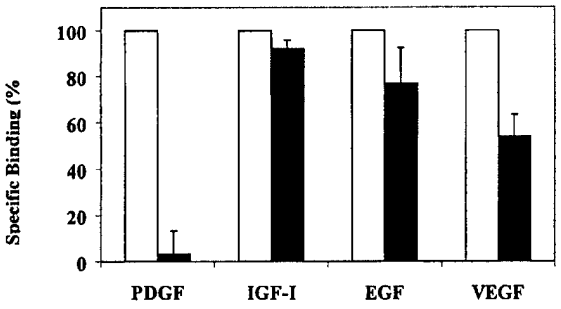

Figure 7 Inhibition of [125-I]-labeled growth factor binding to NIH3T3 cells overexpressing the complementary receptor tyrosine kinase, for PDGFR (PDGF), EGFR (EGF), IGFR (IGF) or Flk-1 (VEGF)

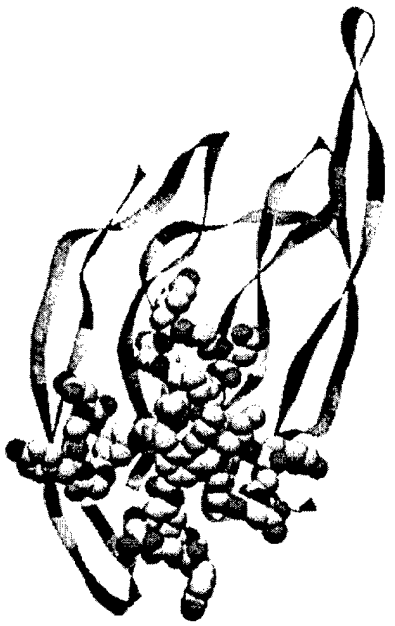

Figure 8 Front view of the postulated interaction between GFB-111 and PDGF

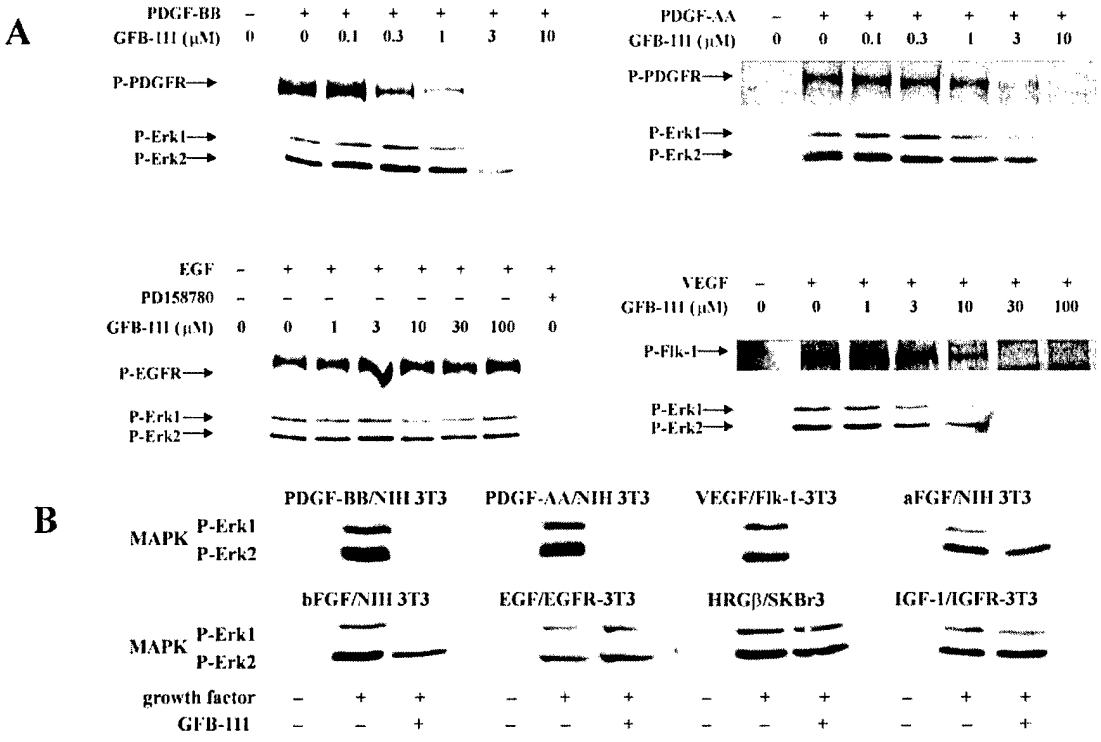

Figure 9 Effects of GFB-111 on growth factor stimulated receptor tyrosine autophosphorylation and activation of MAPK

Similar growth inhibition in nude mice was seen with other tumor cell lines, such as human lung adenocarcinoma A-549 and the rat glioma C6. However, little effect was seen on the growth of the human medulloblastoma DaOY (Table 2).

Although excellent inhibition of tumor growth by GFB-111 was seen, the mechanism by which the synthetic molecule exerts this effect was not clear. An intriguing result is the equipotent effect seen with tumors that depend on PDGF (U87) and those that do not (A549), suggesting an alternative mechanism to direct effects on the tumor cells. One possibility was that GFB-111 interferes with the growth of blood vessels in the tumor since PDGF is known to be important in promoting angiogenesis. In the U87MG nude mouse xenograft experiment, tumor biopsy specimens were taken at the end of the experiment, fixed and processed into paraffin blocks. The tissue sections were immunostained with the vascular marker Factor VIII and are shown in Figure 11. Tumors from animals treated with 50, 100 and 200 mg per kg GFB-111 showed a dose dependent decrease in immunostaining, in marked contrast to tumors from the untreated animals which showed extensive staining (vascularization). A more detailed quantification of microvessels in the tumor preparations showed that U87MG and A-549 tumors were sensitive to GFB-111 inhibition of angiogenesis whereas DaOY tumors showed no effect.

Conclusion

In this review we have described the recent progress that we have made in establishing a novel approach to disrupting the interaction between a growth factor and its receptor tyrosine kinase. We have outlined a strategy that mimics the use of peptide loop recognition domains as seen in antibody complementary determining regions. The synthetic growth factor binding agents (GFBs) are composed of four synthetic peptide loop domains linked to a core calixarene based scaffold. The potential of the approach has been firmly established by targeting the interaction between PDGF and its receptor tyrosine kinase. We show that one effective member of the GFB family is able not only to block the interaction of PDGF with PDGFR but also to inhibit its signaling function. This potent effect further translates into an ability to slow down the growth of human tumors in nude mouse models through an antiangiogenic mechanism.

This study represents the first example of a potential new approach to controlling cell signaling through the selective disruption of protein–protein interactions. The key to the strategy will be to develop a range of GFBs with different surface recognition characteristics that can be then applied to different growth factors.

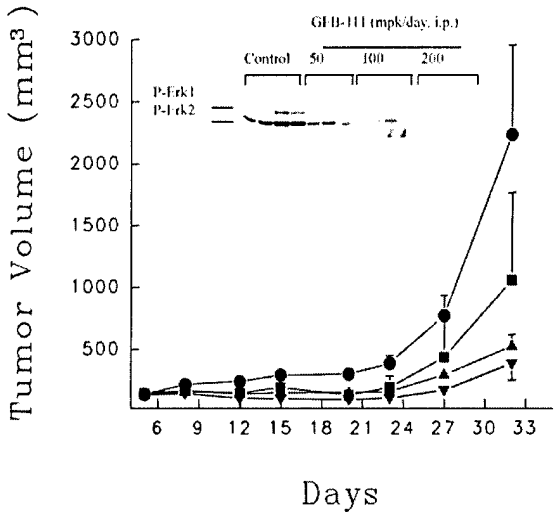

Figure 10 Inhibition of the growth of the human glioblastoma U87MG by GFB-111 in nude mice. Insert: Extent of phosphorylated/activated Erk1/Erk2 in tumors *in vivo*

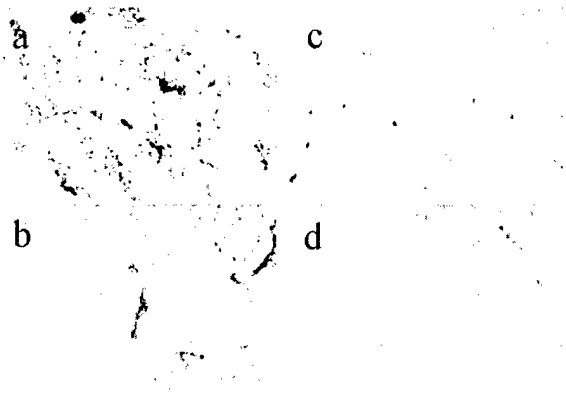

Figure 11 Extent of angiogenesis determined by immunostaining for Factor VIII complex technique; control (**a**), 50 mg/kg (**b**), 100 mg/kg (**c**), 200 mg/kg (**d**)

Table 2 GFB-111 inhibition of tumor growth in nude mice

		% Tumor Growth Inhibition Experiment			
Cell line	*Tumor Origin*	*1*	*2*	*3*	*4*
U87-MG	human brain	61% (35) 50 mpk	56% (32) 50 mpk	81% (32) 100 mpk	88% (32) 200 mpk
A-549	human lung	62% (30) 50 mpk	53% (31) 50 mpk	64% (27) 50 mpk	N/D
C6	rat brain	54% (15) 50 mpk	64% (15) 50 mpk	46% (18) 50 mpk	N/D N/D
DaOY	human brain	21% (48) 50 mpk	0% (37) 50 mpk	N/D	N/D

We are currently investigating different core scaffold structures and alternative recognition elements that will enhance selective binding to growth factor surfaces.

Acknowledgments
This work was supported by NIH PO1 CA78038-01A1 and United States Army grant DAMD17-99-1-9458.

References

Anderson M, Ostman A, Kreysing J, Backstrom G, van de Poll M and Heldin C-H. (1995). *Growth Factors,* **12,** 159–164.

Babine RE and Bender SL. (1997). *Chem. Rev.,* **97,** 1359–1472.

Bach AC, Eyerman CJ, Gross JD, Bower MJ, Harlow RL, Weber PC and DeGrado WF. (1994). *J. Am. Chem. Soc.,* **116,** 3207–3219.

Blaskovich MA, Lin Q, Delarue FL, Sun J, Park HS, Coppola D, Hamilton AD and Sebti SM. (2000). *Nature Biotechnology,* **18,** 1065–1070.

Brandon C and Tooze J. (1991). *Introduction to Protein Structure,* Garland: New York.

Campion SR and Niyogi SK. (1994). *Prog. Nucl. Acid Res. Mol. Biol.,* **49,** 353–383.

Duan D, Pazin MJ, Fretto LJ and Williams LT. (1991). *J. Biol. Chem.,* **266,** 413–418.

Engstom U, Engstrom A, Ernlund A, Werstermark B and Heldin C-H. (1992). *J. Biol. Chem.,* **267,** 16581–16587.

Fenstermaker RA, Poptie E, Bonfield TL, Knauss TC, Corsillo L, Piskurich JF, Kaetzel CS, Jentoft JE, Gelfand C, DiCorleto PE and David M Kaetzel J. (1993). *J. Biol. Chem.,* **268,** 10482–10489.

Fiona J and William GJ. (1994). *New Molecular Targets for Cancer Chemotherapy,* Kerr DJ, Workman P Eds., CRC Press: Boca Raton, 52.

Hamuro Y, Calama MC, Park HS and Hamilton AD. (1997). *Angew. Chemie Int. Ed. Engl.,* **36,** 2680–2683.

Hart CE, Forstrom JW, Kelly JD, Seifert RA, Smith RA, Ross R, Murray MJ and Bowen-Pope DE. (1988). *Science,* **240,** 1529–1531.

Hartwell LH, Szankasi P, Roberts CJ, Murray AW and Friend SH. (1997). *Science,* **278,** 1064–1068.

Heldin C-H. (1992). *EMBO J.,* **11,** 4251–4259.

Henriksen R, Funa K, Wilander E, Backstrom T, Ridderheim M and Oberg K. (1993). *Cancer Res.,* **53,** 4550–4554.

Johnson A, Betsholtz C, von der Helm K, Heldin CH and Westermark B. (1985). *Proc. Natl. Acad. Sci. USA,* **82,** 1721–1725.

LaRoclelle WJ, Pierce JH, May-Siroff M, Giese N and Aaronson SA. (1992). *J. Biol. Chem.,* **267,** 17074–17077.

Middaugh CR, Mach H, Burke CJ, Volkin DB, Dabora JM, Tsai PK, Bruner MW, Ryan JA and Marfa KE. (1992). *Biochemistry,* **31,** 9016–9024.

Muller YA, Li B, Christinger HW, Wells JA, Cunningham BC and de Vos AM. (1997). *Proc. Natl. Acad. Sci. USA,* **94,** 7192–7197.

Oefner C, Arcy AD, Winkler FK, Eggimann B and Hosang M. (1992). *EMBO J.,* **11,** 3921–3926.

Oefner C, Arey AD, Winkler FK, Eggimann B and Hosang M. (1996). *EMBO J.,* **11,** 3921–3926.

Ostman A, Andersson M, Hellman U and Heldin C-H. (1991) *J. Biol. Chem.,* **266,** 10073–10077.

Rockwell P and Goldstein NI. (1995). *Mol. Cell. Differ.,* **3,** 315–335.

Sebti SM and Hamilton AD. (2000). *Expert Opinion On Investigational Drugs.*

Seymour L, Dajee D and Bezwoda WR. (1993). *Breast Cancer Research and Treatment,* **26,** 247–252.

Sun J, Blaskovich MA, Knowles D, Qian Y, Ohkanda J, Bailey RA, Hamilton AD and Sebti SM. (1999). *Cancer Res.,* **59,** 4919–4926.

Thompson LD, Pantoliani MW and Springer BA. (1994). *Biochemistry,* **33,** 3831–3840.

CHEMCOMM Communication
www.rsc.org/chemcomm

Disruption of protein–protein interactions: design of a synthetic receptor that blocks the binding of cytochrome *c* to cytochrome *c* peroxidase

Yen Wei,*[ab] George L. McLendon,*[a] Andrew D. Hamilton,*[c] Martin A. Case,[a] Cherie B. Purring,[a] Qing Lin,[c] Hyung Soon Park,[c] Chang-Sun Lee[c] and Tianning Yu[a]

[a] *Department of Chemistry, Princeton University, Princeton, New Jersey 08544, USA. E-mail: glm@princeton.edu; Fax: 609-258-6746; Tel: 609-258-1595*
[b] *Department of Chemistry, Drexel University, Philadelphia, Pennsylvania 19104, USA. E-mail: weiyen@drexel.edu; Fax: 215-895-1265; Tel: 215-895-2650*
[c] *Department of Chemistry, Yale University, New Haven, Connecticut 06520, USA. E-mail: ahamilton@ursula.chem.yale.edu; Fax: 203-432-3221; Tel: 203-432-5570*

Received (in Cambridge, UK) 1st May 2001, Accepted 14th June 2001
First published as an Advance Article on the web 6th August 2001

Synthetic receptor 1 has been found *via* fluorescence titration to compete effectively with cytochrome *c* peroxidase for binding cytochrome *c* (Cc), forming 1:1 Cc:1 complex with a binding constant of $(3 \pm 1) \times 10^8$ M^{-1}, and to disrupt Cc:Apaf-1 complex, a key adduct in apoptosis.

Protein–protein recognition is critical to virtually all cellular processes. Consequently, molecules which could specifically disrupt the high affinity natural protein complexes found physiologically could provide an important route to modulate cellular processes. However, there are few examples of such a modulation.[1] Since high affinity protein–protein complexes generally involve large surface areas,[2] it has been argued that small synthetic molecules which bind at the interaction surface are unlikely to compete with high affinity natural protein partners. Here, we show that a synthetic receptor molecule of structure **1** can bind cytochrome *c* (Cc) with a sufficiently high

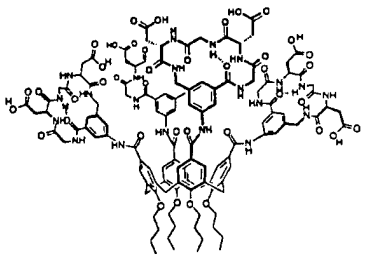

1

affinity to displace a natural high affinity protein partner, cytochrome *c* peroxidase (CcP). Cytochrome *c* provides an important model for such studies for several reasons. First, the structure of Cc is well characterized.[3] Second, the Cc:CcP complex is unusually well characterized, both from structural and thermodynamic viewpoints.[4,5] Finally, the key role of Cc in mediating apoptosis[6–8] makes it a particularly interesting target.

Several previous studies have explored the binding of small molecules to Cc.[3,9] However, in few previous cases was the binding sufficiently strong and specific to be shown to compete with the binding of natural partner proteins at relevant concentrations ($< 10^{-6}$ M). Preliminary data on Cc binding by **1** suggested the possibility of specific and high affinity binding.[10] To test this possibility, we have carried out a series of spectroscopic studies and established that the synthetic receptor **1** is indeed capable of disrupting the physiological complex of Cc with CcP by binding competitively to Cc. From the concentration of **1** needed to disrupt the Cc:CcP binding, we can estimate that the dissociation constant (K_d) for the Cc:**1** complex is near the nanomolar level ($\sim 10^{-8}$ M) in a phosphate buffer (10 mM, pH 6.0). Furthermore, the competitive displacement of CcP from its natural protein partner by **1** suggests that they share a similar binding site on the surface of Cc.

The competitive binding experiments were based on the quenching of strong fluorescence of magnesium(II) CcP (MgCcP) by Cc and the reversal of that quenching by addition of receptor **1**. The reaction schemes are illustrated in eqns. (1) and (2). It has been demonstrated that the magnesium substitution of iron in the native CcP does not alter the binding characteristics of CcP with Cc.[5] The use of MgCcP is advantageous because of its strong, interference-free fluorescence signals. In a typical experimental procedure, 3.0 mL of 0.077 μM solution of MgCcP[5] in 10 mM degassed potassium phosphate buffer (KPhos, pH 6.0) was prepared in a quartz cuvette of 1 cm pathlength equipped with magnetic stirrer. The fluorescence spectrum of the solution was recorded on a PTI fluorimeter (Photon Technology International, NJ) with an excitation wavelength of 556 nm and a scan rate of 1 nm s^{-1} at 15.0 °C (Fig. 1a). The solution was titrated *in situ* with a 3.5 μM solution of yeast Cc (Sigma) to an equivalent point [CcP]:[Cc] = 1. Upon Cc:CcP complex formation, the fluorescence signals of MgCcP at 598 and 653 nm were quenched by resonant energy transfer (Fig. 1b). Then a 4.48 μM solution of receptor **1**[10] in 10 mM KPhos (pH 6.0) was added in aliquots of 10 to 20 μL. The fluorescence spectrum was measured after each addition until the [**1**]:[Cc] molar ratio reached 5 or higher (Figs. 1c and 1d). Upon addition of receptor **1**, the intensity of the fluorescence signals of MgCcP increased, indicating that CcP is gradually freed from the Cc:CcP complex.

$$\text{Cc} + \text{CcP} \leftrightharpoons \text{Cc:CcP} \quad (1)$$

$$\text{Cc:CcP} + \mathbf{1} \leftrightharpoons \text{Cc:}\mathbf{1} + \text{CcP} \quad (2)$$

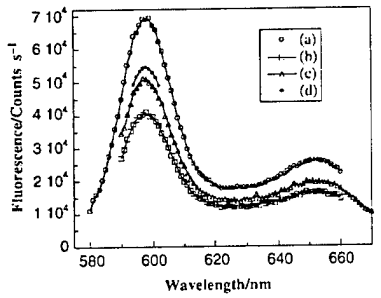

Fig. 1 Representative fluorescence spectra of (a) MgCcP (0.075 μM), (b) MgCcP (0.075 μM) with 0.077 μM of Cc, and the MgCcP:Cc complex titrated with (c) 0.11 and (d) 0.28 μM of **1**. Excitation at 556 nm at 15.0 °C in 10 mM KPhos buffer (pH 6.0).

DOI: 10.1039/b104142h

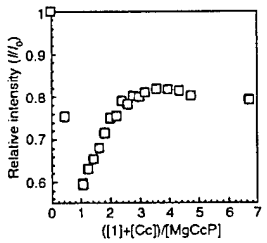

Fig. 2 Plots of the relative fluorescence intensity (I/I_o) at 598 nm against the normalized concentration ([Cc] + [1])/[CcP] (ex. 556 nm). [Cc] = 0.077 μM, [MgCcP] = 0.075 μM in 10 mM KPhos buffer (pH 6.0) at 15.0 °C.

Fig. 2 shows the plots of relative intensity of the fluorescence at 598 nm against the normalized concentration, ([Cc] + [1])/[CcP]. At [Cc]/[CcP] = 1 and before addition of **1**, the fluorescence intensity (I) of MgCcP was reduced to ~57% of the initial value (I_o), which is in agreement with that reported in the literature.[5] Addition of **1** resulted in a sharp increase in the relative intensity (I/I_o) until ([Cc] + [1])/[CcP] reached about 2, *i.e.* [**1**]/[Cc] ≈ 1, after which the intensity levelled off, suggesting the formation of 1:1 Cc:**1** complex. The intensity does not increase to the original level because of partial photodegradation of MgCcP. The recovery of fluorescence suggests that receptor **1** effectively disrupts the Cc:CcP complex at nanomolar concentrations (*i.e.* ~0.08 μM), and releases CcP free into solution. Under these conditions, the interaction between **1** and Cc appears stronger than that between CcP and Cc, with a K_d value < 100 nM.

The binding constant (K_b) for Cc:**1** complex can be estimated from the competitive titration results using a standard nonlinear curve-fitting. The competition equilibrium constant K_c for eqn. (2) can be expressed [eqn. (4)] in terms of the K_b's for eqn. (1) ($K_{b1} = 2 \times 10^7$ M^{-1})[5] and for eqn. (3) (K_{b2}). Assuming that the concentration of free Cc in eqn. (3) at equilibrium is negligible, a quadratic equation can be derived as shown in eqn. (5), where $A = [Cc]_{Total}$, $B = [CcP]_{Total}$, $x = [1]_{Total}$, and $y = (I_{obs} - I_f)/(I_i - I_f)$ with I_i and I_f being the fluorescence intensities at ([Cc] + [1])/[CcP] of 1 and of ≥2, respectively. From the solution for y in eqn. (5), K_c was obtained. A set of typical results are shown in Fig. 3, from which K_{b2} was estimated to be $(3 \pm 1) \times 10^8$ M^{-1}.

$$Cc + \mathbf{1} \leftrightharpoons Cc{:}\mathbf{1} \quad (3)$$

$$K_c = K_{b2}/K_{b1} \quad (4)$$

$$(B^2K_c - B^2)y^2 + (K_cBx - ABK_c + AB + B^2)y - AB = 0 \quad (5)$$

The titration of the MgCcP solution with **1** in the absence of Cc showed little change in the fluorescence of MgCcP in the range of [1]/[MgCcP] from 0 to 5, indicating that there is no significant interaction between **1** and CcP. The region of Cc

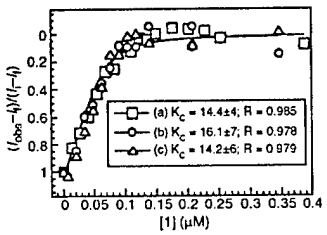

Fig. 3 Typical curve-fitting results for the fluorescence titration of 1:1 Cc:CcP complex with the receptor **1**. The values of $y = (I_{obs} - I_f)/(I_i - I_f)$ for emissions at (a) 598 nm at 15.0 °C, (b) 598 nm at 25.0 °C and (c) 653 nm at 25.0 °C are plotted against the concentration of **1**. The experimental data are fitted according eqn. (5) to estimate K_c values. Excitation at 556 nm, [MgCcP] = 0.076 μM, [Cc] = 0.077 μM in 10 mM KPhos buffer (pH 6.0).

involved in binding to CcP contains an array of positively charged residues that interacts with a complementary patch of negative residues on CcP.[4] The polyanionic receptor **1** competes successfully with CcP, presumably by binding to a similar site on the surface of Cc. The CcP molecules are freed from the interactions with Cc, leading to the observed recovery of fluorescence.

The binding of **1** with Cc has been independently confirmed by direct fluorescence titration of **1**. Receptor **1** exhibits a broad fluorescence peak at ~432–443 nm with excitation wavelength of 298 nm. Addition of Cc results in a rapid decrease in the fluorescence intensity, which levels off as Cc concentration increases. Further quantitative interpretations of such data are precluded at the present time, since the receptor molecules (**1**), due to their surfactant-like structure, tend to aggregate, which interferes with the determination of binding stoichiometry. Reducing the concentration of **1** prevents the aggregation but the decrease in fluorescence signal to noise ratio impedes quantitative analysis.

The ability to bind to Cc with high affinity is of great interest, given the major role of Cc as a signal protein for activating Apaf-1 (the apoptosis protease activating factor-1) protein in apoptosis.[6–8] The binding constant for the 2:1 Cc:Apaf-1 complex was estimated to be ~10^{11} M^{-1} from the fluorescence polarization titration measurements, in which Apaf-1 was added to nanomolar concentrations of horse heart zinc(II) Cc and the increase in polarization was monitored.[8] Upon formation of the Cc:Apaf-1 complex, receptor **1** was added to the system. At a [**1**]/[Cc:Apaf-1] molar ratio of ~200, the relative fluorescence polarization decreased significantly from 1.9 to 1.3. The preliminary data indeed suggest that **1** can disrupt the Cc:Apaf-1 interactions. More detailed results of further studies will be reported in due course.

In conclusion, we have demonstrated that the physiological complex of Cc with CcP can be disrupted by a synthetic receptor (**1**). Receptor **1** competes effectively with CcP for binding Cc, forming 1:1 Cc:**1** complex with a binding constant of ~10^8 M^{-1}. Investigation is in progress to evaluate the effects of the structure of synthetic receptors on their competitive binding with various proteins, including Apaf-1, and protein–protein complexes.

Y. Wei thanks Drexel University for granting him a sabbatical leave at Princeton University and Drs V. Lai, S. Springs and S. Hatch for many helpful discussions.

Notes and references

1 (*a*) D. W. Banner, *Nature*, 2000, **404**, 449; (*b*) W. E. Stites, *Chem. Rev.*, 1997, **97**, 1233.
2 (*a*) C. Branden and J. Tooze, *Introduction to Protein Structure*, Garland, New York, 1991, p. 187; (*b*) D. R. Davies, E. A. Padlan and S. Sheriff, *Annu. Rev. Biochem.*, 1990, **59**, 439; (*c*) H. S. Park, Q. Lin and A. D. Hamilton, *J. Am. Chem. Soc.*, 1999, **121**, 8.
3 R. A. Scott and A. G. Mauk, *Cytochrome c—A Multi-disciplinary Approach*, U. Sci. Books, Sausalito, CA, USA, 1996.
4 H. Pelletier and J. Kraut, *Science*, 1992, **258**, 1748.
5 G. McLendon, Q. Zhang, S. A. Wallin, R. M. Miller, V. Billstone, K. G. Spears and B. M. Hoffman, *J. Am. Chem. Soc.*, 1993, **115**, 3665.
6 H. Zou, W. J. Henzel, X. Liu, A. Lutschg and X. Wang, *Cell*, 1997, **90**, 405.
7 P. Li, D. Nijhawan, I. Budihardjo, S. M. Srinivasula, M. Ahmad, E. S. Alnemri and X. Wang, *Cell*, 1997, **91**, 479.
8 C. Purring, H. Zou, X. Wang and G. McLendon, *J. Am. Chem. Soc.*, 1999, **121**, 7435.
9 (*a*) M. Marjatta and P. K. Kinnunen, *Biochem.*, 1996, **35**, 4529; (*b*) T. E. Meyer, Z. G. Zhao, M. A. Cusanovich and G. Tollin, *Biochem.*, 1993, **32**, 4552; (*c*) M. Antalik, M. Bona, Z. Gazova and A. Kuchar, *Biochim. Biophys. Acta*, 1992, **1100**, 155; (*d*) D. W. Concar, D. Whitford and R. J. P. Williams, *Eur. J. Biochem.*, 1991, **199**, 553; (*e*) K. K. Clark-Ferris and J. Fisher, *J. Am. Chem. Soc.*, 1985, **107**, 5007.
10 Y. Humuro, M. C. Calama, H. S. Park and A. D. Hamilton, *Angew. Chem., Int. Ed. Engl.*, 1997, **36**, 2680.

Comptes Rendue-Submitted

Design and Synthesis of Multiple-Loop Receptors Based on a Calix[4]arene Scaffold for Protein Surface Recognition

Qing Lin and Andrew D. Hamilton*

Department of Chemistry, Yale University, New Haven, Connecticut 06520

This paper is dedicated to the memory of John A. Osborn who was an insightful scientist, an amusing companion and, in his time, an imposing centre half.

Abstract

We have recently reported a synthetic protein binding agent with four fold symmetry containing four identical peptide loops attached to the four phenyl groups of a calix[4]arene core. One of these first generation derivatives not only bound strongly to cytochrome c but also blocked its ability to interact with protein partners or simple reducing agents. In developing second generation protein binding agents with better affinity and selectivity we required a synthetic approach that would lead to a less symmetrical arrangement of the peptide loops around the core calix[4]arene scaffold. We herein report an important step in the wider application of this strategy with the preparation of a series of unsymmetrical receptors in which two different loops are attached to the core calixarene.

Introduction

Protein-protein interactions play a key role in all biological processes including cell growth and differentiation.[1] In many cases, these interactions are mediated through a large surface contact as seen in protein oligomerization and antibody-antigen complexes. The design of synthetic agents that can recognize and bind to specific regions of a protein surface should offer new approaches to the development of enzyme inhibitors[2] and protein antagonists,[3] We have recently introduced a new class of protein surface receptors in which four identical peptide loops are attached to a central calixarene scaffold.[4] The peptide loops are based around a cyclic tetrapeptide which is cyclized through a 4-aminomethyl benzoic acid group. The hydrophobic spacer provides not only a rigidification of the macrocyle but also a point of attachment through 5-amino substituents on the phenyl ring. The amine groups are then linked to the calixarene through carboxylic acid activation. The resulting design contains a concave molecular surface approximately 450-500 A^2 in area whose recognition characteristics can be readily changed by varying the sequences of the cyclic peptides as well as attaching different peptide loops.

[Insert structure 1 and Figure 1]

For example, compound **1** containing four peptide loop with the sequence Gly-Asp-Gly-Asp has a hydrophobic core comprising the calixarene and aminomethylbenzoate spacer and a hydrophilic periphery defined by the eight carboxylate groups in the peptide ring. A calculated structure for the tetra-loop derivative (Figure 1) shows the concentric arrangement of the hydrophilic and hydrophobic domains and the large surface area (~450$Å^2$) available for contact to a protein target. We have shown that this derivative

binds tightly to the cationic surface of cytochrome c and disrupts its interaction with its native protein partner, cytochrome c peroxidase.[5] The exact site on the surface of cytochrome *c* where **1** has not yet been definitively established. However, one strong possibility is the region close to the heme edge, surrounded by the group of positively charged residues (Lys-17, 18, 21, 77, 88), which forms the primary interaction surface with electron transfer partners such as cytochrome *c* oxidase and cytochrome *c* peroxidase. Docking a calculated structure for **1** with this region on the X-ray structure of cytochrome *c*[6] (Figure 2) confirms that four peptide loops can contact four of the five lysine residues and cover a large area of the protein surface. Consistant with this structure we have shown that compound **1** not only disrupts the cytochrome c/cytochrome c peroxidase complex[5] but also the approach of reducing agents to the heme edge.[7] In phosphate buffer Fe(III) cytochrome *c* (1.57×10^{-5}M) is rapidly reduced by excess ascorbate (2.0×10^{-3}M) with a pseudo first-order rate constant of 0.109 ± 0.0001 sec^{-1}. In the presence of **1** (1.91×10^{-5}M) the rate of cytochrome *c* reduction is diminished ten-fold (kobs = 0.010 ± 0.001 sec-1) in a similar manner to that seen with the cytochrome *c*-cytochrome *c* peroxidase complex.[5]

[Insert Figure 2]

The design and simple synthesis of **1** results in a protein binding agent with four fold symmetry containing four identical loops on the four phenyl groups of the calix[4]arene core. While leading to ready access of **1** in large quantities, this feature is limiting particularly since the distribution of charged and hydrophobic domains on protein surfaces in invariably irregular. We therefore needed a synthetic approach that would lead to a less symmetrical arrangement of the peptide loops around the core

scaffold. In the present paper we report an important step in the wider application of this strategy with the preparation of a series of unsymmetrical receptors in which two different loops are attached to the core calixarene (Figure 3).

[Insert Figure 3]

Results and Discussion

Calix[4]arene has been extensively used in the supramolecular chemistry due to its well-defined shape.[8] However, few examples exist in which the upper rim of calixarene has been differentially functionalized.[9] In our effort to attach two different peptide loops onto the calixarene scaffold, we envisioned that three partially protected calix[4]arene tetracarboxylic acid derivatives, such as (**2**), (**3**), (**4**), should lead to unsymmetrical receptors through sequencial coupling steps. Initial attempts to selectively protect butoxycalix[4]arene tetracarboxylic acid were unsuccessful, resulting in inseparable mixtures. However, stepwise functionalization of the upper rim of calix[4]arene could be carried out efficiently and gave all three partially protected derivatives in good yields (Scheme 1).[10] Treating butoxycalix[4]arene with 1 eq. Cl_2CHOCH_3 in the presence of 1 eq. $TiCl_4$ gave primarily mono-formylated product in 60% yield. Subsequent oxidation and protection afforded a mono-calix[4]arene carboxylester. p-Nitro benzyl ester was chosen due to its easy removal by hydrogenation after coupling to the peptide loops (Scheme 2). Further formylation with excess $TiCl_4$ and oxidation with $NaClO_2$ furnished the final product as a mono-protected butoxycalix[4]arene tetracarboxylic acid (**2**). The other scaffolds were prepared in an analogous manner. Formylation of butylcalix[4]arene with $SnCl_4$ gave a mixture of bis-formylated derivatives which could not be separated by flash chromatography. The

mixture was carried on to the bis-ester stage after which the two isomers can be easily separated by column in a 1:1.3 cis:trans ratio. The bis-acids were protected as para-nitrobenzyl ester respectively. Further formylation and oxidation afforded the final products, cis-calix[4]arene bisacid bisester (**3**) and trans-calix[4]arene bisacid bisester (**4**), which set up all three required scaffolds for our receptor constructions.

[Insert Scheme 1]

The use of the scaffold **2** for the preparation of the unsymmetrical receptors is illustrated in Scheme 2. The first coupling proceeded using a straightforward acid chloride method.[11] After removal of the para-nitrobenzyl protecting group under hydrogenation conditions, the acid was converted to a Yamaguchi type anhydride[12], and subsequently reacted with the second peptide loop to give the fully protected calix[4]arene tetra-cyclic peptide receptor. Removal of the protecting groups by TFA treatment gave the final product. A series of X-3-XYZW-1-X′Y′Z′W′ receptors were prepared in good yields by this route (Table 1).

[Insert Scheme 2]

Similar routes were sucessfully performed on the preparations of cis-A2B2 and trans-A2B2 types of receptors (Scheme 3).

[Insert Scheme 3 and Table 1]

In summary, we have developed an efficient route for stepwise functionalizations of the upper rim of calix[4]arene. It should be noted that functional groups other than carboxylate can also be incorporated into the synthetic scheme. A series of unsymmetrical receptors based on partially protected calix[4]arene tetra-carboxylic acid

was thus contructed. The biological testing of unsymmetrical receptors for various protein targets is underway and will be reported in due course.

Experimental Details

Butoxycalix[4]arene mono carboxylic acid

A 50 mL round flask was charged Cl_2CHOCH_3 (98 μL, 1.08 mmol), butoxycalix[4]arene (0.636 g, 0.98 mmol) and dry CH_2Cl_2 (20 mL), and the solution was cooled to -10 °C. $TiCl_4$ (0.13 mL, 1.19 mmol) was added and the mixture was stirred at -10 °C → -5 °C for 1 hr. The reaction was quenched with 50 mL H_2O, and the organic layer was separated and dried over Na_2SO_4. After evaporation, the residue was purified by flash chromatography (SiO_2, 5% EtOAc/Hexane) to give the monoaldehyde as an oil (0.393 g, 60%): ^{1}H NMR ($CDCl_3$, 500 MHz) δ 9.60 (s, 1H), 7.03 (s, 2H), 6.77 (m, 4H), 6.71 (m, 2H), 6.44 (m, 3H), 4.52 (d, J = 13.6 Hz, 2H), 4.47 (d, J = 13.4 Hz, 2H), 3.97 (m, 4H), 3.94 (m, 6H), 3.92 (m, 2H), 3.26 (d, J = 13.6 Hz, 2H), 3.19 (d, J = 13.5 Hz, 2H), 1.91 (m, 8H), 1.53 (m, 4H), 1.44 (m, 4H), 1.05 (m, 12H); ^{13}C NMR ($CDCl_3$, 125 MHz) δ 191.7, 162.0, 156.7, 156.2, 136.0, 135.8, 134.7, 134.6, 130.9, 130.0, 128.8, 128.2, 127.9, 122.2, 121.8, 75.0, 74.8(2), 32.4, 32.3(2), 32.2, 30.9, 30.7, 19.6, 19.4, 19.3, 19.2, 14.1, 14.0, 13.9; To the solution of the aldehyde (0.39 g, 0.58 mmol) in 10 mL CH_2Cl_2 and 30 mL Acetone was added H_2NSO_3H (0.60 g, 6.2 mmol) in 5 mL H_2O and $NaClO_2$ (0.64 g, 5.8 mmol) in 5 mL H_2O, and the mixture was stirred at r.t. overnight. The organic solvents were then removed under reduced pressure and the aqueous solution was extracted with CH_2Cl_2. The organic layer was separated and dried over Na_2SO_4. After evaporation, the

residue was puried by flash chromatography (SiO_2, 3% MeOH / CH_2Cl_2) to give the final product as a white powder (0.260 g, 65%): mp 187-188°C; ^{1}H NMR ($CDCl_3$, 300 MHz) δ 11.13 (s, b, 1H), 7.36 (s, 2H), 6.67 (m, 6H), 6.53 (m, 3H), 4.49 (d, J = 13.5 Hz, 2H), 4.46 (d, J = 13.2 Hz, 2H), 4.00 (t, J = 7.2 Hz, 2H), 3.90 (m, 6H), 3.24 (d, J = 13.5 Hz, 2H), 3.18 (d, J = 13.5 Hz, 2H), 1.95 (m, 8H), 1.48 (m, 8H), 1.03 (m, 12H); ^{13}C NMR ($CDCl_3$, 75 MHz) δ 172.3, 161.5, 156.3, 135.4, 135.2, 134.8, 134.2, 130.3, 128.3, 128.0, 127.9, 122.5, 122.0, 121.7, 74.7, 74.6, 32.1, 30.7, 19.1, 13.9(2); HR FAB-MS *m/e* calcd for $C_{45}H_{56}O_6$ 692.4077 $[M]^+$, found 692.4079.

Butoxycalix[4]arene mono carboxylic acid 4-nitrobenzyl ester

To a solution of Butoxycalix[4]arene mono carboxylic acid (0.255 g, 0.37 mmol) in 20 mL dry CH_2Cl_2 was added oxalylic chloride (0.40 mL, 4.4 mmol) and catalytic amount of DMF (0.4 μL), and the mixture was stirred at r.t. overnight. The solvent and excess reagent were removed in vacuo and the residue was redissolved in 10 mL dry CH_2Cl_2, 4-Nitrobenzyl alcohol (0.58 g, 3.8 mmol) and DIEA (0.2 mL, 1.1 mmol) were added to above solution, and the mixture was stirred at r.t. overnight. The solvent was evaporated and the residue was purified by flash chromatography to give the title compound as a white powder (0.227 g, 75%): mp 57-58°C; ^{1}H NMR ($CDCl_3$, 300 MHz) δ 8.27 (d, J = 8.7 Hz, 2H), 7.50 (d, J = 8.7 Hz, 2H), 7.22 (s, 2H), 6.76 (m, 6H), 6.40 (d, J = 7.5 Hz, 2H), 6.22 (t, J = 7.5 Hz, 1H), 5.34 (s, 2H), 4.48 (d, J = 12.9 Hz, 2H), 4.44 (d, J = 12.3 Hz, 2H), 3.98-3.82 (m, 8H), 3.22 (d, J = 13.5 Hz, 2H), 3.16 (d, J = 13.5 Hz, 2H), 1.89 (m, 8H), 1.46 (m, 8H), 1.01 (m, 12H); ^{13}C NMR ($CDCl_3$, 75 MHz) δ 165.9, 161.0, 156.8, 156.3, 147.5, 143.9, 135.8, 135.4, 134.9, 134.7, 129.8, 128.6, 128.3, 127.8, 123.7, 122.8, 122.0,

121.5, 74.9, 74.8, 64.3, 32.3, 32.2, 30.9, 19.4, 19.3, 19.2, 14.1, 14.0(2); HR FAB-MS *m/e* calcd for $C_{52}H_{62}NO_6$ 828.4475 $[M+H]^+$, found 828.4476.

Butoxycalix[4]arene mono-4-nitrobenzyl carboxylate tris-carboxylic acid (2)

The solution of Butoxycalix[4]arene mono carboxylic acid 4-nitrobenzyl ester (0.226 g, 0.27 mmol), dichloromethyl methyl ether (0.30 mL, 3.3 mmol) in 20 mL dry CH_2Cl_2 was cooled to -10 °C, and $TiCl_4$ (0.40 mL, 3.65 mmol) was added. The mixture was stirred overnight while warming up to r.t. The reaction was then quenched with 20 mL 1.0 N HCl and the organic layer was separated and dried over Na_2SO_4. After evaporation of solvents, the residue was purified by flash chromatography (SiO_2, 30% EtOAc/Hexane) to give the trisaldehyde as a white foam (0.193 g, 78%): ^{1}H NMR ($CDCl_3$, 300 MHz) δ 9.62 (s, 2H), 9.55 (s, 1H), 8.24 (d, J = 8.7 Hz, 2H), 7.53 (d, J = 8.7 Hz, 2H), 7.30 (s, 2H), 7.22 (s, 4H), 7.12 (s, 2H), 5.32 (s, 2H), 4.52 (d, J = 7.8 Hz, 2H), 4.47 (d, J = 7.8 Hz, 2H), 3.97 (m, 8H), 3.37 (d, J = 9.6 Hz, 2H), 3.32 (d, J = 9.6 Hz, 2H), 1.88 (m, 8H), 1.45 (m, 8H), 1.01 (t, J = 7.2 Hz, 12H); To above aldehyde in 6 mL CH_2Cl_2 and 18 mL Acetone was added H_2NSO_3H (0.30 g, 3.1 mmol) in 2 mL H_2O and $NaClO_2$ (0.32 g, 2.9 mmol) in 2 mL H_2O, and the mixture was stirred at r.t. overnight. The organic solvents were then removed under reduced pressure and the precipitate was filtered off and dried in vacuo to give the title compound as an off-white powder (0.173 g, 85%): mp >300°C (dec.); ^{1}H NMR (DMSO-d_6, 500 MHz) δ 8.22 (d, J = 7.9 Hz, 2H), 7.73 (s, 2H), 7.71 (s, 2H), 7.47 (d, J = 8.2 Hz, 2H), 6.89 (s, 2H), 6.88 (s, 2H), 5.20 (s, 2H), 4.36 (d, J = 6.0 Hz, 2H), 4.34 (d, J = 5.7 Hz, 2H), 4.06 (m, 4H), 3.79 (t, J = 6.5 Hz, 2H), 3.76 (t, J = 6.7 Hz, 2H), 3.42

(d, J = 12.6 Hz, 2H), 3.40 (d, J = 12.8 Hz, 2H), 1.86 (m, 8H), 1.57 (m, 4H), 1.33 (m, 4H), 0.97 (m, 12H); LR FAB-MS *m/e* calcd for $C_{55}H_{61}NO_{14}$ 959.4 $[M]^+$, found 959.5.

trans-Butoxycalix[4]arene bis(4-nitrobenzylcarboxylate) (A); cis-Butoxycalix[4]arene bis(4-nitrobenzylcarboxylate) (B)

To a 100 mL flask was charged butoxycalix[4]arene (1.35 g, 2.1 mmol), Cl_2CHOCH_3 (0.76 mL, 8.4 mmol) and 50 mL dry CH_2Cl_2, and the solution was cooled to -10 °C. $SnCl_4$ (1.0 M in CH_2Cl_2, 8.4 mL, 8.4 mmol) was added and the mixture was stirred at -10 °C for 30 min. The reaction was then quenched with 30 mL H_2O, and the organic layer was separated and dried over Na_2SO_4. After evaporation of solvents, the residue was purified by flash chromatography (SiO_2, 10% EtOAc/Hexane) to give the bis-aldehyde as an oil (0.76 g, 52%). To the solution of the aldehyde (0.76 g, 1.1 mmol) in 20 mL CH_2Cl_2 and 60 mL Acetone was added H_2NSO_3H (0.90 g, 9.3 mmol, dissolved in 5 mL H_2O) and $NaClO_2$ (0.96 g, 8.7 mmol, dissolved in 5 mL H_2O), and the mixture was stirred at r.t. overnight. The organic solvents were then removed under reduced pressure and the precipitate was filtered off and dried in vacuo to give the mixed cis and trans biscarboxylic acid product as a white powder (0.78 g, 98%): mp > 290°C (dec.); LR FAB-MS *m/e* calcd for $C_{46}H_{56}O_8$ 736.4 $[M]^+$, found 736.3. To a solution of Butoxycalix[4]arene bis-carboxylic acid (0.780 g, 1.06 mmol) in 30 mL dry CH_2Cl_2 was added oxalylic chloride (0.80 mL, 9.2 mmol) and catalytic amount of DMF (0.2 μL), and the mixture was stirred at r.t. overnight. The solvent and excess reagent were removed in vacuo and the residue was redissolved in 30 mL dry CH_2Cl_2. 4-Nitrobenzyl alcohol (0.86 g, 5.6 mmol) and DIEA (0.6 mL, 3.3 mmol) were added to above solution,

and the mixture was stirred at r.t. overnight. The solvent was evaporated and the residue was applied to a flash chromatography to give the trans- (**A**) and cis- (**B**) title compounds: **A** (0.244 g, 23%); ^{1}H NMR ($CDCl_3$, 500 MHz) δ 8.27 (d, J = 8.6 Hz, 4H), 7.54 (d, J = 8.5 Hz, 4H), 7.35 (s, 4H), 6.69 (m, 6H), 5.32 (s, 4H), 4.48 (d, J = 13.5 Hz, 4H), 3.95 (m, 8H), 3.24 (d, J = 13.6 Hz, 4H), 1.90 (m, 8H), 1.47 (m, 8H), 1.02 (m, 12H); ^{13}C NMR ($CDCl_3$, 75 MHz) δ 165.9, 161.3, 156.6, 147.6, 144.0, 135.6, 134.8, 130.0, 128.6, 128.3, 123.8, 122.9, 122.3, 75.2, 75.1, 64.8, 32.4, 32.3, 31.0, 19.4, 14.2, 14.1; LR FAB-MS *m/e* calcd for $C_{46}H_{56}O_8$ 736.4 $[M]^+$, found 736.3; **B** (0.312 g, 29%): ^{1}H NMR ($CDCl_3$, 500 MHz) δ 8.24 (d, J = 8.4 Hz, 4H), 7.51 (d, J = 8.4 Hz, 4H), 7.37 (s, 2H), 7.36 (s, 2H), 6.55 (d, J = 7.4 Hz, 2H), 6.54 (d, J = 7.3 Hz, 2H), 6.39 (t, J = 7.4 Hz, 2H), 5.37 (s, 4H), 4.50 (d, J = 13.8 Hz, 1H), 4.46 (d, J = 13.7 Hz, 2H), 4.42 (d, J = 13.6 Hz, 1H), 4.01-3.83 (m, 8H), 3.29 (d, J = 13.8 Hz, 1H), 3.22 (d, J = 13.7 Hz, 2H), 3.15 (d, J = 13.6 Hz, 1H), 1.87 (m, 8H), 1.45 (m, 8H), 1.00 (m, 12H); ^{13}C NMR ($CDCl_3$, 125 MHz) δ 165.9, 161.4, 156.6, 147.6, 143.8, 136.0, 135.3, 135.1, 134.4, 130.3, 129.9, 128.5, 128.1, 127.9, 123.8, 123.0, 121.8, 75.0, 74.9, 64.6, 32.3, 31.0 (2), 19.3 (2), 14.0 (2); LR FAB-MS *m/e* calcd for $C_{46}H_{56}O_8$ 736.4 $[M]^+$, found 736.3.

cis-Butoxycalix[4]arene bis(4-nitrobenzylcarboxylate) biscarboxylic acid (3)

To a 250 mL flask was charged cis-Butoxycalix[4]arene bis(4-nitrobenzylcarboxylate) (0.422 g, 0.42 mmol), dichloromethyl methyl ether (0.33 mL, 3.7 mmol) and 30 mL dry CH_2Cl_2, and the solution was cooled to -10 °C. $TiCl_4$ (0.40 mL, 3.7 mmol) was added and the mixture was stirred at -10 °C → r.t. overnight. The reaction was quenched with 10 mL 1.0 N HCl, and the organic layer was separated and dried over Na_2SO_4. The solvent

was evaporated and the residue was purified by flash chromatography (SiO_2, 30% EtOAc / Hexane) to give the aldehyde as an oil (0.270 g, 61%); The aldehyde was dissolved in 15 mL CH_2Cl_2 and 45 mL Acetone. H_2NSO_3H (0.45 g, 4.7 mmol, dissolved in 3 mL H_2O) and $NaClO_2$ (0.48 g, 4.4 mmol, dissolved in 3 mL H_2O) were then added to the solution and the mixture was stirred at r.t. overnight. The organic solvents were removed under reduced pressure and the precipitate was filtered off and dried in vacuo to give the title compound as a yellow powder (0.245 g, 88%): mp 168-170°C; ^{1}H NMR (DMSO-d_6, 500 MHz) δ 8.19 (d, J = 7.2 Hz, 4H), 7.57 (d, J = 7.6 Hz, 4H), 7.37 (s, 2H), 7.35 (s, 2H), 7.30 (s, 4H), 5.34 (s, 4H), 4.35 (m, 4H), 3.92 (m, 8H), 3.43 (m, 4H), 1.85 (m, 8H), 1.44 (m, 8H), 0.97 (m, 12H);); LR FAB-MS *m/e* calcd for $C_{62}H_{66}N_2O_{16}$ 1095.2 $[M]^+$, found 1094.5.

trans-Butoxycalix[4]arene bis(4-nitrobenzylcarboxylate) biscarboxylic acid (4)

The solution of trans-Butoxycalix[4]arene bis(4-nitrobenzylcarboxylate) (0.231 g, 0.23 mmol), dichloromethyl methyl ether (0.18 mL, 2.0 mmol) in 20 mL dry CH_2Cl_2 was cooled to -10 °C. $TiCl_4$ (0.22 mL, 2.0 mmol) was added and the mixture was stirred at -10 °C → r.t. overnight. The reaction was quenched with 10 mL 1.0 N HCl, and the organic layer was separated and dried over Na_2SO_4. After evaporation of solvents, the residue was purified by flash chromatography (SiO_2, 25% EtOAc / Hexane, then 30% EtOAc / Hexane) to give the aldehyde (0.170 g, 70%); ^{1}H NMR ($CDCl_3$, 300 MHz) δ 9.38 (s, 2H), 8.27 (d, J = 8.1 Hz, 4H), 7.65 (s, 4H), 7.61 (d, J = 8.7 Hz, 4H), 6.89 (s, 4H), 5.42 (s, 4H), 4.49 (d, J = 13.5 Hz, 4H), 4.05 (t, J = 7.5 Hz, 4H), 3.88 (t, J = 6.9 Hz, 4H), 3.33 (d, J = 13.8 Hz, 4H), 1.87 (m, 8H), 1.51 (m, 4H), 1.36 (m, 4H), 1.02 (t, J = 6.8 Hz,

6H), 0.99 (t, J = 6.9 Hz, 6H); To the solution of the aldehyde in 12 mL CH_2Cl_2 and 36 mL Acetone was added H_2NSO_3H (0.45 g, 4.7 mmol, dissolved in 3 mL H_2O) and $NaClO_2$ (0.48 g, 4.4 mmol, dissolved in 3 mL H_2O), and the mixture was stirred at r.t. overnight. The organic solvents were removed under reduced pressure and the precipitate was filtered off and dried in vacuo to give the title compound as a white powder (0.123 g, 70%): mp 300-305°C; ^{1}H NMR (DMSO-d_6, 300 MHz) δ 8.18 (d, J = 8.7 Hz, 4H), 7.85 (s, 4H), 7.41 (d, J = 8.7 Hz, 4H), 6.85 (s, 4H), 5.12 (s, 4H), 4.36 (d, J = 13.5 Hz, 4H), 4.10 (t, J = 8.0 Hz, 4H), 3.76 (t, J = 6.2 Hz, 4H), 3.45 (d, J = 13.8 Hz, 4H), 1.85 (m, 8H), 1.59 (m, 4H), 1.30 (m, 4H), 0.99 (t, J = 7.5 Hz, 6H), 0.96 (t, J = 7.5 Hz, 6H);); LR FAB-MS *m/e* calcd for $C_{62}H_{66}N_2O_{16}$ 1095.2 $[M]^+$, found 1094.4.

General procedure for preparation of A3B type receptors

5,11,17-Tris(*cyclo*-GDDDSp)-23-*cyclo*-GDGYSp-25,26,27,28-tetrakis(butoxy)calix[4]arene

A solution of **1** (6.4 mg, 0.0067 mmol), $(COCl)_2$ (20 μL, 0.23 mmol), DMF (0.1 μL) in 2.0 mL dry CH_2Cl_2 was stirred at r.t. overnight. The solution was evaporated to dryness and the residue was then redissolved in 2.0 mL dry CH_2Cl_2. To the solution was added *cyclo*-GD^{p}D^{p}D^{p}Sp-NH_2 (13.8 mg, 0.02 mmol), DIEA (8.0 μL, 0.046 mmol), and the mixture was stirred at r.t. for 20 hr. The solvent was then removed by evaporation and the residue was purified by gel filtration (Sephadex LH-20, CH_2Cl_2 as eluent) to give a white solid (20 mg, 100%). The solid was then dissolved in 5 mL MeOH, and the solution was added 10% Pd/C (15.0 mg, 0.014 mmol) and stirred under H_2 atmosphere for 12 hr. After TLC showed the disappearance of S.M., the catalyst was removed by

filtration through celite and the solution was collected and evaporated. The residue was purified by gel filtration (Sephadex LH-20, CH_2Cl_2 as eluent) to afford tris-loop mono-acid product (11.3 mg, 60% for three steps). The monoacid was dissolved in 1 mL dry THF, and the solution was added 2,4,6-trichlorobenzyl chloride (1.0 μL, 0.006 mmol), TEA (1.0 μL) and the mixture was stirred at r.t. 2 hr. The solvent and reagents were removed in vacuo and the residue was dissolved in 2.0 mL dry CH_2Cl_2. To the solution was added *cyclo*-GD^{P}GY^{P}Sp-NH_2 (7.5 mg, 0.012 mmol), DMAP (2.0 mg, 0.016 mmol), and the mixture was stirred at r.t. for 4 hr. The solvent was then removed by evaporation and the residue was purified by gel filtration (Sephadex LH-20, CH_2Cl_2 as eluent) to give the fully protected product as a white solid (10.8 mg). Further treatment of the product with 25% TFA/ CH_2Cl_2 for 1.5 hr afforded the title compound as a white solid (8.8 mg, 75% for three steps): Anal HPLC showed a single peak; ES-MS *m/e* calcd for $C_{139}H_{154}N_{24}O_{49}$ $[M]^-$ 2944.82, found 2925.50 ± 0.55.

5,11,17-Tris(*cyclo*-GDGYSp)-23-carboxylic acid-25,26,27,28-tetrakis(butoxy)calix[4]arene

ES-MS *m/e* calcd for $C_{123}H_{134}N_{18}O_{33}$ $[M]^-$ 2392.45, found 2393.6.

5,11,17-Tris(*cyclo*-GDGYSp)-23-*cyclo*-GDDGSp-25,26,27,28-tetrakis(butoxy)calix[4]arene

ES-MS *m/e* calcd for $C_{143}H_{156}N_{24}O_{41}$ $[M]^-$ 2866.88, found 2867.37 ± 0.46.

5,11,17-Tris(*cyclo*-GDGYSp)-23-*cyclo*-GDDYSp-25,26,27,28-tetrakis(butoxy)calix[4]arene

ES-MS *m/e* calcd for $C_{150}H_{162}N_{24}O_{42}$ $[M]^-$ 2973.00, found 2973.75 ± 0.87.

5,11,17-Tris(*cyclo*-GDGYSp)-23-*cyclo*-GDDDSp-25,26,27,28-tetrakis(butoxy)calix[4]arene

ES-MS *m/e* calcd for $C_{145}H_{158}N_{24}O_{43}$ $[M]^-$ 2924.91, found 2926.01 ± 0.31.

5,11,17-Tris(*cyclo*-GDDDSp)-23-*cyclo*-GDGYSp-25,26,27,28-tetrakis(butoxy)calix[4]arene

ES-MS *m/e* calcd for $C_{139}H_{154}N_{24}O_{49}$ $[M]^-$ 2944.82, found 2925.50 ± 0.55.

5,11,17-Tris(*cyclo*-GDGDSp)-23-*cyclo*-GDDYSp-25,26,27,28-tetrakis(butoxy)calix[4]arene

ES-MS *m/e* calcd for $C_{135}H_{150}N_{24}O_{45}$ $[M]^-$ 2828.75, found 2828.74 ± 0.45.

5,11,17-Tris(*cyclo*-GDGDSp)-23-*cyclo*-GDGYSp-25,26,27,28-tetrakis(butoxy)calix[4]arene

ES-MS *m/e* calcd for $C_{133}H_{148}N_{24}O_{43}$ $[M]^-$ 2770.71, found 2771.22 ± 1.30.

General procedure for preparation of A2B2 type receptors

5,11-Bis(cyclo-GDDGSp)-17,23-bis(cyclo-GDDYSp)-25,26,27,28-tetrakis(butoxy)calix[4]arene

A solution of **2** (11.2 mg, 0.011 mmol), $(COCl)_2$ (30 μL, 0.35 mmol), DMF (0.1 μL) in dry CH_2Cl_2 (2.0mL) was stirred at r.t. overnight. The solution was evaporated and dried. The residue was redissolved in dry CH_2Cl_2 (2.0 mL), and added *cyclo*-GD^{p}D^{p}GSp-NH_2 (16.0 mg, 0.026 mmol), DIEA (10 μL, 0.058 mmol) and stirred at r.t. for 20 hr. The mixture was then applied to a Sephadex LH-20 column with CH_2Cl_2 eluent, and the product was collected and applied to flash chromatography (SiO_2,10% MeOH/ CH_2Cl_2) to give a white solid (12.7 mg). The solid was redissolved in MeOH (5 mL), added 10% Pd/C (15.0 mg, 0.014 mmol), and stirred under H_2 atmosphere for 8 hr. After TLC showed the disappearance of S.M., the catalyst was removed by filtration through celite and the solution was collected and evaporated to dryness. The residue was applied to Sephadex LH-20 column to give bis-acid intermediate (7.0 mg, 33% for three steps). The bis-acid was dissolved in 2mL dry THF, and the solution was added 2,4,6-trichlorobenzyl chloride (4.0 μL, 0.024 mmol), DIEA (5.0 μL) and the mixture was stirred at r.t. for 2 hr. The solution was then evaporated and dried in vacuo. The residue was dissolved in dry CH_2Cl_2 (2.0 mL) and to the solution was added *cyclo*-GD^{p}D^{p}Y^{p}Sp-NH_2 (20.0 mg, 0.026 mmol), DMAP (5.0 mg, 0.04 mmol). The mixture was stirred at r.t. overnight. The solution was then applied to a Sephadex LH-20 column with CH_2Cl_2 as the eluent. The appropriate portion was collected to give the fully protected product as a white solid (8.0 mg). Further treatment with 25% TFA/CH_2Cl_2 (4 mL) for 2 hr afforded the title compound as a white solid (6.0 mg, 58% for three steps): Anal HPLC showed a single peak; ES-MS *m/e* calcd for $C_{142}H_{156}N_{24}O_{46}$ $[M]^-$ 2934.87, found 2935.78.

5,17-Bis(cyclo-GDGYSp)-11,23-bis(cyclo-GDDGSp)-25,26,27,28-tetrakis(butoxy)calix[4]arene

A solution of **3** (8.0 mg, 0.017 mmol), $(COCl)_2$ (20 μL, 0.23 mmol), DMF (0.1 μL) in dry CH_2Cl_2 (2.0mL) was stirred at r.t. overnight. The solution was evaporated to dryness and the residue was then redissolved in 2.0 mL dry CH_2Cl_2. To the solution was added *cyclo*-GD^{p}D^{p}GSp-NH_2 (25.0 mg, 0.041 mmol), DIEA (8.0 μL, 0.046mmol) and stirred at r.t. for 20 hr. The mixture was applied first to a gel filtration column (Sephadex LH-20, CH_2Cl_2), then a silica gel column (10% MeOH/ CH_2Cl_2) to give a white solid (13.5 mg). The solid was then dissolved in 5 mL MeOH, and the solution was added 10% Pd/C (15.0 mg, 0.014 mmol) and stirred under H_2 atmosphere for 8 hr. After TLC showed the disappearance of S.M., the catalyst was removed by filtration through celite and the solution was collected and evaporated. The residue was purified by gel filtration (Sephadex LH-20, CH_2Cl_2 as eluent) to give the bis-acid product (18.4 mg, 61% for three steps). The product was dissolved in dry THF (2 mL), and the solution was added 2,4,6-trichlorobenzyl chloride (4.0 μL, 0.024 mmol), DIEA (5.0 μL) and the mixture was stirred at r.t. for 2.5 hr. The solution was then evaporated and dried in vacuo. The residue was dissolved in2.0 mL dry CH_2Cl_2 and the solution was added *cyclo*-GD^{p}GY^{p}Sp-NH_2 (20.0 mg, 0.031 mmol), DMAP (6.0 mg, 0.048 mmol). The mixture was stirred at r.t. overnight. The solution was then applied to a Sephadex LH-20 column with CH_2Cl_2 as the eluent. The appropriate portion was collected to give the fully protected product as a white solid (10.8 mg). Further treatment of the solid with 25% TFA/ CH_2Cl_2 (4 mL) for 2 hr afforded the title compound as a white solid (12.4 mg, 42%

for three steps): Anal HPLC showed a single peak; ES-MS *m/e* calcd for $C_{138}H_{152}N_{24}O_{42}$ $[M]^-$ 2818.80, found 2818.79 ± 0.72.

Acknowledgement.

We thank the National Institutes of Health (GM35208) and the US Army (DAMD17-99-1-9458) for financial support of this work.

References

1. Stites, W.E. *Chem. Rev.* **1997**, *97*, 1233-1250. Toogood, P. *J. Med. Chem.* **2002**, *45*, 00-00.

2. Tilley, J.W.; Chen, L.; Fry, D.C.; Emerson, S.D.; Powers, G.D. et al. *J. Am. Chem. Soc.* **1997**, *119*, 7589-7590.

3. Zutshi, R.; Franciskovich, J.; Shultz, M.; Schweitzer, B.; Bishop, P.; Wilson, M.; Chmielewski, J., *J. Am. Chem. Soc.* **1997**, *119*, 4841-4845.

4. Park, H.S.; Lin, Q.; Hamilton, A.D. *J. Am. Chem. Soc.* **1999**, *121*, 8-13.

5. Wei, Y.; McLendon, G. L.; Hamilton, A. D.; Case, M. A.; Purring, C. B.; Lin, Q.; Hyung Soon Park, Chang-Sun Lee, Tianning Yu. *J. Chem. Soc. Chem. Commun*, **2001**, 1580-1581.

6. Pelletier, H.; Kraut, J. *Science* **1992**, *258*, 1748-1755.

7. Hamuro, Y.; Calama, M. C.; Park, H. S.; Hamilton, A. D. *Angew. Chemie Int. Ed. Engl,* **1997**, *36*, 2680-2683.

8. For reviews, see: (a) Gutsche, C.D. Calixarenes Revisited. In Monographs in Supramolecular Chemistry; Stoddart, J.F., Ed.; Royal Society of Chemistry, London, **1998**. (b) Bohmer, V. *Angew. Chem. Int. Ed. Engl.* **1995**, *34*, 713-745.

9. For a few examples, see: (a) Pinkhassik, E.; Stibor, I.; Casnati, A.; Ungaro, R. *J. Org. Chem.* **1997**, *62*, 8654-8659. (b) Kanamathareddy, S.; Gutsche, C.D. *J. Am. Chem. Soc.* **1998**, *120*, 12226-12231. (c) Timmerman P.; Verboon, W.; Reinhoudt, D.N.; Arduini, A.; Grandi, S.; Sicui, A.R.; Pochini, A.; Ungaro, R. *Synthesis* **1994**, 185. (d) Arduini, A.; McGregor, W.M.; Pochini, A.; Secchi, A.; Ugozzoli, F.; Ungaro, R. *J. Org. Chem.* **1996**,

61, 6881-6887. (e) Arduini, A.; mirone, L.; Paganuzzi, D.; Pinalli, A.; Pochini, A.; Secchi, A.; Ungaro, R. *Tetrahedron*, **1996**, *52*, 6011-6018.

10 Arduini, A.; Fanni, S.; Manfredi, G.; Pochini, A.; Ungaro, R.; Sicuri, A.R.; Ugozzoli, F. *J. Org. Chem.* **1995**, *60*, 1448-1453.

11. For synthesis of cyclic peptides, see: Lin, Q.; Park, H.S.; Hamuro, Y.; Lee, C.S.; Hamilton, A.D. *Biopolymers (Peptide Science)* **1998**, *47*, 285-297.

12 Inanaga, J.; Hirata, K.; Saeki, H.; Katsuki, T.; Yamaguchi, M. *Bull. Chem. Soc. Jpn.* **1979**, *52*, 1989-1993.

Table 1 Unsymmetrical Receptors.

sequence	yield	molecular weight	
		expected($M+H^+$)	determined(ES-MS)
X-3(GDDD)-GDGY	45%	2945.82	2925.50 ± 0.55
X-3(GDGY)-GDDG	45%	2867.88	2867.37 ± 0.46
X-3(GDGY)-GDDY	52%	2974.00	2973.75 ± 0.87
X-3(GDGY)-GDDD	51%	2925.91	2926.01 ± 0.31
X-3(GDGD)-GDGY	43%	2771.71	2771.22 ± 1.30
X-3(GDGD)-GDDD	57%	2781.65	?
X-3(GDGD)-GDDY	54%	2829.75	2828.74 ± 0.45
trans-X-2(GDDG)-2(GDGY)	26%	2819.80	2818.79 ± 0.72
cis-X-2(GDDG)-2(GDDY)	19%	2935.88	2935.62 ± 0.07

Figure Captions

Figure 1 The calculated structure for tetra-loop calixarene derivative **1**,

Figure 2 The calculated complex structure between cytochrome *c* and compound **1**, the contacting basic residues of cytochrome *c* are shown in polytube model.

Figure 3. Design of unsymmetrical ligands based on a calix[4]arene scaffold.

Scheme 1. a) 1 eq. Cl_2CHOCH_3, 1 eq. $TiCl_4$, CH_2Cl_2, -10°C; b)$NaClO_2$, H_2NSO_3H, CH_2Cl_2, Acetone, H_2O; c) $(COCl)_2$, cat. DMF, CH_2Cl_2; d) *p*-nitrobenzyl alcohol, DIEA, CH_2Cl_2; e) Cl_2CHOCH_3, $TiCl_4$ (excess), CH_2Cl_2, -10°C; f) Cl_2CHOCH_3, $SnCl_4$, CH_2Cl_2, -10°C.

Scheme 2. a) $(COCl)_2$, cat. DMF, CH_2Cl_2; b) cyclo-(Gly-Asp(O^tBu)-Asp(O^tBu)-Asp(O^tBu)-Spc)-NH_2, DIEA, CH_2Cl_2; c) 10% Pd/C, H_2, MeOH; d) 2,4,6-trichlorobenzol chloride, TEA, THF; e) cyclo-(Gly-Asp(O^tBu)-Gly-Tyr(O^tBu)-Spc)-NH_2, DMAP, Benzene/CH_2Cl_2; f) 25% TFA/ CH_2Cl_2.

Scheme 3. a) $(COCl)_2$, cat. DMF, CH_2Cl_2; b) *cyclo*-(Gly-Asp(O^tBu)-Asp(O^tBu)-Gly-Spc)-NH_2, DIEA, CH_2Cl_2; c) 10% Pd/C, H_2, MeOH; d) 2,4,6-trichlorobenzol chloride, TEA, THF; e) *cyclo*-(Gly-Asp(O^tBu)- Asp(O^tBu)-Tyr(O^tBu)-Spc)-NH_2, DMAP, Benzene/CH_2Cl_2; f) 25% TFA/CH_2Cl_2; g)) *cyclo*-(Gly-Asp(O^tBu)-Gly-Tyr(O^tBu)-Spc)-NH_2, DMAP, CH_2Cl_2.

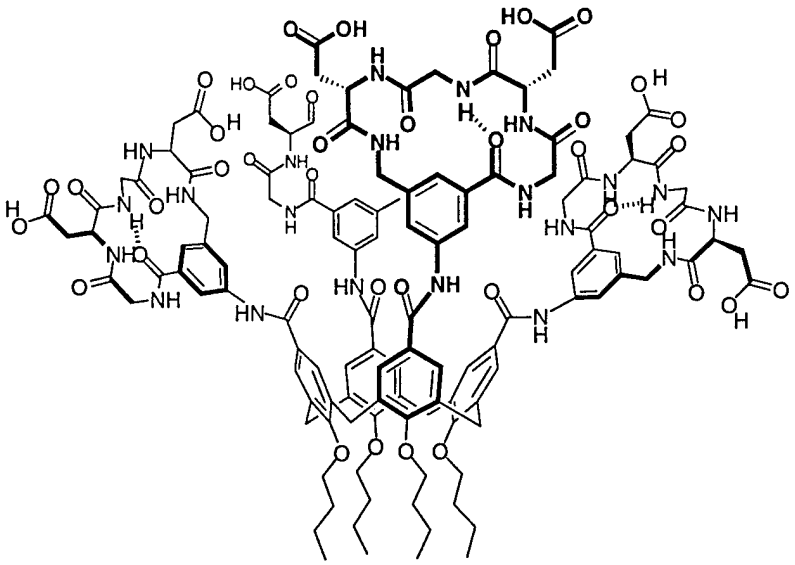

1

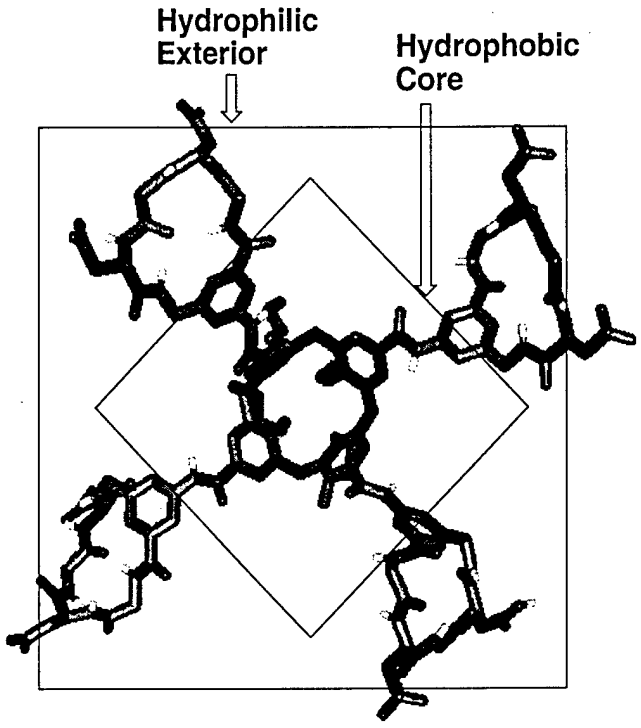

Figure 1 The calculated structure for tetra-loop calixarene derivative **1**,

Figure 2 The calculated complex structure between cytochrome *c* and compound **1**, the contacting basic residues of cytochrome *c* are shown in polytube model.

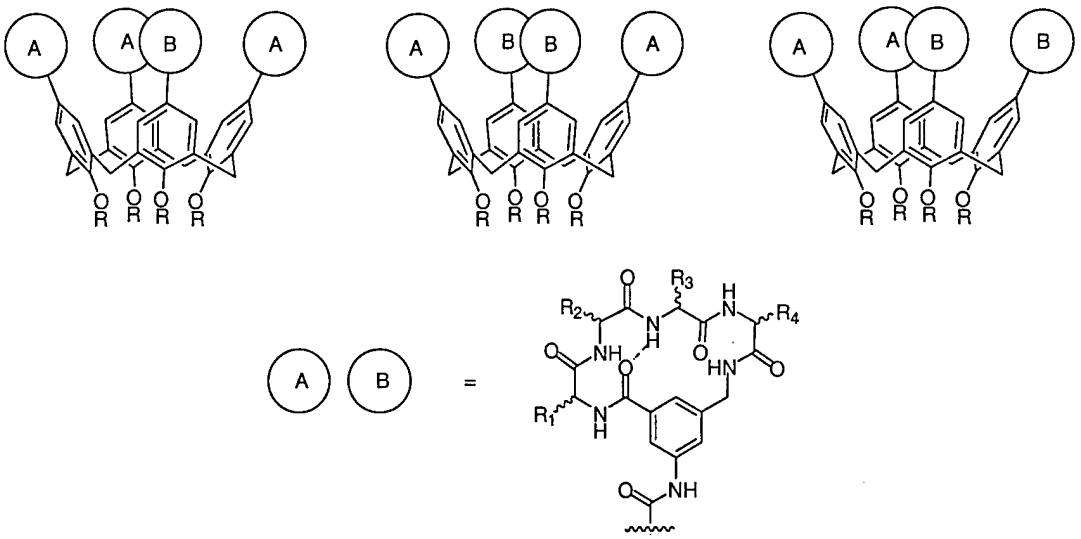

Figure 3. Design of unsymmetrical ligands based on a calix[4]arene scaffold.

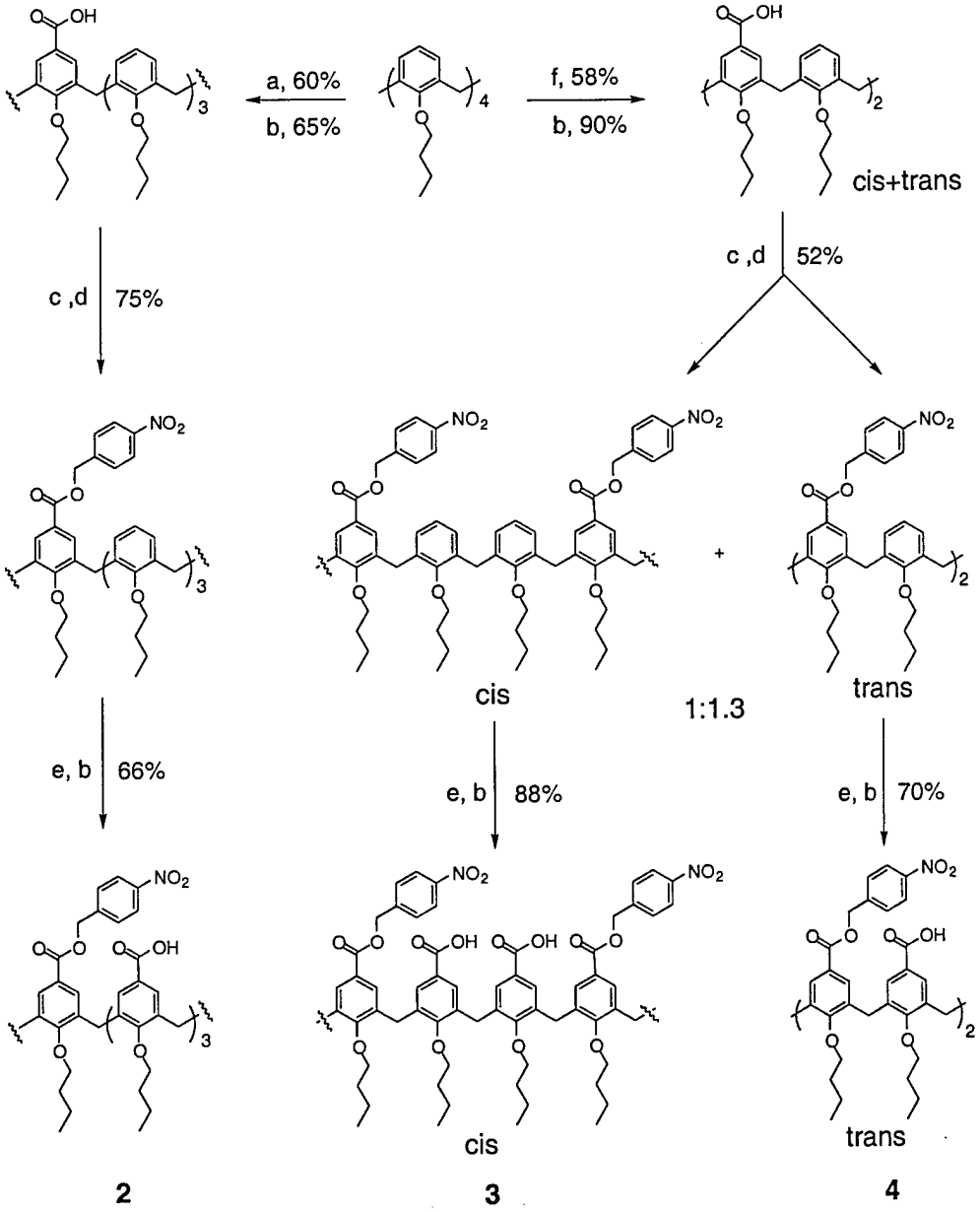

Scheme 1

a) 1 eq. Cl_2CHOCH_3, 1 eq. $TiCl_4$, CH_2Cl_2, -10°C; b)$NaClO_2$, H_2NSO_3H, CH_2Cl_2, Acetone, H_2O; c) $(COCl)_2$, cat. DMF, CH_2Cl_2; d) *p*-nitrobenzyl alcohol, DIEA, CH_2Cl_2; e) Cl_2CHOCH_3, $TiCl_4$ (excess), CH_2Cl_2, -10°C; f) Cl_2CHOCH_3, $SnCl_4$, CH_2Cl_2, -10°C.

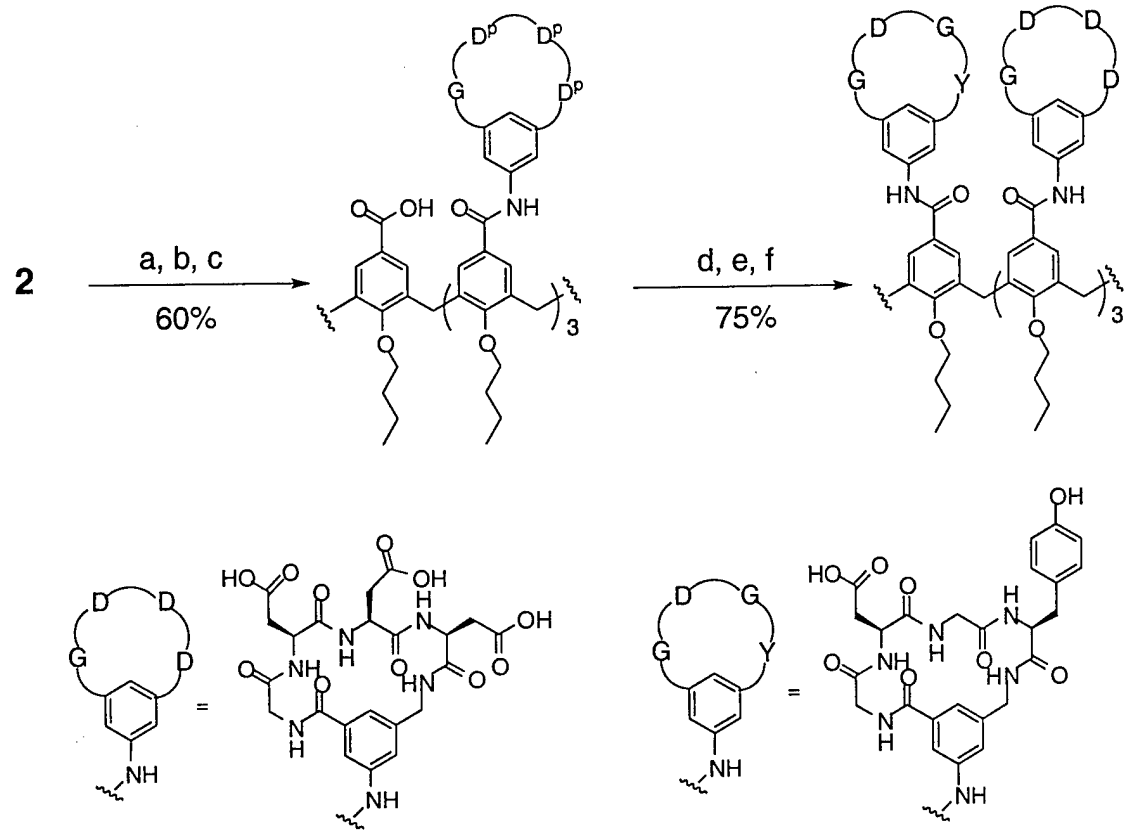

Scheme 2.

a) $(COCl)_2$, cat. DMF, CH_2Cl_2; b) cyclo-(Gly-Asp(O^{t}Bu)-Asp(O^{t}Bu)-Asp(O^{t}Bu)-Spc)-NH_2, DIEA, CH_2Cl_2; c) 10% Pd/C, H_2, MeOH; d) 2,4,6-trichlorobenzol chloride, TEA, THF; e) cyclo-(Gly-Asp(O^{t}Bu)-Gly-Tyr(O^{t}Bu)-Spc)-NH_2, DMAP, Benzene/CH_2Cl_2; f) 25% TFA/ CH_2Cl_2.

Scheme 3.

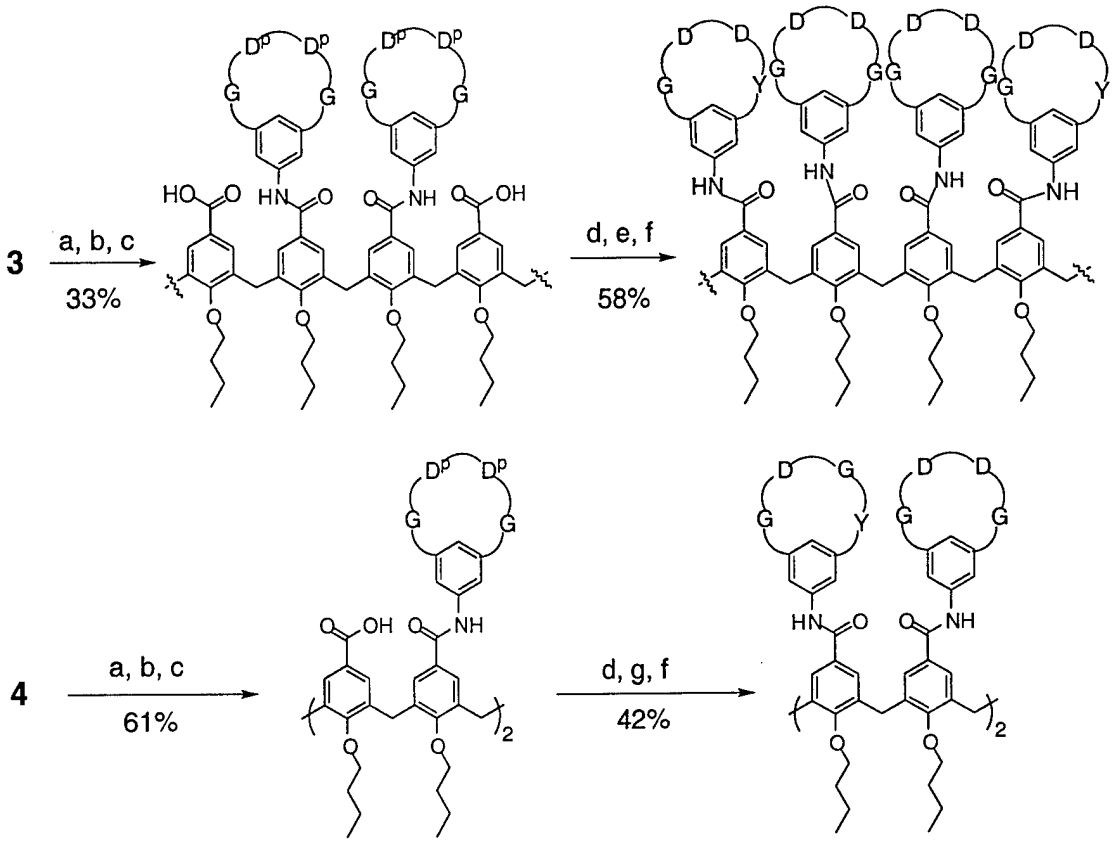

a) $(COCl)_2$, cat. DMF, CH_2Cl_2; b) *cyclo*-(Gly-Asp(O^{t}Bu)-Asp(O^{t}Bu)-Gly-Spc)-NH_2, DIEA, CH_2Cl_2; c) 10% Pd/C, H_2, MeOH; d) 2,4,6-trichlorobenzol chloride, TEA, THF; e) *cyclo*-(Gly-Asp(O^{t}Bu)- Asp(O^{t}Bu)-Tyr(O^{t}Bu)-Spc)-NH_2, DMAP, Benzene/CH_2Cl_2; f) 25% TFA/CH_2Cl_2; g)) *cyclo*-(Gly-Asp(O^{t}Bu)-Gly-Tyr(O^{t}Bu)-Spc)-NH_2, DMAP, CH_2Cl_2.